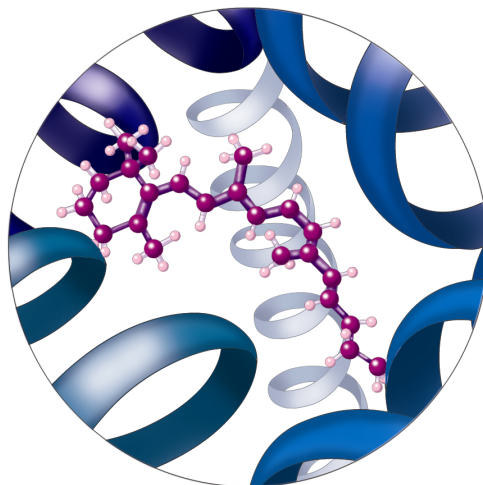


Department of Engineering Physics and Mathematics  
Laboratory of Biomedical Engineering  
Helsinki University of Technology

Espoo 2003

## THE RELATION BETWEEN SPECTRAL AND THERMAL PROPERTIES OF VERTEBRATE VISUAL PIGMENTS

Petri Ala-Laurila



TEKNILLINEN KORKEAKOULU  
TEKNISKA HÖGSKOLAN  
HELSINKI UNIVERSITY OF TECHNOLOGY  
TECHNISCHE UNIVERSITÄT HELSINKI  
UNIVERSITE DE TECHNOLOGIE D'HELSINKI



Helsinki University of Technology Laboratory of Biomedical Engineering  
Department of Engineering Physics and Mathematics  
Teknillinen korkeakoulu Lääketieteellisen tekniikan laboratorio  
Teknillisen fysiikan ja matematiikan osasto  
Espoo 2003

## THE RELATION BETWEEN SPECTRAL AND THERMAL PROPERTIES OF VERTEBRATE VISUAL PIGMENTS

Petri Ala-Laurila

Dissertation for the degree of Doctor of Science in Technology to be presented with due permission of the Department of Engineering Physics and Mathematics for public examination and debate in Auditorium F1 at Helsinki University of Technology (Espoo, Finland) on the 13th of December, 2003, at o'clock 12 noon.

Helsinki University of Technology  
Department of Engineering Physics and Mathematics  
Laboratory of Biomedical Engineering

Teknillinen korkeakoulu  
Teknillisen fysiikan ja matematiikan osasto  
Lääketieteellisen tekniikan laboratorio

Cover picture: Anne Ikonen

© Petri Ala-Laurila

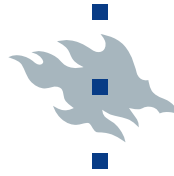
ISBN 951-22-6830-2 (printed)

ISBN 951-22-6831-0 (pdf)

Picaset Oy  
Helsinki 2003



TEKNILLINEN KORKEAKOULU  
TEKNISKA HÖGSKOLAN  
HELSINKI UNIVERSITY OF TECHNOLOGY  
TECHNISCHE UNIVERSITÄT HELSINKI  
UNIVERSITE DE TECHNOLOGIE D'HELSINKI



HELSINGIN YLIOPISTO  
HELSINGFORS UNIVERSITET  
UNIVERSITY OF HELSINKI

## THE RELATION BETWEEN SPECTRAL AND THERMAL PROPERTIES OF VERTEBRATE VISUAL PIGMENTS

Petri Ala-Laurila

This thesis for the degree of Doctor of Science in Technology has been  
carried out at two departments:

Department of Engineering Physics and Mathematics  
Laboratory of Biomedical Engineering  
Helsinki University of Technology

&

Department of Biosciences  
Division of Animal Physiology  
University of Helsinki

Espoo 2003

© Petri Ala-Laurila

ISBN 951-22-6830-2 (printed)  
ISBN 951-22-6831-0 (pdf)

Picaset Oy  
Helsinki 2003

“Dabei findet man denn wohl den Künstler beneidenswert, der durch Nachbildung und Nachahmung auf alle Weise jenen großen Intentionen sich mehr nähert, sie besser begreift als der bloß Beschauende und Denkende. Doch muß am Ende jeder tun, was er vermag, und so spanne ich denn alle Segel meines Geistes auf, um diese Küsten zu umschiffen.”

*“At this stage one naturally envies the artist, who, through reproducing and imitating these great visions, comes closer to them in every way than the person who merely looks and thinks. Still, after all, each can do only what lies in his power, and so I spread all the sails of my spirit that I may circumnavigate these coasts.”*

- Goethe, *Italienische Reise* -



## Abstract

This thesis investigates the relation between three important functional properties of visual pigments: 1) the absorbance spectrum, 2) the energy needed for activation and 3) the thermal stability.

The study is based on measurement of spectral absorbance and spectral sensitivity in 10 visual pigments in rod and cone photoreceptor cells from the retinas of 6 vertebrate species and on data from the literature. Absorbance spectra were recorded by single-cell microspectrophotometry (MSP) and spectral sensitivities by electroretinogram recording (ERG) across the isolated retina. For each pigment, measurements were conducted at two or more temperatures in the range 0–40 °C. The photoactivation energies of the visual pigments were determined from the temperature-dependence of spectral sensitivity in the long-wavelength range. Thermal activation rates of rod and cone pigments were collected from the literature.

One objective was to test the hypothesis that there is a strict coupling between the energy needed for photoactivation ( $E_a$ ) and the wavelength of maximum absorbance ( $\lambda_{\max}$ ) of visual pigments. The greater goal was to clarify the relation between the energies required for thermal and photic activation and thus explain the experimentally observed correlation between  $\lambda_{\max}$  and the rate of spontaneous, thermal activation of pigments.

The measurements showed that there is no necessary physical coupling between  $E_a$  and  $\lambda_{\max}$ . A strict inverse proportionality ( $E_a \propto 1/\lambda_{\max}$ ) holds only in the simple case where spectral tuning is achieved by a change of chromophore, with no change in the protein (opsin) part of the pigment. On the other hand, a significant correlation between  $E_a$  and  $1/\lambda_{\max}$  was found in the full set of 12 visual pigments considered (including two invertebrate pigments).

A new model for thermal activation is proposed, with a consequent dependence of the activation rate on  $\lambda_{\max}$ . The crucial point is that the statistics of thermal activation is determined by the presence of internal energy in a large number of vibrational modes of the visual pigment molecule. The great discrepancy between photoactivation energies and thermal activation energies as estimated in earlier work then disappears as an analytical artifact. The main conclusion is that thermal and photic activation of visual pigments may follow the same molecular route from a very early stage (isomerization of the chromophore in the native conformation of rhodopsin). Furthermore, the model accurately predicts the correlation between the wavelength of maximum absorbance and the rate of thermal activation observed in the whole set of visual pigments studied.

**Keywords:** rhodopsin, photoreception, activation energy, thermal noise, spectral sensitivity, absorbance, vision, retina

## Acknowledgements

The research reported in this thesis was carried out in the Laboratory of Biomedical Engineering at Helsinki University of Technology and at the Department of Biosciences at the University of Helsinki during the years 1999–2003.

I want to thank both of my supervisors Professor Ari Koskelainen and Professor Kristian Donner. I am grateful to Professor Koskelainen for introducing me to the field of vision research, for the wide freedom to concentrate on this project and for patiently trying to transfer to me the careful mind of an experimentalist at the early stage of this project. I also want to thank Professor Koskelainen for his guidance as well as the excellent research facilities obtained for the biophysics group. I am deeply thankful to Professor Kristian Donner for our fruitful debate and regular meetings, which have had a most profound impact on this thesis. Professor Donner's encouraging attitude, wide knowledge of this research field, interesting ideas and his special sense of humour were indispensable power sources for this work. In addition to the scientific contribution, I want to thank both of my supervisors for the numerous good laughs, educational conversations and interesting experiences during the years of this work.

I want to thank Professor Toivo Katila for providing an excellent research environment for this thesis in the Laboratory of Biomedical Engineering. I am thankful to all the people in the laboratory for the friendly working atmosphere.

I want to thank Mr. Rauli Albert, Ms. Pia Saarinen and Dr. Nanna Fyhrquist-Vanni for their significant contribution to the experimental part of this project as well as for the great company. I am grateful to Mr. Sami Minkkinen and Mr. Antti Huotarinen for their contribution to this work during their special assignment projects. I want to thank Ms. Soile Nymark, Ms. Hanna Suominen, Ms. Mirka Jokela-Määttä, Mr. Johan Pahlberg, Ms. Lotta Haldin, Dr. Ann-Christine Aho, Ms. Liisa-Ida Sorsa, Mr. Kim Simelius, Mr. Matti Stenroos and Dr. Timo Mäkelä as well as all the people who attended the monthly Vision and Hearing seminars for their help in many sorts of issues during this work. Thanks to the company of all these skilful colleges and friends of mine, the work with this thesis was a much more enjoyable journey.

To pre-examiners Professor Carter Cornwall and Professor Matti Weckström I want to express my gratitude for their expert criticism and comments on the manuscript of this thesis. I want to thank Dr. Victor Govardovskii for building the microspectrophotometer used in the experimental part of this thesis at the Department of Biosciences and for his expert comments. I thank Dr. Simo Hemilä

and Emeritus Professor Tom Reuter for many fruitful discussions. To Professor Eric Warrant I am thankful for encouraging me greatly during this project and for the wonderful opportunity to take part in the vision research expedition in the Pacific Ocean. I want to thank Ms. Anne Ikonen for drawing the cover page picture, Ms. Sisko Pietiläinen and her colleagues for taking care of the experimental animals and the personnel of the workshop at the Department of Engineering Physics and Mathematics for their skilful work.

The financial support of the Finnish Graduate School of Molecular Nanotechnology, the Emil Aaltonen Foundation, the Ella and Georg Ehrnrooth Foundation, the Foundation of Technology in Finland and the Oskar Öflund Foundation is gratefully acknowledged.

I thank my parents Eija-Liisa and Pekka for their love and support during the years of this work and much earlier. I am grateful to my brother Juha and his family among all my relatives and friends for being there. Finally, I want to express my deepest gratitude to my cute wife Suvi for sharing her life and love with me during the years of this work. Her smiles, understanding attitude and all the fun together were the best part of all.

Espoo, October 2003

Petri Ala-Laurila

# Contents

<b>List of publications</b>	<b>12</b>
<b>Author's contribution</b>	<b>13</b>
<b>List of abbreviations and symbols</b>	<b>14</b>
<b>1 Introduction</b>	<b>16</b>
<b>2 Visual pigments and their functional properties</b>	<b>18</b>
2.1 General characteristics .....	18
2.1.1 Location and structure .....	18
2.1.2 Classification of vertebrate visual pigments.....	21
2.1.3 Visual pigment function and signal transduction in vertebrate photoreceptor cells.....	22
2.2 Activation of visual pigments .....	25
2.2.1 General aspects.....	25
2.2.2 Activation by light.....	26
2.2.3 Spontaneous activation.....	29
2.3 Spectral absorbance and spectral sensitivity of visual pigments.....	41
2.3.1 General characteristics.....	41
2.3.2 Physical interpretation of visual pigment spectra.....	46
<b>3 Aims of the study</b>	<b>59</b>
<b>4 Materials and methods</b>	<b>61</b>
4.1 A general note on experimental techniques .....	61
4.2 Visual pigments, animals and preparations.....	63

4.3	Single-cell microspectrophotometry (MSP) (II–III).....	66
4.4	Electroretinogram recording (ERG) (I–IV).....	69
4.5	General analysis (I–IV) .....	73
4.6	Methods for models (IV, V).....	77
<b>5</b>	<b>Results</b>	<b>79</b>
5.1	Temperature effects on spectral sensitivity (I–IV).....	79
5.2	Photoactivation energy estimates and their relation to $1/\lambda_{\max}$ (I–IV).....	82
5.3	Model for thermal activation of visual pigments (V).....	83
<b>6</b>	<b>General discussion</b>	<b>85</b>
6.1	The validity of the physical models for spectral sensitivity and photoactivation energy .....	85
6.2	The relation between the wavelength of maximum absorbance ( $\lambda_{\max}$ ) and photoactivation energy ( $E_a$ ).....	87
6.3	The relation between the wavelength of maximum absorbance ( $\lambda_{\max}$ ) and thermal activation rates of visual pigments.....	88
<b>7</b>	<b>Conclusions</b>	<b>91</b>
	<b>References</b>	<b>92</b>

## List of publications

This thesis is based on the following five publications, which are referred to by their Roman numerals in the text:

- I Koskelainen, A., Ala-Laurila, P., Fyhrquist, N., & Donner, K. (2000). Measurement of thermal contribution to photoreceptor sensitivity. *Nature* **403**, 220–223.
- II Ala-Laurila, P., Saarinen, P., Albert, R., Koskelainen, A., & Donner, K. (2002). Temperature effects on spectral properties of red and green rods in toad retina. *Visual Neuroscience* **19**, 781–792.
- III Ala-Laurila, P., Albert, R.-J., Saarinen, P., Koskelainen, A., & Donner, K. (2003). The thermal contribution to photoactivation in A2 visual pigments studied by temperature effects on spectral properties. *Visual Neuroscience* **20**, 411–419.
- IV Ala-Laurila, P., Pahlberg, J., Koskelainen, A., & Donner, K. (2003). On the relation between the photoactivation energy and the absorbance spectrum of visual pigments. *Vision Research* (accepted for publication).
- V Ala-Laurila, P., Donner, K., & Koskelainen, A. (2003). Thermal activation and photoactivation of visual pigments. *Biophysical Journal* (accepted for publication).

## **Author's contribution**

The author has been involved in all aspects of the research reported in papers I–V. He has participated in the planning, execution, interpretation and analysis of the experiments. He has developed and refined the experimental designs and the methods of analysis. The physical model for thermal activations of visual pigments presented in paper V was discovered and developed by the author. He has participated actively in the writing of papers II–V and he has been responsible for the graphic realization of most of the figures in the original papers.

## List of abbreviations and symbols

$A$	absorbance
$A_B$	pre-exponential factor in the Arrhenius model
$A_H$	pre-exponential factor in the Hinshelwood model
A1	visual pigments containing 11- <i>cis</i> -retinal as chromophore
A2	visual pigments containing 11- <i>cis</i> -3,4-dehydroretinal as chromophore
$\bar{\alpha}(\lambda)$	the average absorption coefficient of a chromophore at certain wavelength ( $\lambda$ )
BB	Birge-Barlow hypothesis (see section 2.2.3)
$c$	concentration
$c$	speed of light
cDNA	complementary deoxyribonucleic acid
cGMP	guanosine 3',5'-cyclic monophosphate
$\Delta G$	the free energy change of a reaction
$\Delta H$	the enthalpy change of a reaction
$\Delta S$	the entropy change of a reaction
$\Delta$ -spectrum	the difference between logarithmic spectral sensitivities measured at different temperatures ('c' = "cold", 'w' = "warm"): $\Delta = \text{Log } S_w - \text{Log } S_c$
$\epsilon$	molar extinction coefficient
$E$	energy
$E_a$	the minimum energy needed for photoactivation of a visual pigment molecule from the ground state to the first electronically excited state
$E_{a,B}$	the apparent Arrhenius activation energy
$E_{a,H}$	the apparent activation energy based in the Hinshelwood model
ERG	electroretinogram
$F$	fraction of molecules with energy greater than a certain criterion
GMP	guanosine monophosphate
GPCR	G-protein-coupled receptor
$h$	Planck constant
HB	hypothesis proposed by Horace Barlow (1957) (see section 2.2.3)
$I$	light intensity (photons/(area $\times$ time))
$K$	the final slope of logarithmic sensitivity vs. frequency spectrum: $K = \partial \text{Log } S / \partial (1/\lambda)$
$k$	molecular rate constant of thermal isomerizations

$k$	Boltzmann constant
$L$	long-wavelength-sensitive
$l$	solution thickness
$\lambda$	wavelength
$\lambda_{\max}$	wavelength of maximum absorbance
$\lambda_0$	wavelength corresponding to minimum energy needed for photoactivation ( $\lambda_0 = hc/E_a$ )
$M$	mid-wavelength-sensitive
$m$	parameter in Lewis model ( $m + 1 =$ the number of vibrational modes involved in visual pigment activation)
MSP	microspectrophotometry
M/LWS	mid- and long-wavelength-sensitive
MI	metarhodopsin I
MII	metarhodopsin II
MIII	metarhodopsin III
$N$	number of atoms in a molecule
$n$	number of “square terms” for energy in the Hinshelwood model
O.D.	optical density
OS	photoreceptor outer segment
PSB	protonated Schiff base
$R$	molar gas constant
$r^2$	coefficient of determination
$S$	spectral sensitivity
SEM	standard error of mean
SLB	Stiles-Lewis-Barlow hypothesis (see section 2.2.3)
$S_0$	the ground state
$S_1$	the first electronically excited state
$T$	absolute temperature
TM	transmembrane

# 1 Introduction

Light is potentially the most powerful source of information about the environment available to an animal. It propagates faster than any other signal, it has useful qualities such as wavelength distribution and pattern of polarisation, and it is abundantly available at least in the daytime (except e.g. in the deepest waters or caves). Thus, it is not surprising that vision has become the primary sense especially in quickly moving animal species. The ability of visual systems to cope effectively with the vast variety of natural light environments, differing greatly both in light intensity and spectral composition, is quite astonishing. A common example of the challenges solved by our own visual system is our ability to see faint stars, which may be some 10 log units less intense than the scenery viewed on a bright sunny day. To understand the capacity of vision to function over such an enormous range of intensity and to find the absolute limits of visual performance, we must start from the molecular mechanisms of the very first steps in vision.

It has been known since the early discoveries by Boll (1876, 1877) and Kühne (1877, 1879) that a photosensitive substance, called a visual pigment or rhodopsin, constitutes the interface between the physiological world of vision and the physical world of light. George Wald and his co-workers showed that the rhodopsin protein binds a vitamin A derivative (the chromophore) as a cofactor (Wald, 1933, 1935), and that isomerization of the chromophore by a quantum of light is the very first step in seeing (Wald, 1968). Since these early investigations, visual pigments have been the subject of extensive study.

Novel approaches in biochemistry, molecular biology and biophysics, such as gene-targeting techniques, fast laser spectroscopy and X-ray crystallography, have provided a new level of understanding visual pigment structure and function. Today rhodopsin is the best-studied member of a wide and important group of G-protein-coupled receptor proteins (GPCRs) involved in many different cellular signalling processes including chemoreceptors facing the outside world (olfaction and taste) as well as internal hormone and neurotransmitter receptors. Compared with other GPCRs, rhodopsin offers some unique experimental advantages, e.g., the possibility of extremely precise, synchronous activation by light and subsequent monitoring of the activation process by spectroscopic methods. Studies are facilitated by the high concentration of rhodopsin in specialized regions of photoreceptor cells (in vertebrates, the rod or cone outer segment). Electrophysiological recording of the light-sensitive circulating current of photoreceptor cells can take advantage of the powerful natural amplification (the phototransduction cascade) to study events originating in single rhodopsin

molecules. Thus, studies on rhodopsin have also helped us to understand the structure and function of GPCRs in general.

Visual pigments vary with respect to two key functional properties: spectral sensitivity and thermal stability. Spectral sensitivity expresses the relative probabilities for the pigment to be activated by electromagnetic radiation of different wavelengths. This defines the limits to the visible band of electromagnetic radiation, i.e., the wavelength range called “light”. Furthermore, color vision results from the presence of at least two spectrally different visual pigments in different photoreceptor types. In addition to their activation by light, visual pigments can also be activated by their own thermal energy (Autrum, 1943; Barlow, 1956). At least in their physiological expression, thermal activations of the visual pigments are indistinguishable from activations by light (Baylor *et al.*, 1980). At the level of the light-sensitive circulating current in photoreceptor cells, they cause a random light-like activity (the “dark light”) that constitutes an irreducible intrinsic noise of the visual system and sets an ultimate limit to visual sensitivity (Autrum, 1943; Barlow, 1956; Aho *et al.*, 1988).

It is evident that spectral sensitivity and thermal stability, must both have been of critical importance in the evolution of visual pigments. An ideal pigment should be spectrally tuned for maximal quantum catch in a given light environment and at the same time be as stable as possible. The objective of the present thesis is to clarify the relationship between these two crucial properties.

## 2 Visual pigments and their functional properties

### 2.1 General characteristics

#### 2.1.1 Location and structure

In vertebrates, visual pigments are situated in the outer segment membranes of two morphologically distinguished photoreceptor types, rods and cones. In rods, visual pigments are packed in separate disc membranes of the outer segment. In cones, visual pigments are embedded in the folded plasma membrane of the outer segment. Rod and cone pigments have diverged to fulfill the different requirements of twilight (scotopic) and day (photopic) vision (Schultze, 1866; for review see Ebrey & Koutalos, 2001). The distinctions between rods and cones, based on morphology on one hand and visual pigment identity on the other have proved contradictory in some cases. For instance, it has been shown, that the same pigment can be found both in a rod and a cone photoreceptor in the same retina (Ma *et al.*, 2001).

All visual pigments possess a similar main structure consisting of two principal units shown in Fig. 1. The backbone of the molecule is a large (~ 40 kDa) apoprotein known as opsin, to which a small prosthetic group, termed the chromophore, is attached covalently. Opsin consists of a single chain of *ca.* 340–390 amino acids, the sequence of which varies between visual pigments. It is a typical 7-TM receptor protein, where seven  $\alpha$ -helical coils traverse the membrane forming a pocket-like structure shown in panel A in Fig. 1. Inside this pocket, the aldehyde terminus of the chromophore is attached to opsin at the lysine 296 residue in the centre of the seventh transmembrane helix via a protonated Schiff base (PSB) linkage (Bownds, 1967; Ovchinnikov, 1982; Hargrave *et al.*, 1983). The positive charge of the Schiff base linkage is stabilized by a negatively charged counterion, glutamate 113 (Zhukovsky & Oprian, 1989; Sakmar *et al.*, 1989; Nathans, 1990a). Thus, lysine 296 and glutamate 113 are highly conserved amino acid residues, which have an important role in regulating the spectral absorbance and stability of the opsin-bound chromophore.

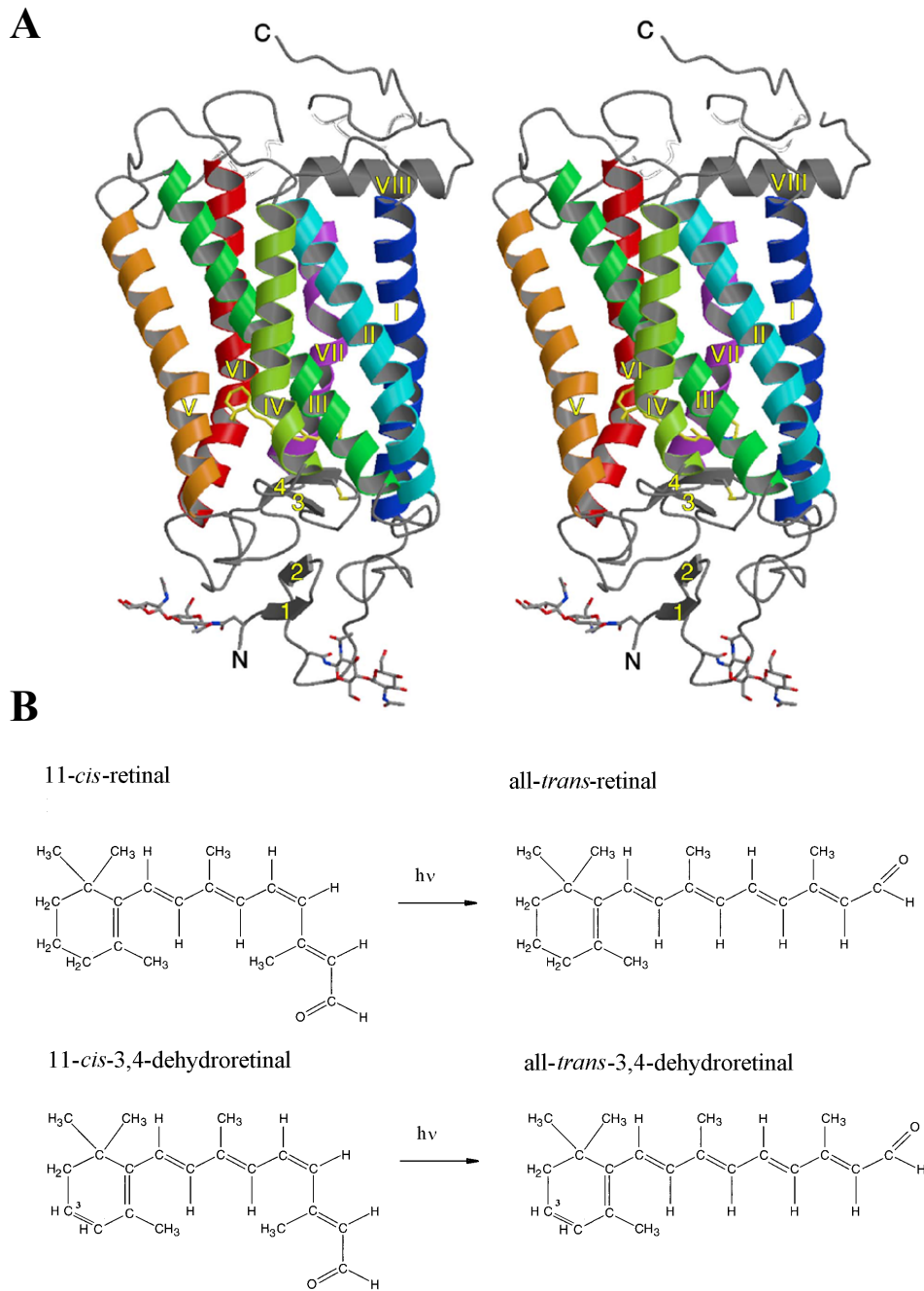


**Fig. 1. (A)** Stereoscopic ribbon drawing of rhodopsin parallel to the plane of the membrane. Reprinted with permission from Palczewski *et al.* (2000). Copyright 2000 [AAAS](#) (the original figure kindly provided by Dr. Palczewski). **(B)** The chemical structures of 11-*cis* and all-*trans* isomers of the vertebrate visual pigment chromophores.

The chromophore is the functional light-absorbing part of a visual pigment molecule. In vertebrate visual pigments, two different chromophores have been found, as shown in panel B in Fig. 1. The most common is 11-*cis*-retinal (A1 chromophore), which is the aldehyde of vitamin A1. Some amphibians, fishes and reptiles have 11-*cis*-3,4-dehydroretinal (A2 chromophore), the aldehyde of vitamin A2. The important structural difference between these two chromophores is the addition of a double bond between the carbons at the positions 3 and 4 in the  $\beta$ -ionone-ring. The switch of the chromophore from A1 to A2 has two important functional effects: 1) the absorbance spectrum of the resulting pigment is broader, and the absorbance spectrum is shifted towards longer wavelengths (Dartnall & Lythgoe, 1965; Bridges, 1967; for review see Bridges, 1972) and 2) the thermal stability of the pigment is lowered (Dartnall, 1955; Bridges, 1956, 1967; Williams & Milby, 1968; Donner *et al.*, 1990).

The structure of visual pigment has been the subject of extensive study. The best-examined pigment is bovine rhodopsin. This pigment was also the first one for which the primary structure was deduced by direct amino acid sequencing (Ovchinnikov *et al.*, 1982; Hargrave *et al.*, 1983) and later by cloning the cDNA sequence (Nathans & Hogness, 1983). By the year 2000, the amino acid sequences of more than 100 visual pigments had been deduced from DNA and cDNA sequences (for reviews see Yokoyama & Yokoyama, 2000; Ebrey & Koutalos, 2001). Among these are also the cDNA sequences of all the human opsin genes (Nathans & Hogness, 1984; Nathans *et al.*, 1986). The opsin of any visual pigment can now be expressed in cultured cells. Thus, many functionally important amino acids controlling the spectral properties of visual pigments have been identified. In addition, these techniques have been of great importance in studying the molecular basis of generic retinal diseases, such as retinitis pigmentosa. A recent breakthrough was the determination of the three-dimensional structure of bovine rhodopsin by X-ray crystallography extending to 2.8 angstroms resolution (Palczewski *et al.*, 2000). This study refined the structural model of the seven transmembrane helices of opsin, which had first been visualized in electron microscopic (Schertler *et al.*, 1993) and cryo-electron microscopic (Unger *et al.*, 1997) studies on two-dimensional crystals of bovine and frog rhodopsin, respectively. X-ray crystallography has offered the possibility to identify those regions of opsin that interact directly with the chromophore. This knowledge is of fundamental importance in the attempt to understand the relation between rhodopsin structure and function.

### 2.1.2 Classification of vertebrate visual pigments

Visual pigments originate from a common ancestor (for review see Goldsmith, 1990; Yokoyama, 1996). In spite of the relatively constant basic structure of opsin, the visual pigments possess sufficient freedom for spectral tuning to match their sensitivity to very different light environments as well as a large variation e.g. in thermal stability and speed of regeneration after bleaching. As shown in Fig. 2, vertebrate visual pigments are classified according to their chromophore and opsin into different groups. Pigments with 11-*cis*-retinal as chromophore are called rhodopsins or A1 pigments, whereas pigments containing 11-*cis*-3,4-dehydroretinal are called porphyropsins or A2 pigments. Molecular phylogeny, based on the opsin gene sequence, groups vertebrate opsins into six families. These are shown in panel B in Fig. 2 (for reviews see Yokoyama, 1996; Yokoyama & Yokoyama, 2000).

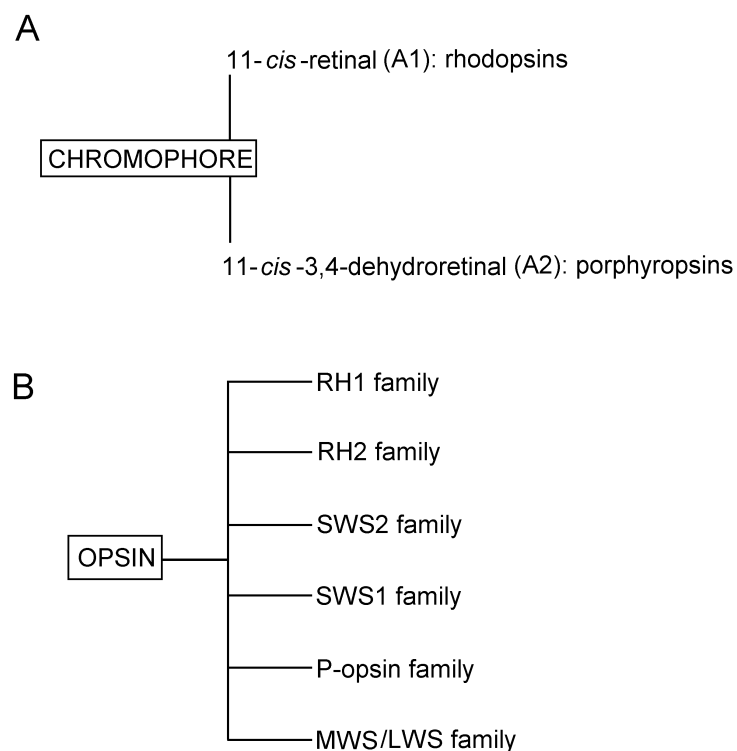


**Fig. 2.** Classification of vertebrate visual pigments. **A)** According to the chromophore vertebrate pigments are classified into rhodopsins and porphyropsins. **B)** According to the opsin sequence all vertebrate pigments fall into six groups (for review see Yokoyama, 1996).

In addition to the simple nomenclature presented above, there exists a wide terminology of visual pigments in literature. The term rhodopsin, originally given by Kühne (1877, 1879), is often used as a general term to refer to all visual pigments. Cones and their visual pigments are commonly named “blue-“, “green-“ and “red-sensitive” depending on the color appearance of light corresponding to the wavelength of maximum absorption ( $\lambda_{\max}$ ). Vertebrate rods are called “green” ( $\lambda_{\max} = ca. 430 \text{ nm}$ ) or “red” ( $\lambda_{\max} = ca. 500 \text{ nm}$ ) according to the color appearance of the transmitted light. In this thesis, the aforementioned classification and terminology of visual pigments is used. Other naming criteria can also be found especially in older literature. For example, Wald *et al.* (1953) reserved the terms rhodopsin and porphyropsin only for rod pigments and called the corresponding cone pigments iodopsins and cyanopsins, respectively. (for review see Ebrey & Koutalos, 2001)

### **2.1.3 Visual pigment function and signal transduction in vertebrate photoreceptor cells**

#### *Activation*

The first step in seeing occurs when the configuration of the chromophore is changed by light. Absorption of a photon isomerises the chromophore from its kinked 11-*cis*-configuration to a straight all-*trans*-configuration (Wald, 1968). This triggers a series of conformation changes in the protein, as a result of which rhodopsin reaches its activated form, called metarhodopsin II. Thus, the information of photon absorption is transferred from the chromophore to the cytoplasmic surface of rhodopsin. In the dark state, the 11-*cis* form of chromophore acts as an inverse agonist stabilizing the protein in its inactive conformation. As a result of isomerization, the chromophore becomes an agonist and triggers the transition of the rhodopsin into its active form.

#### *Phototransduction*

Rhodopsin activation is followed by a biochemical cascade of reactions, by which the information of the absorbed photon is amplified and transferred into an electrical signal within the photoreceptor cell. This process is called phototransduction. Phototransduction in vertebrate rods is one of the best-studied cellular signaling pathways. The main stages of phototransduction after visual pigment activation can be summarized as follows: The activated form of rhodopsin (metarhodopsin II) activates multiple molecules of the photoreceptor G-protein (transducin), each of which can activate one subunit of a phosphodiesterase molecule. Each activated phosphodiesterase molecule catalyses the hydrolysis of

multiple molecules of guanosine 3',5'-cyclic monophosphate (cGMP), the internal messenger in the photoreceptor cells, to guanosine monophosphate (GMP). As the concentration of cGMP drops, the cGMP-gated channels in photoreceptor outer segment close leading to a decrease in the current flowing into the cell in darkness ("dark current") and thus to a hyperpolarization of the cell (for reviews see Arshavsky *et al.*, 2002; Burns & Lamb, 2003). Hyperpolarization causes a decrease in the synaptic release of glutamate, through which the information is transferred to the next layer of neurons (bipolar and horizontal cells). Soon after activation, metarhodopsin II as well as the activated forms of transducin and phosphodiesterase are inactivated in a sequence of processes.

#### *Summary of primary functional properties*

The only light-sensitive mechanism in the whole visual pathway is the very first step, the *cis-trans* isomerization of the chromophore. Later stages amplify the signal and process the information about single-photon absorption events in both the time and space domains. At these later stages, no direct information about the light environment can be added: all the information is already present in the spatio-temporal pattern of visual pigment activations in different photoreceptor types. On the other hand, possible "false" events produced by thermal activations of visual pigment molecules represent noise that is transmitted to the later stages of visual information processing. Thus, the properties of the visual pigments set ultimate limits to visual performance. It must be assumed that these properties have been subject to strong selection pressures during evolution.

The most important functional requirements of visual pigments can be summarized in the following way:

- **High quantum efficiency of photoactivation.** Quantum efficiency defines, which fraction of the molecules that absorb a photon are activated.
- **Optimized spectral sensitivity.** In addition to quantum efficiency, the effectiveness of photon utilization depends on the spectral sensitivity of the pigment. To maximize the photon catch, the spectral sensitivity of the pigment should be tuned to match the spectral composition of light available.
- **Fast activation and effective signal transduction.** Fast activation of visual pigment by light and effective signal transfer to the next stage of the phototransduction cascade are necessary requirements for the fastness of vision.
- **Effective termination of rhodopsin activity and regeneration of the native pigment.** To avoid noise in the system and to recover sensitivity

after intense light stimuli, the activated visual pigment has to be quickly turned off and the native pigment regenerated. This is important for temporal resolution and to preserve sensitivity under steady illumination.

- **Low level of spontaneous activations.** Especially in dim light, the rate of spontaneous activations of visual pigments has to be minimized to improve the signal-to-noise ratio of vision.

The first property, quantum efficiency, seems to have reached some functional maximum during evolution to fulfill the requirements of effective photon utilization. Dartnall (1968) originally showed that all visual pigments have a rather constant quantum efficiency of photoactivation (*ca.* 0.67) over wide wavelength and temperature domains. Thus, on the average two of three absorbed photons activate the pigment. Compared with other photochemical reactions, this is a very high quantum efficiency. In addition, the quantum efficiency of rhodopsin is at least two times higher than that of a naked 11-*cis*-retinal protonated Schiff base in solution (not complexed with opsin) (Freedman *et al.*, 1986), which shows that opsin has an important role in controlling the quantum efficiency of visual pigments (for review see Birge, 1990).

The other requirements listed above have different priorities for rod and cone pigments. According to the current view, rod visual pigments diverged from cone pigments in the course of evolution to meet the requirements of scotopic vision (Yokoyama & Yokoyama, 2000). In rods, a high sensitivity and a low level of intrinsic noise are very important characteristics, because visual information is limited by the sparseness of photons in dim light. Rod pigments are, indeed, thermally extremely stable molecules; at room temperature each of them is activated on average only once in *ca.* 3000 years (Baylor *et al.*, 1980). The high stability of rod pigments has made it possible to pack a large number of them into each rod photoreceptor without incurring an unacceptable noise level. A typical rod contains about  $10^8$ – $10^9$  rhodopsin molecules depending on photoreceptor size. The high density of thermally stable visual pigments allows rods to operate as efficient single photon detectors in dim light (Hecht *et al.*, 1942; van der Velden, 1946; Barlow, 1956; Sakitt, 1972; Baylor *et al.*, 1979; Aho *et al.*, 1987; Rieke & Baylor, 1998; Rieke, 2000). In cones, the visual pigments are tuned according to the needs of a photopic light environment, where the number of photons available is not a limiting factor in general. In bright light, the speed of vision and ability to adapt over a wide intensity range are more important characteristics than high sensitivity. Thus, the inactivation, regeneration and modulatory steps of phototransduction are much faster and the rate of spontaneous activations of visual pigments is on average 4 log units higher in cones than in rods (Barlow, 1958; Baylor *et al.*, 1984; Schnapf *et al.*, 1990; Donner, 1992; Rieke & Baylor, 2000; Sampath & Baylor, 2002; V).

Visual pigment evolution can be thought as an optimization problem, where the key characteristics are listed above. In order to understand this optimization it is important to know to what extent these characteristics can be tuned separately and in what ways they are coupled. One can ask, for example, how scotopic vision is optimized. Because the quantum efficiency appears to be a practically constant property of visual pigments, the interesting question from the point of view of maximizing visual sensitivity in a given light environment is the relation between spectral sensitivity and thermal stability. Both of these properties can be tuned over a wide range in visual pigments. If there is a physical coupling between spectral sensitivity and thermal stability of visual pigments, then this is a limiting condition that has to be taken into account in order to understand how the best signal-to-noise ratio can be achieved in visual pigment evolution. The speed of pigment regeneration, on the other hand, is not particularly important for vision in very dim light. A more detailed discussion about the thermal stability and the spectral sensitivity of visual pigments is presented in sections 2.2.3 and 2.3, respectively. The coupling between these two quantities will be discussed in sections 5.3 and 6.3.

## **2.2 Activation of visual pigments**

### **2.2.1 General aspects**

Visual pigments can be activated by light and by heat. The former process is called photoactivation, whereas the latter is called spontaneous or thermal activation. Rod pigments combine an extremely fast photoisomerization process with a very low probability of thermal isomerization. To understand this fortunate design, both activation mechanisms have to be profoundly understood. The mechanism of photoactivation is quite well understood based on studies on a few model pigments, especially bovine rhodopsin. On the other hand, the reaction mechanism that generates spontaneous activations is still unclear. Several models have been proposed for the molecular mechanism of thermal activation of rhodopsin (see below), but none of them explains satisfactorily the experimental data available. Contrary to the photoactivation process, which can be experimentally triggered by brief pulses of light and elucidated at submolecular resolution with fast spectroscopic methods, spontaneous activations are difficult to study. The stochastic occurrence of spontaneous pigment activations does not allow the same elegant approaches as applied in the case of photoactivation.

The current knowledge of photoactivation and its mechanism is summarized in section 2.2.2. Thermal activations of visual pigments and the prevailing hypothesis of their molecular mechanisms are discussed in section 2.2.3.

## 2.2.2 Activation by light

In photoactivation, absorption of a photon triggers the initial event of vision, the *cis-trans* isomerizations of the chromophore inside the opsin (Wald, 1968). This reaction is one of the fastest photochemical reactions ever studied (Schoenlein *et al.*, 1991). *Cis-trans* isomerizations is complete in only 200 fs, as revealed by novel ultrafast spectroscopic methods using laser pulses delivered on femtosecond-scale (Schoenlein *et al.*, 1991; Wang *et al.*, 1994). The *cis-trans* isomerization of the chromophore is followed by the formation of a sequence of spontaneous transient states in the chromophore-(all-*trans*-retinyldine)-opsin complex, which have been characterized by their different absorption properties. The sequence of transient states leads within milliseconds from the initial photon absorption to an equilibrium between metarhodopsin I (MI) and metarhodopsin II (MII), the active form of rhodopsin. This equilibrium is the final phase of the activation process, which is followed by the dissociation of MII via metarhodopsin III (MIII) to free all-*trans*-retinal and opsin. The kinetics and energetics of *cis-trans* isomerization and the following sequence of transient states of the photolysis of vertebrate visual pigments are summarized in Fig. 3. Invertebrate visual pigments differ from vertebrate pigments in the later intermediates of the visual pigment photolysis (Nakagawa *et al.*, 1999), but this is beyond the scope of the present thesis (for review see Shichida & Imai, 1998).

The energy barrier for the *cis-trans* isomerization of the chromophore has to be passed for photoactivation to occur. In general photochemistry, the minimum energy needed for the electronic excitation of a molecule from its ground state to the 1st electronically excited state is called the photoactivation energy ( $E_a$ ). As shown in Fig. 3, excitation of rhodopsin from the ground state ( $S_0$ ) to the 1st electronically excited state ( $S_1$ ) happens as a result of photon absorption. The delocalized  $\pi$ -electrons along the conjugated chain of the chromophore are the electrons involved in electronic excitation. According to the Franck-Condon principle, the electronic excitation can be presented as a vertical line from the ground-state potential energy surface to the potential surface of the first electronically excited state, because the time needed for electronic excitation is much shorter than the nuclear vibration period. The excited state relaxes to the ground-state surface forming the primary transient photoproduct, photorhodopsin, first discovered in low temperature spectrophotometry and laser photolysis studies (Shichida *et al.*, 1984; Yoshizawa *et al.*, 1984). Of course, relaxation can also lead

back to the ground state of rhodopsin, but the high quantum efficiency of photoactivation (0.67) (Dartnall, 1968) shows that relaxation towards photo-rhodopsin is favoured.

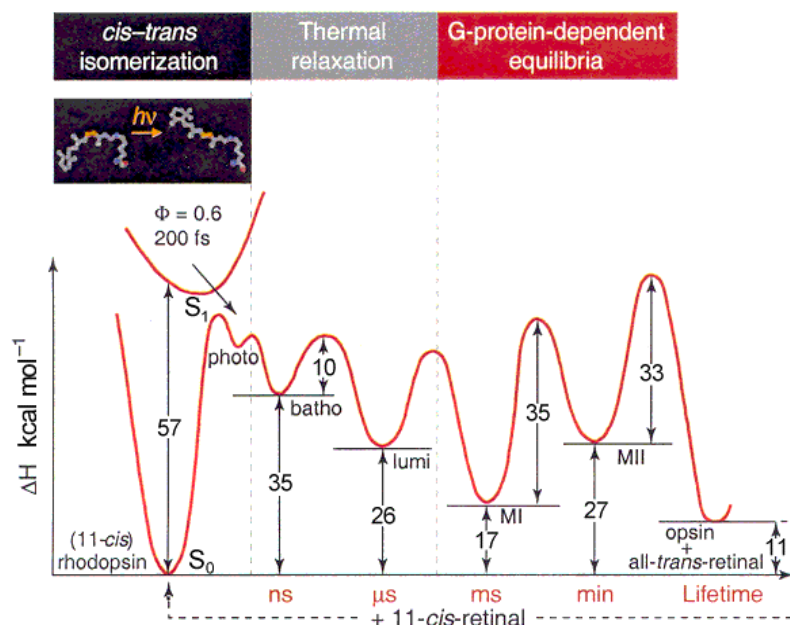


**Fig. 3.** A schematic two-dimensional drawing of the ground- and excited-state enthalpy surfaces of the photoactivation pathway of bovine rhodopsin and its intermediates. The enthalpies and activation enthalpies of bovine rhodopsin and its intermediates are based on calorimetric and kinetic experiments (Cooper, 1979; Imai *et al.*, 1994; Cooper & Converse, 1976; Cooper, 1981; for review see Shichida & Imai, 1998). The vertical energy difference between the ground state ( $S_0$ ) and the 1st electronically excited state ( $S_1$ ) is based only on the absorption maximum (500 nm) of bovine rhodopsin (Cooper, 1979). The figure is reprinted with minor modifications from Okada *et al.* 2001, Copyright (2001), with permission from Elsevier.

With the aid of femtosecond transient absorption spectroscopy, resonance Raman spectroscopy, and fluorescence measurements, it has been possible to study both the ground- and the excited-state dynamics and energetics. The data provided by these methods have been used for theoretical calculations of the excited-state potential energy surface. On the basis of these studies, the following conclusions have been drawn: 1) the chromophore tunnels from the excited state to the photoproduct ground state at *ca.* 50–60 femtoseconds after the photon absorption (Kakitani *et al.*, 1998; Mathies, 1999). 2) The isomerization is as fast as the period of torsional vibrations of the chromophore (Loppnow & Mathies, 1988; Wang *et al.*, 1994). 3) The ground-to-excited state energy gap at the surface crossing region is approximated to be only *ca.* 6 kcal/mol based on modeling of bovine

rhodopsin (Mathies, 1999). 4) The chromophore leaves the excited state at *ca.* 46 kcal/mol above the ground state according to the general rhodopsin model based mostly on studies on bovine rhodopsin (Mathies, 1999). Activation energies of visual pigments have also been estimated by photocalorimetry, bleaching studies as well as by measuring the temperature effects in the long-wavelength domain of the absorption spectrum. The last-mentioned is the method applied in this thesis. The results for activation energies of visual pigments obtained by these different methods are compared in General discussion (at the end of section 6.1).

Photorhodopsin relaxes via bathorhodopsin and lumirhodopsin to reach an equilibrium between MI and MII (for review see Shichida & Imai, 1998). The formation of MII, the active form of rhodopsin, is accompanied by deprotonation of the Schiff base linkage (Arnis & Hofmann, 1993) and a large hypsochromic shift (blue shift,  $\Delta\lambda_{\max} \approx 100$  nm) in the absorption maximum (for review see Shichida & Imai, 1998). MII dissociates to all-*trans*-retinal and free opsin via MIII. Bathorhodopsin (Yoshizawa & Kito, 1958), lumirhodopsin (Hubbard *et al.*, 1959) and MI-II (Matthews *et al.*, 1963) can be trapped by experiments performed at very low temperature. Thus, these intermediates were distinguished by spectroscopy much before laser techniques allowed the discovery of photorhodopsin (Shichida *et al.*, 1984) and some other intermediates in between these classical ones (Hug *et al.*, 1990; Thorgeirsson *et al.*, 1993; Tachibanaki *et al.*, 1998). Later studies have also shown that two different forms of MII exist (Arnis & Hofmann, 1993; Szundi *et al.*, 1998). In addition to spectroscopic classification of batho-, lumi- and MI and II, the enthalpies of these intermediates compared with ground-state rhodopsin have been estimated by photocalorimetry (Cooper, 1979, 1981). The enthalpies are summarized in Fig. 3.

The free energy changes ( $\Delta G$ ) of the reaction steps in photoactivation can be used to assess the spontaneity of the reactions. For a reaction occurring at constant absolute temperature ( $T$ ):

$$\Delta G = \Delta H - T\Delta S, \tag{1}$$

where according to a common notation,  $\Delta H$  is the enthalpy change of the reaction and  $\Delta S$  is the entropy change of the reaction.

In photoactivation, photon energy is the primary source for the chemical free energy needed for all the later steps of the activation process. Cooper (1979) showed that bathorhodopsin has 35 kcal/mol higher enthalpy than the ground state of rhodopsin. Thus, most of the photon energy is stored by switching the opsin-bound chromophore into its *trans*-configuration. All steps after the initial photoactivation take place spontaneously indicating that the chemical free energy is

decreasing ( $\Delta G < 0$ ) in each reaction step. Although the enthalpy change is positive ( $\Delta H > 0$ ) as MI is converted to MII (see Fig. 3), this process is still spontaneous, indicating lowering of the total free energy. Therefore, there has to be an increase in the entropy ( $\Delta S > 0$ ) and thus the disorder of the protein must increase within the MII formation.

Thermodynamics does not, however, offer any information about the absolute rate of reactions. The kinetics of a reaction sets limits to the structural changes, which are possible within the limited time of the reaction. It is intuitively easy to understand that large conformation changes need time to occur. This reasoning can be applied to the analysis of the photoactivation reaction of visual pigments. The light-induced isomerization of the chromophore is complete within only 200 fs after photon absorption (Schoenlein *et al.*, 1991; Wang *et al.*, 1994). Up to this point the reaction is too fast to involve any significant structural changes in opsin (for review see Filipek *et al.*, 2003). The *cis-trans* isomerization is believed to happen by a fast torsion around the Schiff-base side of the C11=C12 double bond of the opsin-bound chromophore (Okada *et al.*, 2001). During the formation of later intermediates, the chromophore-opsin interactions play a more important role leading to larger conformation changes in the opsin part of the molecular complex. Especially, the transition from MI to MII is accompanied by a large change in opsin conformation. Site-directed mutagenesis and spin-label experiments with controlled modifications in the opsin structure have helped to resolve structural changes during the later steps of photoactivation. In these studies, many functionally important regions of rhodopsin have been found and the movement of opsin helices during photoactivation monitored (for review see Filipek *et al.*, 2003). These conformation changes finally transfer the information of the photon absorption from the core of the protein into its surface region.

### 2.2.3 Spontaneous activation

#### *General characteristics*

The notion that spontaneous activations occur in visual pigments dates back to the 1940's. Originally, Autrum (1943) proposed that thermal activations of visual pigments set an ultimate limit to visual sensitivity. Soon after this, Hecht *et al.* (1942) argued on the basis of psychophysical experiments that the absorption of as few as 5–7 quanta is sufficient for the perception of light. Their photometric estimate of quantum catch was later proved to be too low, however, and the statistics of detection in their experiments could no longer be explained only by quantal fluctuations in the number of photon absorptions (cf. Barlow, 1977;

Donner, 1992). Horace Barlow (1956) gave a theoretical explanation. He argued that “photon-like” thermal activations of visual pigment molecules provided an explanation for why the variability of light detection is larger than would result from Poisson fluctuations of the number of light quanta absorbed. He also estimated the upper limit of this internal noise component based on the absolute sensitivity of human scotopic vision obtained from psychophysical measurements.

The first direct experimental evidence for spontaneous activations of visual pigments in vertebrate photoreceptors came when Baylor *et al.* (1980) showed by suction pipette recording from single toad rods that spontaneous discrete events in the light-sensitive current of the photoreceptor occurred in total darkness. In addition to the discrete events, a continuous noise component was present. The discrete “bumps” (discrete noise) were indistinguishable from photon-triggered events in both amplitude and waveform. It is now generally accepted that the discrete events in the dark current are generated by thermal activations of visual pigment molecules. Because both single-photon events and spontaneous events have similar amplitude and kinetics, it is assumed that they are generated via similar amplification stages. Thus, the only reasonable assumption is that they are generated at the first step of phototransduction, which is the activation of a visual pigment molecule. Contrary to discrete noise, continuous noise in the dark current appears to be generated by spontaneous activations of phosphodiesterase molecules (Rieke & Baylor, 1996).

The first recordings by Baylor *et al.* (1980) have been followed by many studies in which the rates of spontaneous activations have been estimated not only from rods of several species but also from some cones (see Tables 1 and 2 in paper V for references). As suggested by early psychophysical experiments (Barlow, 1958), the rate of spontaneous events is much higher in cones than in rods. Because of this high rate, discrete events are superimposed. Their amplitude is also small because of the low gain in cone phototransduction. Thus, single discrete events cannot be distinguished in the dark current of cones. The rate of discrete events in cones can, however, be estimated from the power spectra of noise recordings and the estimated amplitude of the single-photon response. Noise recordings from cones have also shown that the dominant noise component can vary depending on the cone type. Rieke & Baylor (2000) showed on salamander cones that the main noise component of long-wavelength-sensitive (L) cones is discrete noise, whereas the main noise component of short-wavelength-sensitive (S) cones is continuous noise.

The most important functional consequence to be expected from spontaneous activations is that they set an absolute limit on visual sensitivity in dim light (Autrum, 1943; Barlow, 1956). This idea has received strong experimental

support from Aho *et al.* (1988, 1993), who measured the behavioural sensitivity of common toads and frogs at different temperatures. The measured absolute visual sensitivity of dark-adapted toads was about that allowed by known rates of spontaneous activations. The same was true of the most sensitive retinal ganglion cells (the output stage of the retina). Moreover, sensitivity dropped with increasing temperature as would be expected based on the increased rate of thermal isomerizations as measured in toad rods (Baylor *et al.*, 1980). The extremely rare occurrence of spontaneous events in rods and their role as the limiting factor of visual sensitivity at least in some cases suggest that evolution has minimized the rate of thermal isomerizations of rhodopsin (for further discussion, see Barlow, 1988).

*The temperature dependence of spontaneous activations and the Arrhenius equation*

The frequency of discrete events depends on temperature. Thermal events become more frequent at higher temperatures, the rise being quite similar in the vertebrate pigments studied so far (*ca.* 3–4 fold per 10 °C) (Baylor *et al.*, 1980; Matthews, 1984; Sampath & Baylor, 2002). Although there is a large difference between the absolute rate of discrete events measured in rods and that in cones, the temperature dependence of discrete events appears to be fairly similar in both photoreceptor types.

Baylor *et al.* (1980) used Arrhenius analysis to characterize the temperature dependence of the rate of spontaneous activations in the rods of the cane toad (*Bufo marinus*). This approach has also been used in the subsequent studies where the temperature dependence of the rate of spontaneous activations has been studied in the green rods of the cane toad (Matthews, 1984) and the long-wavelength-sensitive cones of the tiger salamander (Sampath & Baylor, 2002). The expression proposed by Arrhenius is the most common way to describe the temperature dependence of the rate constant of a chemical reaction:

$$k = A_B e^{-\frac{E_{a,B}}{RT}}, \quad (2)$$

where  $k$  is the molecular rate constant (in this case the frequency of thermal isomerizations),  $A_B$  is the Arrhenius pre-exponential factor,  $E_{a,B}$  is the apparent Arrhenius activation energy of the reaction,  $R$  is the gas constant and  $T$  is the absolute temperature. According to this relation, the temperature dependence of the reaction comes mostly from the exponential term ( $\exp(-E_{a,B}/RT)$ ), although  $A_B$  may have a weak temperature dependence. The subscript ‘B’ is used in the pre-

exponential factor ( $A_B$ ) as well as in the Arrhenius activation energy ( $E_{a,B}$ ) to emphasize that the Arrhenius model is based on Boltzmann statistics.

The apparent activation energy can be easily read from the experimental data determined by plotting  $\ln k$  (or  $\log k$ ) against  $1/T$ :

$$\ln k = \ln A_B - \frac{E_{a,B}}{RT}. \quad (3)$$

The graphical representation of this formula (logarithmic  $k$  vs.  $1/T$ ) is called an Arrhenius plot (see Fig. 4). The intercept of the straight line of the Arrhenius plot is  $\ln A_B$  and the slope is  $-E_{a,B}/R$ . A reaction that gives a straight line in this representation is said to show Arrhenius-type behaviour. The rate constants of discrete dark events demonstrate, within experimental error, Arrhenius-type behaviour.

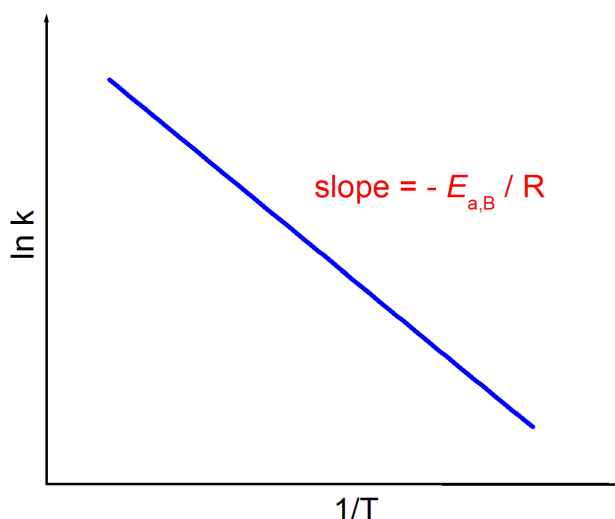


**Fig. 4.** Arrhenius-plot representing the logarithmic rate of the reaction ( $\ln k$ ) as a function of the inverse absolute temperature ( $1/T$ ).

The Arrhenius equation can be regarded as an empirical formula, valid for a number of chemical reactions. The equation is based on a simple physical picture of gaseous collision reactions. Arrhenius' original idea was that the strong temperature dependence of gaseous collision reactions could be explained if only a small fraction of collisions caused the reaction. He thought that the rate of a gaseous collision reaction would be proportional to the number of molecules with high translational energy. Because the number of such molecules can be estimated by

the Boltzmann distribution, the rate of the reaction should be proportional to  $\exp(-E_{a,B}/RT)$ . This reasoning led Arrhenius to the idea that the reaction rate of simple gaseous collision reactions is governed by equation 2 (for further details, see e.g. Mortimer, 1993). Although the Arrhenius theory was originally developed for molecular collisions in gases, it has been used to characterize many other chemical reactions. The so-called transition-state theory or activated complex theory connects the apparent activation energy ( $E_{a,B}$ ) of the Arrhenius equation to the thermodynamic quantities of the reaction. According to this theory, the reaction mechanism can be presented in the following way (Moore, 1962):



where A and B are reactants and  $[AB]^\ddagger$  is a transition state (or an activated complex) of the reaction with high energy content. The rate of the reaction is then proportional to the concentration of the transition state:  $k \propto [AB]^\ddagger$ . The apparent activation energy ( $E_{a,B}$ ) is the height of the energy barrier on the potential energy surface between the transition state and the reactants (see Fig. 5). The number of activated-complex molecules is proportional to  $\exp(-E_{a,B}/RT)$ . Thus, the Arrhenius equation gives the reaction rate in the transition-state theory. In addition, the apparent activation energy ( $E_{a,B}$ ) has a physical interpretation as the energy barrier on the potential energy surface of the reaction, which has to be passed during the reaction.

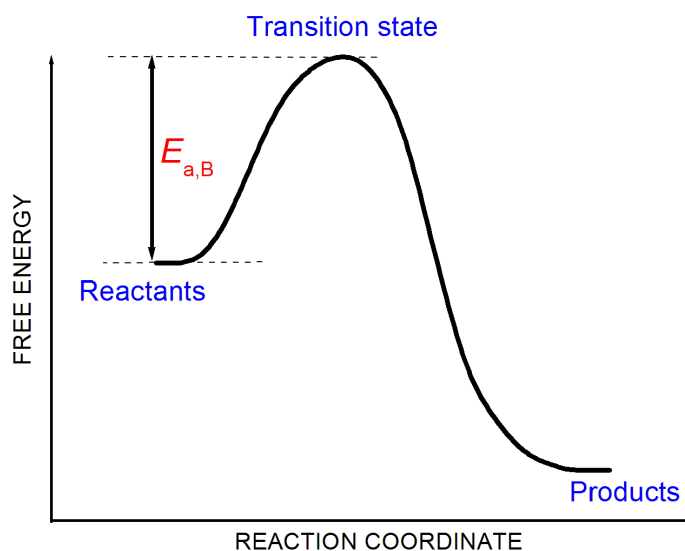


**Fig. 5.** Free energy diagram for a reaction according to the transition-state theory.

Transition-state theory has also been applied to the analysis of the rate of the spontaneous activations of visual pigments. Furthermore, the Gibbs free energy of activation, the enthalpy of activation and the entropy of activation for discrete events have been estimated based on the transition-state theory (Baylor *et al.*, 1980; Matthews, 1984; Sampath & Baylor, 2002). In general, the estimates for the apparent activation energies and the activation enthalpies for thermal isomerizations of different visual pigments are only about half of those estimated for the photoactivation process of visual pigments (Lythgoe & Quilliam, 1938; St. George, 1952; Srebro, 1966; Cooper, 1979; Barlow *et al.*, 1993; Mathies, 1999; Birge & Vought, 2000; I–IV). Because of this evident discrepancy between the energetics of thermal activation and photoactivation, it has been generally believed that these processes follow different molecular mechanisms (Barlow *et al.*, 1993; Birge & Barlow, 1995). Different hypotheses about the possible mechanism of thermal activation are discussed later in this section.

The rate of thermal bleaching has earlier been studied on extracted visual pigments in solution (Lythgoe & Quilliam, 1938; St. George, 1952; Hubbard, 1958a; Williams & Milby, 1968). The apparent Arrhenius activation energy ( $E_{a,B}$ ) estimates deduced from these studies range between 44–100 kcal/mol. However, many of these studies used high temperatures well beyond the physiological temperature range (up to *ca.* 70 °C). Hubbard (1958b) has shown that under these conditions, thermal bleaching can proceed via denaturation of opsin. Thus, the high apparent activation energy estimates obtained in some of these studies probably represent a totally different process, which is not related to photoactivation or thermal activation of visual pigments, but rather to denaturation of protein. The apparent activation energy of thermal isomerizations of 11-*cis*-retinal in different organic solutions (22.4–26.2 kcal/mol) (Hubbard *et al.*, 1965; Hubbard, 1966) is, however, comparable to the values obtained for the apparent activation energy of the spontaneous activations determined in living rod photoreceptors by Baylor *et al.* (1980). Since the studies of 11-*cis*-retinal in organic solutions do not involve opsin, the results can not be distorted by the denaturation of protein. On the other hand, other authors (Birge & Vought, 2000) have argued that the apparent Arrhenius activation energy of 11-*cis*-retinal may not be related to that of intact rhodopsin. They have pointed out that naked 11-*cis*-retinal in solution may behave differently from the protein-bound chromophore which is the protonated Schiff base of 11-*cis*-retinal.

#### *Theory of thermal unimolecular reactions with many degrees of freedom*

So far, the kinetics of spontaneous activations of visual pigments has been studied only in the light of the Arrhenius theory (Baylor *et al.*, 1980; Matthews, 1984; Sampath & Baylor, 2002). The conclusion that there is a large discrepancy

between the photoactivation and thermal activation energies is based on the assumption that Arrhenius analysis gives correct estimates of the latter. One of the principal goals of this thesis is to question the validity of this assumption by questioning the strict physical interpretation of the apparent Arrhenius activation energy of the spontaneous activations of visual pigments (see paper V). To resolve the discrepancy between the apparent Arrhenius activation energies and the photoactivation energies of visual pigments, I suggest another approach to the analysis of the rates of spontaneous activations. This approach is based on the Hinshelwood theory of thermal unimolecular reactions (Hinshelwood, 1933; Moore, 1962; Steinfeld *et al.*, 1999). The main points of this theory are summarized below.

According to Hinshelwood (1933), the activation energy of a unimolecular reaction can be considerably larger than predicted by the Arrhenius theory. The reason for this is that in the simple collision theory on which the Arrhenius analysis is based, it is assumed that the critical energy needed for activation comes only from the two translational degrees of freedom of the colliding particles. However, additional energy is also stored in the internal degrees of freedom of molecules, which include primarily the vibrational modes. According to Hinshelwood, the simple exponential term of Arrhenius equation ( $\exp(-E_{a,B}/RT)$ ) should be replaced by one that takes into account the internal degrees of freedom involved in the activation process. Thus, the reaction rate in the case of unimolecular reactions involving many internal degrees of freedom is, instead of equation 2, given by the following modified equation (Hinshelwood, 1933):

$$k = A_H \cdot e^{-E_{a,H}/RT} \cdot \left[ \frac{1}{\left(\frac{1}{2}n-1\right)!} \left(\frac{E_{a,H}}{RT}\right)^{\frac{1}{2}n-1} + \frac{1}{\left(\frac{1}{2}n-2\right)!} \left(\frac{E_{a,H}}{RT}\right)^{\frac{1}{2}n-2} + \dots + 1 \right], \quad (4)$$

where  $k$  is the molecular rate constant,  $A_H$  is the pre-exponential factor,  $E_{a,H}$  is the activation energy of the thermal reaction called the apparent Hinshelwood activation energy in this thesis,  $R$  is the gas constant,  $T$  is the absolute temperature and  $n$  is the number of “square terms” in which the energy can be acquired. Translational and rotational energy both have one square term per degree of freedom ( $1/2 mv^2$  or  $1/2 I\omega^2$ , respectively) and vibrational energy has one square term for kinetic energy ( $1/2 mv^2$ ) and one square term for potential energy ( $1/2 \kappa x^2$ ).<sup>1</sup> There are  $3N - 6$  vibrations in the molecule, where  $N$  is the number of

---

<sup>1</sup> $m$  = mass,  $v$  = velocity,  $\omega$  = angular velocity,  $I$  = moment of inertia,  $\kappa$  = the spring constant of the oscillator,  $x$  = coordinate

atoms in the molecule. Thus, the upper limit for the square terms of energy coming from the vibrational energy of the atoms can be easily estimated:  $n \leq 2 \times (3N - 6) = 6N - 12$  (cf. Moore, 1962). In equation 4, different notations for the pre-exponential factor and the energy barrier are used than in equation 2 to emphasize that these factors get different values than the corresponding terms in the Arrhenius equation with the same value of  $k$ .

Because  $E_{a,H}$  is large compared to  $RT$  in most chemical reactions, only the first term of the series in equation 4 need to be considered. Thus, equation 4 can be simplified into the following form (see Hinshelwood, 1933, p. 24):

$$k = A_H \cdot \frac{e^{-E_{a,H}/RT} \cdot (E_{a,H}/RT)^{\frac{1}{2}n-1}}{\left(\frac{1}{2}n-1\right)!} \quad (5)$$

The application of the Hinshelwood theory to spontaneous activations is presented in paper V and in the Results and Conclusions sections of this thesis. At this point, it should be noted that equation 5 is a generalized form of the Arrhenius equation: the Arrhenius equation is obtained with  $n = 2$  comprising the translational degrees of freedom of the two colliding particles. The importance of equation 5, however, lies in the fact that the same empirical data of the temperature dependence of the rate of spontaneous activations can be used to derive a considerably higher activation energy in the case of the Hinshelwood model than in the case of the Arrhenius theory. By taking the logarithm of equations 2 and 5 and differentiating with respect to temperature, the difference between the apparent Hinshelwood activation energy ( $E_{a,H}$ ) and the apparent Arrhenius activation energy ( $E_{a,B}$ ) can be obtained (St. George, 1952; V):

$$E_{a,H} - E_{a,B} = (n/2 - 1) \cdot RT \quad , \text{with } n > 2. \quad (6)$$

Thus, the Hinshelwood theory offers a natural and *a priori* plausible way to test the hypothesis proposed in paper V, whether the temperature dependence of spontaneous activations could be explained with the same or closely related energetics, which is found for the photoactivation reaction. This would be possible, if the number of square terms taking part in thermal-isomerization reactions ( $n$ ) is large enough to explain the discrepancy between the apparent Arrhenius energy estimates ( $E_{a,B}$ ) and the photoactivation energy estimates ( $E_a$ ) of visual pigments.

### *Models for molecular mechanisms of spontaneous activations*

The molecular mechanism of spontaneous activations is not understood. This is especially due to the serious discrepancy between the thermodynamic parameters of photoactivation and those deduced from the apparent activation energy for spontaneous activations of rhodopsin. The apparent Arrhenius activation energy (20–25 kcal/mol) (Baylor *et al.*, 1980; Matthews, 1984; Sampath & Baylor, 2002) is lower even than the enthalpy difference between bathorhodopsin and the ground state of rhodopsin (35 kcal/mol) (Cooper, 1979) and the difference compared with the photoactivation energy estimates ( $E_a$ ) is of course much larger (see Fig. 3). The photoactivation energy estimates are typically in the range (40–50 kcal/mol) (Lythgoe & Quilliam, 1938; St. George, 1952; Srebro, 1966; Cooper, 1979; Barlow *et al.*, 1993; Mathies, 1999; Birge & Vought, 2000; I–IV). Thus, it has been proposed that thermal activation and the photon-driven process follow different molecular routes. In the following, I shall discuss the requirements for a good model for thermal activations and present some models put forward in the literature.

There are two experimentally observed relations that should be explained by any good physical model for spontaneous activations:

- 1) The model should explain the temperature dependence of the rate of spontaneous activations as well as its absolute value. As discussed earlier in this section, the rate of spontaneous activations depends strongly on temperature. Any serious physical model for spontaneous activations should explain this temperature dependence.
- 2) The model should also explain the experimentally observed correlation between  $\lambda_{\max}$  and the absolute rate of spontaneous events. It is observed that shifts of  $\lambda_{\max}$  towards longer wavelengths are, on average, associated with increased rates of spontaneous events both in rods and in cones (Donner *et al.*, 1990; Firsov & Govardovskii, 1990; Rieke & Baylor, 2000; V). It is reasonable to assume that this correlation says something important about the molecular mechanism underlying the spontaneous events. Since the rate of spontaneous activations sets an absolute limit to the sensitivity in dim light as discussed in section 2.2.3, it can be expected that evolution should have minimized the rate of spontaneous activations to some limit set by the physical border conditions governing the generation of these events. A good model for thermal isomerizations should elucidate these physical border conditions.

Before this thesis two kinds of models had been proposed to account for the molecular mechanism of spontaneous activations:

**Model I: Single-barrier model.** Horace Barlow (1957), in an attempt to account for the ubiquitous but paradoxical “Purkinje shift” in spectral sensitivity (see below), proposed the first model for thermal activation mechanism. The physical basis of his model was Stiles’ (1948) idea that the photoactivation of the visual pigment requires a certain minimum energy, which need not be totally delivered by a photon but may be supplemented by heat (vibrational modes of the molecule). Barlow made two simplifying assumptions. Firstly, he assumed that a photon whose wavelength corresponds to the peak sensitivity of the absorbance spectrum ( $\lambda_{\max}$ ) provides exactly the minimum energy needed for visual pigment activation ( $E_a = hc/\lambda_{\max}$ ). Secondly, his model assumed the same energy barrier for both thermal and photon-triggered activations of visual pigments. Barlow used the Boltzmann distribution (see equation 2) to predict the rate of thermal isomerizations based on the above assumptions ( $k \propto \exp(-hc/kT\lambda_{\max})$ ). Thus, his model predicted a strict physical coupling between the three important quantities of a visual pigment molecule: the wavelength of maximum absorbance ( $\lambda_{\max}$ ), the rate of thermal isomerizations ( $k$ ) and the minimum energy needed for photoactivation of the visual pigment molecule ( $E_a$ ). According to the model, shifting  $\lambda_{\max}$  towards longer wavelengths would inevitably increase the rate of spontaneous activations as shown by the above expression for  $k$ . This original model proposed by Horace Barlow is referred to as the HB hypothesis in this thesis.

At this point it should be noted that for Barlow’s purpose it would be sufficient to assume only that photoactivation energy is inversely proportional to the wavelength of peak absorbance ( $E_a \propto 1/\lambda_{\max}$ ). This general form will be referred as Stiles-Lewis-Barlow (SLB) hypothesis in this thesis to distinguish it from the HB hypothesis (see paper IV). There are two main differences between the definitions of the HB and the SLB hypothesis as defined here: Firstly, in the SLB hypothesis photoactivation energy ( $E_a$ ) is assumed to be a constant fraction of the value predicted by the original HB hypothesis ( $E_a = A \times hc/\lambda_{\max}$ ). Secondly, the SLB hypothesis is used to refer only to the coupling between photoactivation energy and the wavelength of peak absorbance ( $\lambda_{\max}$ ). Contrary to the HB hypothesis, no assumption is made about the barrier for thermal activation. Although these definitions are not widely used in literature, they are utilized in this thesis technically to clarify the different levels of coupling assumed between the physical properties of visual pigments in different models.

The original HB hypothesis (Barlow, 1957) is a single-barrier model, which fulfills qualitatively requirement 2 of the list above: it predicts the correlation between  $\lambda_{\max}$  and the rate of spontaneous events ( $k$ ). Although there was no direct experimental evidence of the thermal isomerizations of visual pigments, Barlow explained Purkinje shift with the aid of his model. Purkinje shift known in humans and many other species is the phenomenon, where the spectral sensitivity of vision is shifted towards the blue end of the spectrum at low levels of illumination (Hecht & Williams, 1922; Wald, 1945; Hough & Ruddock, 1969). In humans this happens as the cone-driven photopic vision is shifted in dim light to rod-driven scotopic vision. Because the spectral irradiance of moonlight is shifted towards longer wavelengths compared to sunlight, the Purkinje shift seems to go to a wrong direction. Barlow cleverly pointed out that Purkinje shift could be explained if shifting the  $\lambda_{\max}$  of the visual pigment towards longer wavelengths increases thermal noise.

Later, as the apparent Arrhenius activation energy ( $E_{a,B}$ ) was deduced from the temperature dependence of the rate of spontaneous events, the discrepancy between  $E_{a,B}$  and the photoactivation energy estimates ( $E_a$ ) seemed to ruin the HB hypothesis and all analogous single-barrier models. Clearly, requirement 1 was contradicted. In addition, as shown in paper V, the empirical correlation between  $\log k$  and  $1/\lambda_{\max}$  is much shallower than predicted by the HB hypothesis. However, until the model presented in paper V, it has been the only physical hypothesis to predict at least qualitatively the correlation between the position of the peak of the absorbance spectrum ( $\lambda_{\max}$ ) and the frequency of spontaneous events ( $k$ ).

**Model II: Different molecular routes for thermal and photic activation.** The discrepancy between the apparent Arrhenius activation energy ( $E_{a,B}$ ) and the photoactivation energy ( $E_a$ ) can be explained by assuming that thermal activations follow a different molecular route with a low-energy barrier. Barlow *et al.* (1993) and Birge & Barlow (1995) proposed a model based on the idea that the thermal and the photic activation of visual pigments follow different molecular routes. They argued that spontaneous events could arise from a small subpopulation of rhodopsin with a deprotonated Schiff base linkage between the chromophore and lysine 296 in the protein. This will be referred to as the Birge-Barlow (BB) hypothesis in this thesis (cf. Burns & Baylor, 2001). The BB hypothesis is based on molecular modeling as well as on observations of thermal isomerization rates of *Limulus* photoreceptors. This work (Barlow *et al.*, 1993; Birge & Barlow, 1995) predicts for the deprotonation-isomerization reaction an activation energy that is consistent with the apparent Arrhenius activation energies found for thermal isomerizations (Baylor *et al.*, 1980; Barlow *et al.*, 1993). On the other

hand, the BB hypothesis predicts that the rate of thermal isomerizations should depend strongly on pH. Intracellular alkalization should increase the proportion of molecules with deprotonated Schiff base, and hence the rate of thermal isomerizations. Consistent with their hypothesis, Barlow *et al.* (1993) observed in *Limulus* photoreceptors that a pH change caused a change in the rate of thermal events in the predicted direction.

However, later studies on vertebrate photoreceptors have shown that pH does not affect the rate of thermal isomerizations either in rods (Firsov *et al.*, 2002) or in cones (Sampath & Baylor, 2002). Furthermore, the pH dependence observed on *Limulus* photoreceptors by Barlow *et al.* (1993) was much stronger than predicted by the BB hypothesis (Barlow *et al.*, 1993; Birge & Barlow, 1995). It follows from the BB hypothesis that changes in the external and in the internal pH should affect the noise level in the same direction. Thus, the observation that external and internal pH changes affect the noise level in opposite directions in *Limulus* (Corson & Fein, 1980) is also contradictory to the BB hypothesis. In the light of these experimental observations, it appears that this model is inadequate to explain the mechanism of thermal events (for review see Burns & Baylor, 2001).

In general, models assuming different activation energies for thermally induced and photon-induced isomerizations are tempting, because the ground-state potential energy surface of rhodopsin could potentially offer a huge number of different molecular routes. It is possible to assume that the ground-state surface is like a maze, where one or several unlikely or restricted routes can lead through low-energy barriers to the active state of rhodopsin (Kakitani, 1999). The discrepancy between the thermal activation energy estimates and the photoactivation energy estimates could be explained by the existence of these low-energy routes. The rareness of spontaneous events would be explained by the difficulty to find the right complex route through the whole maze. However, an exact hypothesis of the route and the modeled shape of the potential energy surface along the route would be required for a serious hypothesis belonging to this model family. Moreover, if no coupling between photoactivation energy and thermal barrier exists, there is no evident reason, why thermal noise should correlate with  $\lambda_{\max}$ . Thus, the requirement 2 in the list above seems *a priori* difficult for this model family.

## 2.3 Spectral absorbance and spectral sensitivity of visual pigments

### 2.3.1 General characteristics

#### *Absorbance spectra and spectral sensitivity curves*

The absorbance spectra of visual pigments determine the wavelength range of electromagnetic radiation available for vision. This conclusion was originally drawn based on the close similarity between the absorbance spectrum of rhodopsin in solution and the relative sensitivity of the dark-adapted eye at different wavelengths determined by psychophysical measurements (Hecht & Williams, 1922; Wald, 1945; cf. Stiles, 1948). The similarity between the scotopic spectral sensitivity of the dark-adapted eye and the absorbance spectrum of rhodopsin depends on the constant quantum efficiency of photoactivation over a wide wavelength domain (Darnall, 1968). Thus, the only wavelength-selective mechanism is the absorbance spectrum of the visual pigment, which determines the spectral sensitivity of a photoreceptor containing the pigment. This same reasoning is the basis for the principle of univariance according to which the information about the wavelength of a photon is lost in vision as soon as the photon is absorbed (Naka & Rushton, 1966).

Some differences between the relative scotopic spectral sensitivity and the relative absorbance spectra of rods arise due to following reasons. Firstly, absorption by the other components of the eye attenuates light intensity especially in the short-wavelength region. Secondly, the light has to travel axially through the oriented layers of visual pigments in the waveguide formed by the photoreceptor outer segment. The absorption of photons by the pigment layers attenuates the light intensity as a function of the distance travelled. The latter effect, called “self-screening”, tends to flatten the absorbance spectrum. If these differences are taken into account, both the spectral absorbance ( $A$ ) of visual pigments and the spectral sensitivity ( $S$ ) of photoreceptors or the whole visual system can be used for studying the photoexcitation of visual pigments (cf. Cornwall *et al.*, 1984).

The absorbance ( $A$ ) of visual pigments can be measured spectrophotometrically from extracted visual pigments in solution. Since the advent of microspectrophotometry, absorbance measurements have been performed also on intact isolated photoreceptors (Hanaoka & Fujimoto, 1957; Brown, 1961; Liebman & Entine, 1964; Marks *et al.*, 1964; Brown & Wald, 1964; Hárosi & MacNichol, 1974; MacNichol, 1978; for reviews see Liebman, 1972; Bowmaker, 1984; Cornwall *et al.*, 1984). On the other hand, the spectral sensitivity ( $S$ ) of

photoreceptors or the whole visual system can be measured either by electrophysiological methods or by psychophysical methods. Spectral sensitivity measurements are based on determining the intensity that generates a criterion signal of constant size (“threshold”) at each wavelength. The methods used in this thesis, absorbance measurements by microspectrophotometry in intact photoreceptors and electrophysiological spectral sensitivity measurements by the electroretinogram technique, are presented in the methods section (Chapter 4). The exact mathematical formulation of the common definitions of absorbance ( $A$ ) and spectral sensitivity ( $S$ ) are also found in the methods section.

#### *The main bands of the absorbance spectra of visual pigments*

Fig. 6 shows the general shape of a typical absorbance spectrum of rhodopsin. The absorbance spectrum has several peaks called the  $\alpha$ -band, the  $\beta$ -band, the  $\gamma$ -band etc. The  $\alpha$ -band and the  $\beta$ -band correspond to the absorption of light by the opsin-bound chromophore. Other bands, located at shorter wavelengths, correspond to light absorption by the protein part. Thus, only the  $\alpha$ - and  $\beta$ -bands contribute directly to visual excitation. The primary interest lies on the  $\alpha$ -band, which arises from the electronic excitation of the opsin-bound chromophore from the ground state ( $S_0$ ) the first electronically excited state ( $S_1$ ) (Jurkowitz, 1959; Loeb *et al.*, 1959; Wald, 1959). The weaker  $\beta$ -band is not as well studied as the  $\alpha$ -band, mostly because of technical problems arising from its lower amplitude and location in the UV region (e.g. light scattering problems).

#### *Spectral tuning of visual pigments*

The wavelength of maximum absorption ( $\lambda_{\max}$ ) of the  $\alpha$ -band of visual pigment spectra varies between *ca.* 360 nm–630 nm (Shichida & Imai, 1998). The wide range of  $\lambda_{\max}$  values indicates that the position of visual pigment spectra can be rather freely shifted on the wavelength scale to match the varying photic environments present on earth. This process is called spectral tuning. There are three main mechanisms of spectral tuning of visual pigments: 1) changing the amino acid composition of the opsin, 2) changing the chromophore and 3) affecting the spectral properties of the chromophore by a specific chloride binding site in the opsin. Each of these mechanisms is shortly reviewed below.

In mechanism #1, the absorption maximum ( $\lambda_{\max}$ ) of the opsin-bound chromophore is regulated by its interaction with the nearby amino acid residues of opsin in the chromophore-binding pocket. These interactions can shift the absorbance spectrum of the 11-*cis*-retinal protonated Schiff base (PSB) either towards shorter wavelengths (hypsochromic shift) or towards longer wavelengths

(bathochromic shift) from the position of the absorbance spectrum of PSB in organic solution (440 nm) (Kito *et al.*, 1968). In general, any shift of the PSB's spectrum from the reference value in solution by opsin-induced interactions is called an "opsin shift" (Motto *et al.*, 1980). In addition to mechanism #1, mechanism #3 can also be used for the opsin shift. Mechanism #1 offers, however, the latitude of the tunable range of wavelengths and is the main tuning mechanism in visual pigment evolution. Point mutations in the amino acid sequence of opsin offer the organisms a possibility to adapt the spectral sensitivities of their visual pigments to different photic environments by natural selection on an evolutionary time scale.

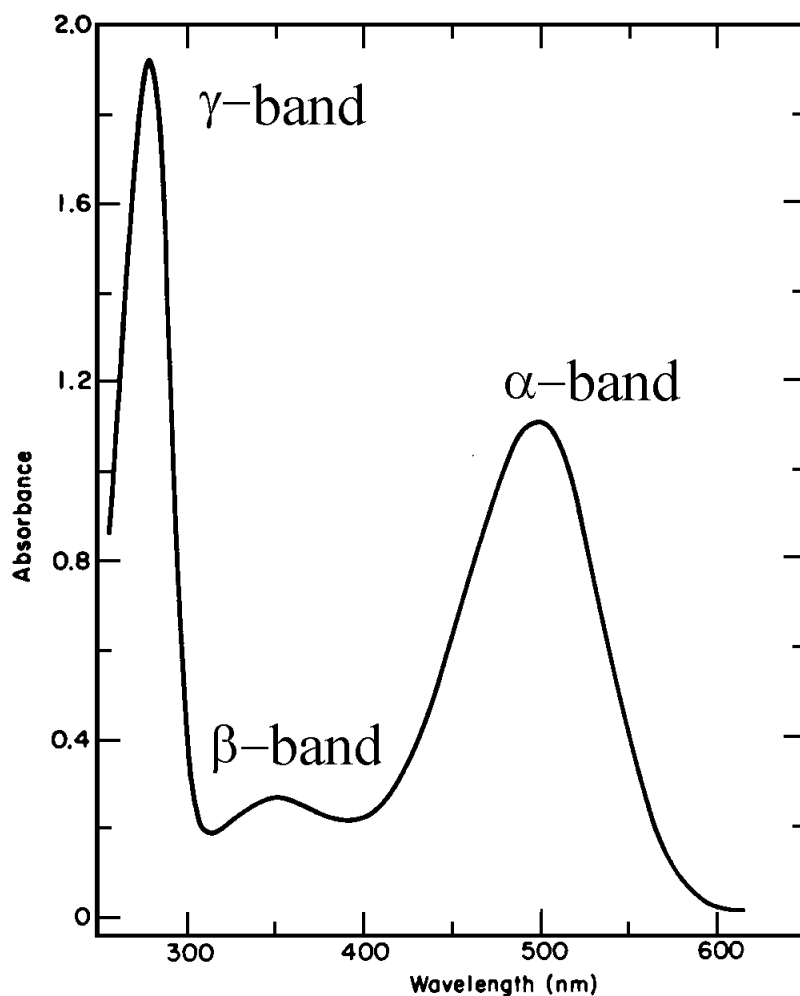


**Fig. 6.** The absorption spectrum of purified extracted bovine rhodopsin in solution. Reprinted with minor modifications from Hong *et al.* (1982), Copyright (1982), with permission from Elsevier.

There is no complete physical theory to explain the opsin shift based on the tertiary structure of opsin. On the other hand, studies with site-directed mutagenesis (Sakmar *et al.*, 1989; Zhukovsky & Oprian, 1989; Nathans, 1990a; Nathans, 1990b; Han *et al.*, 1996a; Han *et al.*, 1996b; Lin & Sakmar, 1996) have shed light on mechanism #1 by revealing many important amino acid residues affecting the absorption properties of opsin-bound chromophore (for review see Sakmar *et al.*, 2002). The key residue is the retinal counterion, glutamate 113 on helix III, which alone explains most of the bathochromic opsin shift from 440 nm to the  $\lambda_{\max}$  value of a typical rod visual pigment at around 500 nm (Sakmar *et al.*, 1989; Zhukovsky & Oprian, 1989; Nathans, 1990a). The problem in studies involving site-directed mutagenesis is that the mutant pigments may be very “unnatural”. Evolutionary genetic methods based on comparisons of the amino acid sequences of closely related natural pigments have helped to find many functionally important amino acid changes used in spectral tuning of natural pigments (for review see Yokoyama & Yokoyama, 1996).

Although there is no complete physical model explaining the opsin shift based on the molecular structure, it is generally known that it involves the opsin-induced perturbation of retinal’s  $\pi$ -electrons. The most important mediators of this perturbation are the dipolar amino acid residues located near the chromophore (Kochendoerfer *et al.*, 1999; Lin & Sakmar, 1999; Sakmar *et al.*, 2002). This perturbation modulates the chromophore’s ground-state ( $S_0$ ) and excited-state ( $S_1$ ) charge distributions and the energy gap between these states. Thus, mechanism #1 can affect both  $\lambda_{\max}$  and the minimum energy needed for photoactivation ( $E_a$ ). The relation of the opsin effects on  $\lambda_{\max}$  and  $E_a$  is studied in papers I–IV of this thesis.

Mechanism #2 offers a simple way of spectral tuning. In vertebrates, it entails a switch between the two possible chromophores: 11-*cis*-retinal (A1) and 11-*cis*-3,4-dehydroretinal (A2). As discussed in section 2.1.1, the A1  $\rightarrow$  A2 chromophore switch shifts  $\lambda_{\max}$  towards longer wavelengths in general (Dartnall & Lythgoe, 1965; Bridges, 1967). Contrary to mutations in the amino acid sequence of opsin, the chromophore switch allows spectral tuning on a physiological time scale. It is used by many species of fish and amphibians to modulate spectral sensitivity during their lifetime (Dartnall & Lythgoe, 1965; Bridges, 1965, 1972; McFarland & Allen, 1977). For example, the common frog (*Rana temporaria*) utilizes A2 chromophore while living in the “reddish” fresh water environment at its early tadpole stage. During metamorphosis it changes to A1 (Reuter, 1969), which is more efficient in catching photons above the water surface, an important light environment for adult frogs. Mechanism #2 can also be utilized to tune the absorbance spectra of visual pigments in different parts of the retina selectively. For example, the adult bullfrog (*Rana catesbeiana*) has A1 chromophore in the

ventral retina but may have even 81–89 % of A2 chromophore in the most dorsal part of the retina (Reuter *et al.*, 1971). This unusual spatial distribution of chromophores is useful for living at the water surface, where the ventral retina looks into the air and the dorsal retina under the water surface. The relation between the effects on  $\lambda_{\max}$  and  $E_a$  generated by mechanism #2 are studied in papers I, III and IV.

Mechanism #3 involves the binding of a chloride ion to a specific high-affinity chloride-binding site on the opsin. The effect of the chloride ions on spectral sensitivity was first found in the long-wavelength-sensitive pigment ( $\lambda_{\max} = 521$  nm) of the Tokay gecko (*Gekko gekko*) (Crescitelli, 1977) and in the long-wavelength-sensitive cone pigment of the chicken (Knowles, 1976, 1980; Fager & Fager, 1979). Since these first observations, the chloride binding site has been found in the opsins of most members of M/LWS (mid- and long-wavelength-sensitive) pigment family (Novitskii *et al.*, 1989; Kleinschmidt & Harosi, 1992) including also human mid (M) and long-wavelength-sensitive (L) cone pigments (Wang *et al.*, 1993). The binding of chloride ion shifts  $\lambda_{\max}$  towards longer wavelengths and may have been a critical innovation in evolution to produce long-wavelength-sensitive cone pigments. Chloride binding site has not been found in other pigment families than M/LWS (Wang *et al.*, 1993). So far all known A1 based visual pigments with  $\lambda_{\max}$  greater than 510 nm use chloride-binding for spectral tuning (Ebrey & Koutalos, 2001). Theoretically, mechanism #3 could allow active tuning of spectral sensitivity by binding or releasing chloride ions in its binding site on a physiological time scale. However, no evidence for this has been found. Furthermore, an electrophysiological study of LWS cones of goldfish (Zak *et al.*, 2001) suggests that these cones lose their phototransduction capacity in the absence of chloride ions.

### *Visual pigment templates*

Dartnall (1953) discovered that the normalized  $\alpha$ -bands of different visual pigments can be described by a common template when plotted on a frequency scale ( $A$  vs.  $1/\lambda$ ). Later, it was demonstrated that a broader template should be used for A2 visual pigments (Bridges, 1967; Munz & Schwanzara, 1967). Ebrey & Honig (1977) studied A1-based visual pigments with a wider range of  $\lambda_{\max}$  values than Dartnall. They showed that, contrary to Dartnall's original result, the shape of the  $\alpha$ -band gets systematically narrower on a frequency scale as  $\lambda_{\max}$  shifts towards longer wavelengths. Many refined templates have been proposed for visual pigments (Metzler & Harris, 1978; Dawis, 1981; Barlow, 1982; Mansfield, 1985; MacNichol, Jr., 1986; Maximov, 1988; Partridge & DeGrip, 1991; Stavenga *et al.*, 1993; Lamb, 1995; Palacios *et al.*, 1996). Mansfield (1985)

and MacNichol (1986) showed that shape-invariance holds to a high degree of accuracy when spectra are plotted on a  $\lambda_{\max}/\lambda$  scale. The most recent and comprehensive formulation is the one by Govardovskii *et al.* (2000). They used Lamb's (1995) template for the  $\alpha$ -band of visual pigments as a basis and derived separate parameter sets for A1- and A2-based visual pigments templates. They showed that the shape of the  $\alpha$ -band of all vertebrate visual pigments with  $\lambda_{\max} > 350$  nm can be described by either of these templates with  $\lambda_{\max}$  as the only variable.

Generalized templates are useful for predicting the absorbance spectra of pigments for which the  $\lambda_{\max}$  values are known. They can also be used for estimating the proportions of different visual pigments in mixtures of pigments with known  $\lambda_{\max}$ . Similarly, the proportion of A1 and A2 pigments can be estimated as absorbance spectra are recorded from a photoreceptor containing a mixture of A1- and A2-based pigments with the same opsin. However, visual pigment templates have no strict physical interpretation. They are empirical descriptions, which rely on curve fitting to the measured spectra.

### 2.3.2 Physical interpretation of visual pigment spectra

#### *The physical formulation of the theory*

Despite the wide knowledge of the structure and the mechanisms of spectral tuning of visual pigments, no comprehensive physical theory exists for predicting their absorbance spectra. Only for the long-wavelength part of the spectrum a physical theory has been available since the 1940's (Stiles, 1948; Lewis, 1955). The theory predicts the shape and the temperature dependence of the long-wavelength region of visual pigment spectra. In addition, this physical model allows the estimation of the minimum energy needed for photoactivation of the visual pigment ( $E_a$ ) (Stiles, 1948; Lewis, 1955; Srebro, 1966; I–IV).

The general ideas of Stiles' theory are illustrated in Fig. 7 (reproduced with minor modifications from paper IV). The top panels A–C show the situation at a low temperature and the middle panels at a higher temperature. As shown in the uppermost pair of panels A and B, a certain minimum energy ( $E_a$ ) is assumed to be needed for the photoactivation of a visual pigment molecule. In addition, Stiles (1948) proposed that  $E_a$  need not be wholly derived from the photon energy but may be supplemented by heat (the appropriate vibrational modes of the visual pigment molecule). Thus, photons with energy less than the minimum energy needed for photoactivation ( $hc/\lambda < E_a$ ) can activate only those visual pigment

molecules that possess sufficient supplementary energy in their internal vibrational modes ( $E_{\text{thermal}} > E_a - hc/\lambda$ ). Furthermore, Stiles assumed that visual pigments are in thermal equilibrium and distributed among different vibrational energy levels according to the Boltzmann distribution (see the two uppermost pair of panels B in Fig. 7). Thus, the number of molecules at each individual energy level ( $E_i$ ) should be proportional to the factor  $\exp(-E_i/kT)$ . As shown in the two uppermost pair of panels C, these assumptions lead to the qualitative notion that the absorbance spectrum of rhodopsin declines in the long-wavelength region ( $\lambda > hc/E_a$ ) in proportion to the visual pigment molecules with sufficient vibrational energy. This qualitative idea is in agreement with experimental data (Denton & Pirenne, 1954; Lewis, 1955; Srebro, 1966; Baylor *et al.*, 1984, 1987; Lamb, 1995, I–IV), which indeed show the predicted type of decline of absorbance spectra in the long-wavelength region (see Fig. 7, panel C). If only the photon energy could contribute to visual pigment activation, the absorbance spectrum should, contrary to experimental data, at all temperatures drop precipitously to zero at the wavelength corresponding to the minimum energy needed for photoactivation ( $\lambda = hc/E_a$ ). In Stiles' model, this will occur only at absolute zero, where all visual pigment molecules are at the ground state (see panels at the bottom of Fig. 7).

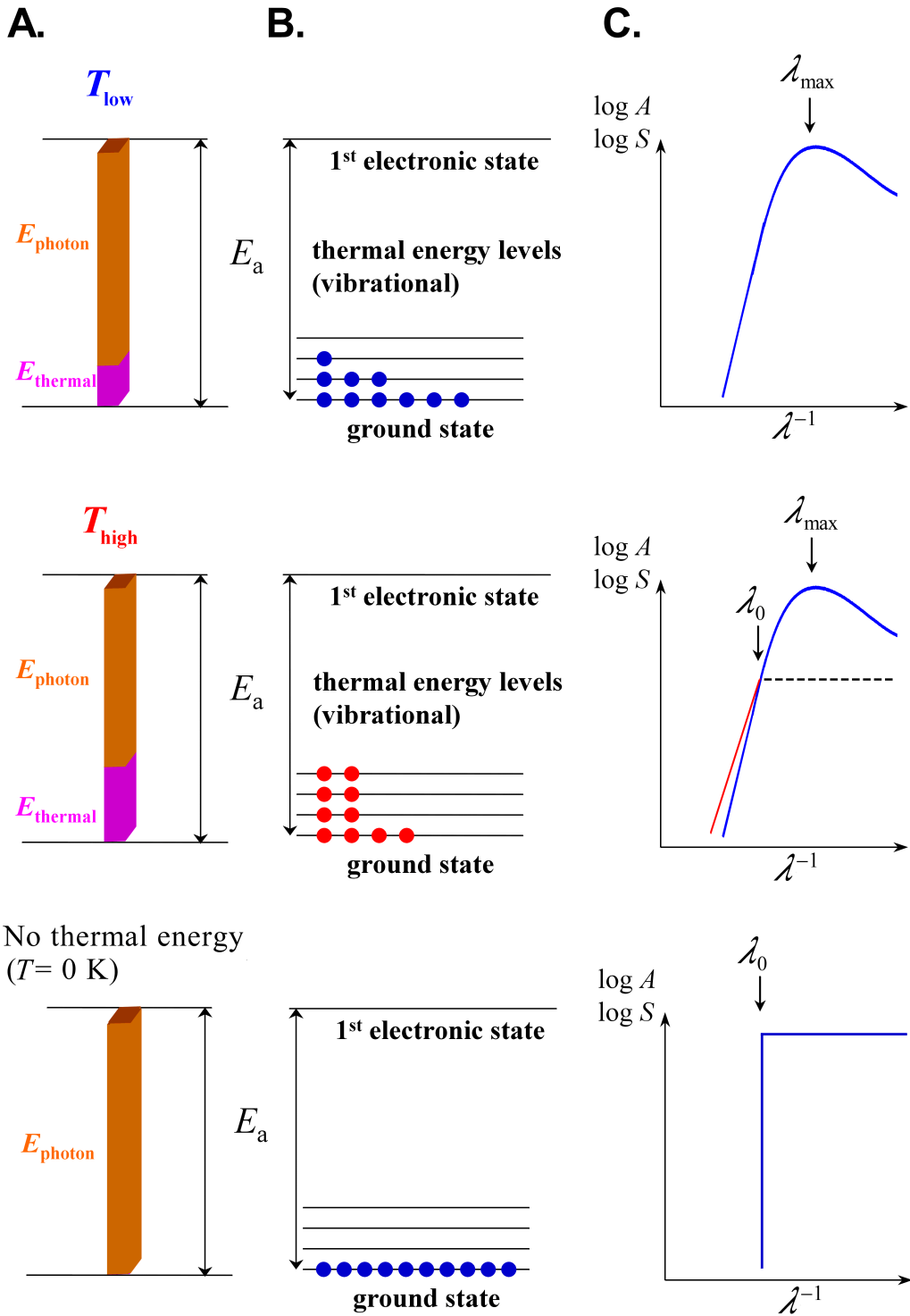


**Fig. 7. (facing page)** Illustration of Stiles' (1948) theory of temperature effects on visual pigment spectra (modified from Fig. 1 in paper IV). The top row of panels represent a low temperature ( $T_{\text{low}}$ ), the middle row a higher temperature ( $T_{\text{high}}$ ) and the bottom row the absolute zero ( $T = 0$  K), where no thermal (vibrational) energy is available. **(A)** Photons with energy less than the minimum energy required for photoactivation ( $E_a$ ) can activate only those pigment molecules that possess sufficient amount of thermal (vibrational) energy ( $E_{\text{thermal}}$ ). **(B)** The distribution of rhodopsin molecules on vibrational levels depends on temperature: higher energy levels become more populated at higher temperature. Stiles (1948) assumed that different energy levels are populated according to the Boltzmann distribution. Lewis (1955) pointed out that for a complex molecule like rhodopsin a distribution derived by Hinshelwood (1933) has to be used. Both models predict that the decline of log visual sensitivity vs. frequency ( $1/\lambda$ ) will follow a straight line in the long-wavelength domain. **(C)** Logarithmic absorbance ( $A$ ) or sensitivity ( $S$ ) plotted vs.  $1/\lambda$ . The slope of the final limb of the spectrum becomes shallower at higher temperatures because of the increased proportion of molecules at higher vibrational levels. The temperature effect starts at  $\lambda_0$  where photon energy equals the minimum energy required for photoactivation ( $E_{\text{photon}} = E_a = hc/\lambda_0$ ). The model is too simple to explain the shape of the visual pigment spectra in the short-wavelength region: The model predicts constant spectral sensitivity or absorbance (dashed line) in the short-wavelength region ( $\lambda < \lambda_0$ ) where photon energy is larger than  $E_a$ .

In order to deduce a quantitative, mathematical model for the long-wavelength tail, Stiles (1948) made the following further assumptions:

- 1) The average absorption coefficient of a chromophore ( $\bar{\alpha}(\lambda)$ ) is at each wavelength ( $\lambda$ ) proportional to the cumulative distribution of pigment molecules on thermal energy levels ( $E_i$ ) greater than  $E_a - hc/\lambda$ . Denoting this cumulative distribution by  $F$ , the above assumption gets the following mathematical form:

$$\bar{\alpha}(\lambda) = A \cdot F, \quad (7)$$

where  $A$  is a constant and

$$F = \sum_{i=j}^{\infty} e^{-E_i/kT}, \quad (8)$$

where  $j$  is the lowest energy level for which  $hc/\lambda > E_a - E_i$ .

- 2) In order to replace equation 7 by an integral, Stiles assumed that there is a great number of vibrational energy levels, which are close to each other.

- 3) In order to integrate the formula obtained by assumption 2, Stiles assumed that the separation between adjacent energy levels ( $\Delta E = E_{i+1} - E_i$ ) is independent of energy  $E_i$ .

Using the above assumptions, Stiles obtained by direct integration the following formulas for the average absorption coefficient of a chromophore ( $\bar{\alpha}(\lambda)$ ):

$$\ln \bar{\alpha}(\lambda) = C + \frac{hc}{kT\lambda}, \quad \text{for } hc/\lambda < E_a, \quad (9)$$

$$\ln \bar{\alpha}(\lambda) = C + \frac{E_a}{kT}, \quad \text{for } hc/\lambda \geq E_a,$$

where  $C$  is a constant.

Because the absorbance ( $A$ ) and the spectral sensitivity ( $S$ ) of pure rhodopsin are directly proportional to the absorbance coefficient of the chromophore group  $\bar{\alpha}(\lambda)$ , Stiles' formula can be used to predict the relative shape of both absorbance and sensitivity spectra. The top and middle panels C in Fig. 7 are generalized representations illustrating spectral sensitivity curves at different temperatures as predicted by Stiles' model and plotted on logarithmic ordinates against wavenumber ( $1/\lambda$ ).

The primary results predicted by Stiles' model can be summarized as follows:

- 1) In the long-wavelength region ( $\lambda > hc/E_a$ ), spectral sensitivity or absorbance declines following a straight line with a constant slope ( $K = \partial \text{Log } S / \partial(1/\lambda) = hc \log e/kT$ ), when plotted on logarithmic ordinates ( $\log S$  or  $\log A$ ) against wavenumber ( $1/\lambda$ ).
- 2) The slope ( $K$ ) depends on temperature and becomes shallower at higher temperatures as the higher vibrational levels of the molecule get more densely populated (see panel B in Fig. 7):  $\partial K / \partial(1/T) = hc \log e/k$ . The ratio of the slopes in the long-wavelength domain at two different temperatures (denoted "warm" and "cold") is inversely proportional to the respective temperatures:  $K_{\text{warm}}/K_{\text{cold}} = T_{\text{cold}}/T_{\text{warm}}$ .
- 3) The theory allows the estimation of the minimum energy needed for photoactivation of a visual pigment molecule ( $E_a$ ). According to the theory,  $E_a$  corresponds to the wavelength ( $\lambda_0$ ), where photon energy is just equal to the minimum energy needed for photoactivation ( $E_a = hc/\lambda_0$ ). At

longer wavelengths ( $\lambda > \lambda_0$ ), temperature should affect spectral sensitivity. Thus, the long-wavelength tails of spectra measured at different temperatures should cross at  $\lambda_0$  (see the middle panel C in Fig 7).

The precision of the above predictions will be discussed under separate subheadings. The most valuable predictions for the purposes of the present thesis are #2 and #3, which allow the estimation of the minimum energy needed for photoactivation ( $E_a$ ).

*Prediction #1: the shape of the visual pigment spectrum*

Prediction #1 is qualitatively accurate. The final limb of all experimentally determined visual pigment spectra follow approximately a straight line as plotted on log sensitivity vs. frequency scale. Quantitatively, the final slopes of experimentally determined visual pigment spectra are somewhat shallower than predicted (70–90% of that predicted by Stiles' theory) (Stiles, 1948; Lewis, 1955; Lamb, 1995; see also Table 3 in the Results section). Thus, Stiles' simple model with its constant slope cannot predict accurately the absolute value of the final slope of different visual pigments. This is evident, as the final slope is known to depend on  $\lambda_{\max}$  so that short-wavelength-sensitive pigments have shallower final slopes than long-wavelength-sensitive pigments (Ebrey & Honig, 1977). Thus, at least one extra parameter depending on  $\lambda_{\max}$  is needed for a physical model explaining accurately the final slope of different visual pigments.

Lewis (1955) refined Stiles' theory by proposing that for a complex molecule with several degrees of freedom the distribution proposed by Hinshelwood (1933) should be used instead of the Boltzmann distribution (cf. section 2.2.3 on how the Arrhenius rate constant for chemical reactions differs from that predicted for thermal unimolecular reactions with many degrees of freedom). The fraction of molecules with energy greater than  $E_i$  is then given by:

$$F = e^{-E_i/kT} \cdot \left\{ \frac{(E_i/kT)^m}{m!} + \frac{(E_i/kT)^{m-1}}{(m-1)!} + \dots + 1 \right\}, \quad (10)$$

where (according to the notation of Lewis) the number of vibrational modes is  $m + 1$ .

To apply equation 10 to spectral sensitivities, Lewis replaced  $E_i$  in equation 10 by the difference between photoactivation energy and photon energy ( $E_i = hc/\lambda_0 - hc/\lambda$ ). Furthermore, he related  $F$  directly to spectral sensitivity at the

corresponding wavelength ( $F = \text{constant} \times S$ ). Lewis also pointed out that the series in equation 10 can be approximated by its first term in the long-wavelength domain, where  $hc/\lambda_0 - hc/\lambda > mkT$ . Using this approximation, equation 10 can be replaced by the following equation in the long-wavelength domain:

$$F = e^{-E_i/kT} \cdot \frac{(E_i/kT)^m}{m!}. \quad (11)$$

Equations 10 and 11 take into account the degrees of freedom of a complex molecule in photoactivation just as equations 4 and 5 described in section 2.2.3 do for the case of thermal activation. Both equations 10 and 11 and the exponential terms of equations 4 and 5 ( $k/A_H$ ) represent the fraction of molecules with energy higher than a certain limit deduced from the Hinshelwood distribution. The difference between these two expressions lies only in the notation used. In equations 4 and 5, the energy limit is denoted by  $E_{a,H}$  as in equations 10 and 11 by  $E_i$ . By denoting  $E_{a,H} = E_i$ ,  $m = 1/2 n - 1$  and taking into account that equations 4 and 5 were deduced for the molar activation energy (R is used instead of k), equations 10 and 11 and the exponential terms of equations 4 and 5, respectively, become identical.

The refinement by Lewis (1955) to Stiles' (1948) model leads to the following prediction for the long-wavelength slope of the absorbance spectrum:

$$K = \frac{\partial \log S}{\partial(1/\lambda)} = \frac{hc \cdot \log e}{kT} - \frac{m \cdot \log e}{\frac{1}{\lambda_0} - \frac{1}{\lambda}}, \quad (12)$$

The effect of the term  $m$  is to make the slope shallower in the vicinity of  $\lambda_0$  and monotonically steeper towards longer wavelengths. At long wavelengths, Lewis's formula for the slope approaches Stiles' prediction ( $hc \log e/kT$ ), the limiting value for the final slope being ( $hc \log e/kT - \lambda_0 m \log e$ ). With small values of  $m$  Lewis' prediction deviates only slightly from Stiles' prediction at the long-wavelength limit. For example, with  $m = 6$ ,  $T = 298$  K and  $\lambda_0 = 586$  nm, Lewis's formula gives a 7% shallower slope than Stiles' formula as a limiting value in the long-wavelength domain (for predictions on the temperature effects in the same case, cf. Fig. 8). Both Lewis' and Stiles' formulas predict a straight line at the long-wavelength limit of the spectrum plotted on  $\log S$  vs.  $1/\lambda$  scale.

The advantage of Lewis' formula is that it allows exact prediction of the shape of the spectral sensitivity curve from long wavelengths down to  $\lambda_0$ . On the other

hand, Lewis' formula contains an extra parameter ( $m$ ) compared to Stiles' simple formula. Thus, the unambiguous estimation of both parameters  $\lambda_0$  (or  $E_a$ ) and  $m$  is a challenging task. An estimate for  $m$  that is independent of the other parameter  $E_a$  can, however, be obtained from the final slope of the  $\log S$  vs.  $1/\lambda_0$  curve (see equation 12). Lewis found a good agreement with experimental data (human scotopic spectral sensitivity) for  $m = 6$ .

It should be noted that both Stiles' original prediction #1 about the shape of the spectrum and the refined theory by Lewis are valid only in the long-wavelength region of the visual pigment spectra, where  $\lambda \geq \lambda_0$ . The constant value predicted by equation 9 for absorbance or spectral sensitivity in the short-wavelength region (dashed lines in panel C in Fig. 7) disagrees with the shape of the experimentally observed visual pigment spectra. Specifically, Stiles' and Lewis' theories do not give any physical interpretation for the peak sensitivity ( $\lambda_{\max}$ ) of visual pigment spectra.

*Prediction #2: Temperature dependence of the long-wavelength slope*

Stiles' model predicts quite accurately the temperature dependence of the long-wavelength slope. The predicted temperature effect in the long-wavelength domain has been detected by psychophysical (de Vries, 1948) and electrophysiological measurements of visual pigment spectra (Denton & Pirenne, 1954; Srebro, 1966; Lamb, 1984; I-III). In addition, studies on pigment extracts have shown that the bleaching rate is temperature-dependent in the long-wavelength domain ( $\lambda > \lambda_0$ ), increasing at higher temperatures as predicted by Stiles' model (St. George, 1952). Both Stiles' original model and Lewis' modification predict the same temperature dependence of the long-wavelength slope ( $\partial K/\partial(1/T) = hc \log e/k$ ). Only in the close vicinity of  $\lambda_0$ , Lewis' model predicts a weaker temperature dependence than Stiles' original model. In this region, equation 10 should be used instead of equation 11. The small difference between Stiles' and Lewis' predictions for the temperature dependence of the spectra is readily perceived if the difference between spectra at different temperatures ("warm" and "cold") is plotted for both models (see Fig. 8).

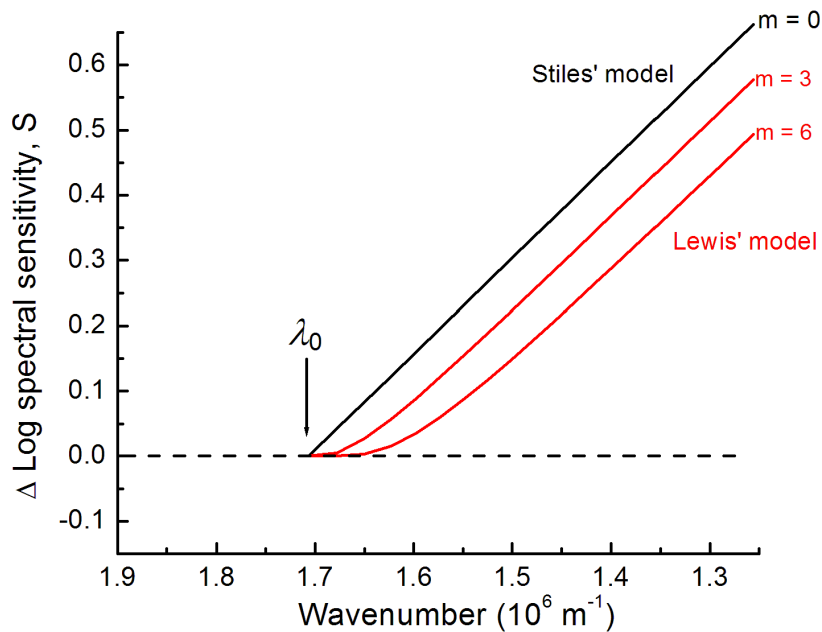


**Fig. 8.** The difference spectra ( $\Delta = \text{Log } S_w - \text{Log } S_c$ ) are plotted for both Stiles' and Lewis' models with the following parameter values:  $\lambda_0 = 586 \text{ nm}$ ,  $m = 6$  (in Lewis' model),  $T_c = 282 \text{ K}$ ,  $T_w = 302 \text{ K}$ .

Temperature effects on pigment spectra have also been studied spectrophotometrically in solutions. These studies include absorbance measurements of solutions containing extracted visual pigments (Yoshizawa, 1972), pure retinal (Jurkowitz, 1959) as well as  $\beta$ -carotene (Loeb *et al.*, 1959; Wald, 1959), which is the precursor of retinal with a closely related molecular structure. Absorbance measurements on extracted visual pigments in solution allow the use of a much wider temperature range than psychophysical and electrophysiological recording techniques. The more precipitous decline of the long-wavelength tail of the spectra at low temperatures observed in these studies is in qualitative agreement with the predictions of Stiles and Lewis. Measurements of absorbance spectra cannot, however, offer accurate information about the final slope in the long-wavelength domain, where the absolute absorbance is very low. Quantitative comparisons between data and the slopes predicted by the theoretical models require physiological or psychophysical sensitivity measurements. Yet, the study of visual pigments in solution over wide temperature ranges offer other kinds of interesting results, which can be interpreted with the aid of basic photochemistry and the simple basic ideas of Stiles' model (cf. Fig. 7).

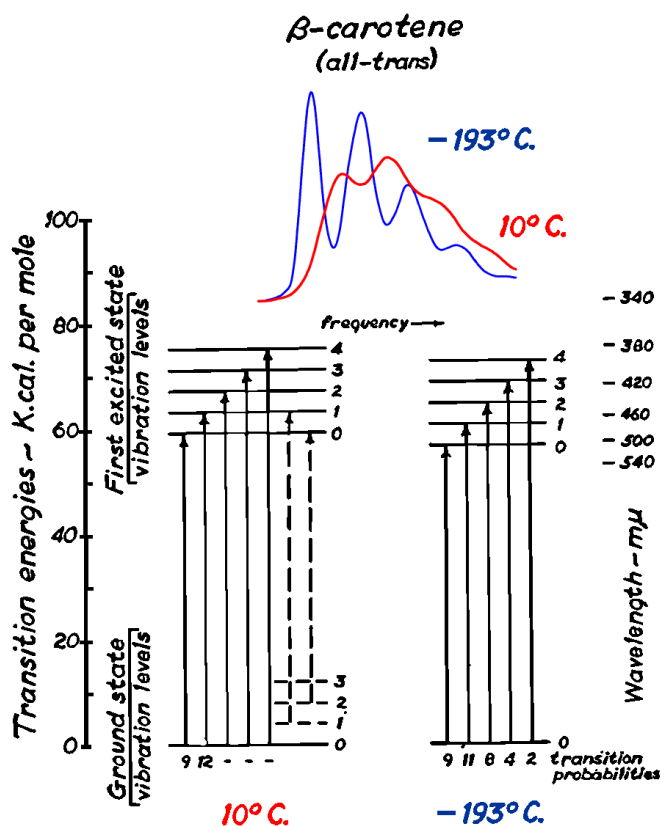


**Fig. 9.** Schematic energy diagrams of all-*trans*  $\beta$ -carotene at 10°C and at -193 °C. Absorbance spectra are shown above the energy diagrams (10°C, red line; -193 °C, blue line). The distinct peaks in the cold spectrum correspond transitions from the 0 vibrational level of the ground state to equally spaced vibrational levels of the 1st electronically excited state. The peaks in the absorbance spectrum become broader and thus more superimposed at the high temperature as a result of transitions from the higher vibrational levels of the ground state (dashed lines). Reprinted by permission from [Nature](#) (Wald, 1959) copyright (1959) Macmillan Publishers Ltd.

Fig. 9 shows the absorbance spectra of  $\beta$ -carotene at -193 °C and +10 °C (Loeb *et al.*, 1959; Wald, 1959) and the energy diagrams constructed for the spectra by Wald (1959). At -193 °C the absorbance spectrum shows five distinct peaks (the fine structure of the spectrum). Most molecules are at the lowest vibrational level of the ground state (level 0) at -193 °C and the peaks correspond to the transitions from the ground-state level 0 to different vibrational levels (0,1,2,3) of the excited state. The 0-0 transition corresponds to the minimum energy needed for photoactivation ( $E_a$ ). The amplitudes of different peaks reflect the transition probabilities. At the higher temperature, the distinct absorbance peaks became wider and smoother as a result of electronic transitions starting from the higher

vibrational levels of the ground state, which become more populated at the higher temperatures. These transitions from the higher vibrational levels of the ground state are illustrated by the vertical dashed lines in Fig. 9. This effect is the one used to predict the long-wavelength tail of the rhodopsin spectrum on the basis of Stiles' model. With the aid of Fig. 9, it is easy to understand that Stiles' and Lewis' models are applicable only at  $\lambda > \lambda_0$ , where the peak corresponding to the transition to the excited-state level 0 dominates. At shorter wavelengths, peaks corresponding to higher energy transitions are superimposed, and more complex physical models would be needed to predict the temperature effects and the shape of the spectrum.

The above results on  $\beta$ -carotenes can be used for understanding the temperature-dependence of the spectrum of the closely related retinal. Contrary to the spectra of  $\beta$ -carotenes at low temperatures, the absorbance spectrum of retinal is smooth without any evident fine structure even at  $-193$  °C (Jurkowitz, 1959). The low-temperature spectra of retinal as well as extracted visual pigments are, however, much narrower than spectra measured at room temperature reflecting the same underlying physics as seen in the case of  $\beta$ -carotene.

*Prediction #3: The estimation of the minimum energy needed for photoactivation ( $E_a$ )*

The procedure for estimating the minimum energy needed for photoactivation ( $E_a$ ) from temperature effects on the long-wavelength region of the spectrum is illustrated graphically in Fig. 8. The method is based on finding the limiting wavelength ( $\lambda_0 = hc/E_a$ ), where photon energy is equal to  $E_a$ . According to Stiles' and Lewis' models,  $\lambda_0$  can be found at the crossing point of the temperature-independent and temperature-dependent areas of the spectrum. Based on experimental data,  $\lambda_0$  can be found by measuring temperature effects in both temperature-dependent and temperature-independent domains and calculating the difference spectra ( $\Delta = \text{Log } S_w - \text{Log } S_c$ ) shown in Fig. 8. Stiles' (1948) model gives the following equation for the long-wavelength (temperature-dependent) part of the difference spectra:

$$\Delta = \text{Log } S_w - \text{Log } S_c = \frac{hc \cdot \log e}{k} \cdot \left( \frac{1}{\lambda_0} - \frac{1}{\lambda} \right) \cdot \left( \frac{1}{T_c} - \frac{1}{T_w} \right). \quad (13)$$

Thus, the slope of the temperature-dependent part of the  $\Delta$ -spectrum depends only on the temperatures at which the original spectra are measured:

$$\frac{\partial(\text{Log } S_w - \text{Log } S_c)}{\partial(1/\lambda)} = -\frac{hc \cdot \log e}{k} \cdot \left( \frac{1}{T_c} - \frac{1}{T_w} \right). \quad (14)$$

By using the constant slope predicted by equation 14, a straight line can be fitted to the data points of the  $\Delta$ -spectrum and the crossing point ( $\lambda_0$ ) between this line and the horizontal one fitted to the temperature-independent domain can be found.

In the case of Lewis' model, equation 13 should be replaced by a more complex formula:

$$\Delta = \frac{hc \cdot \log e}{k} \cdot \left( \frac{1}{\lambda_0} - \frac{1}{\lambda} \right) \left( \frac{1}{T_c} - \frac{1}{T_w} \right) + \log \left\{ \frac{\left( \frac{hc}{kT_w} \right)^m \left( \frac{1}{\lambda_0} - \frac{1}{\lambda} \right)^m \cdot \frac{1}{m!} + \dots + 1}{\left( \frac{hc}{kT_c} \right)^m \left( \frac{1}{\lambda_0} - \frac{1}{\lambda} \right)^m \cdot \frac{1}{m!} + \dots + 1} \right\}. \quad (15)$$

For the same experimental data Lewis' formula gives systematically higher activation energy estimates than Stiles' formula, because it takes into account the curvature of the  $\Delta$ -spectrum near  $\lambda_0$  (see Fig. 8). This more accurate model requires, however, independent estimation of the extra parameter  $m$  based on the final slope of the spectrum (see equation 12). On the other hand, Stiles' model offers a simple graphical means of obtaining a lower limit for  $E_a$  based only on the  $\Delta$ -spectrum. For a constant value of  $m$ , the difference between Stiles' and Lewis'  $E_a$  estimates is constant. Thus, both models give the same estimates for the differences in  $E_a$  between different visual pigments, although the absolute values given by Stiles' formula are lower.

Srebro (1966) derived the following equation for the minimum energy of activation:

$$E_a = \frac{hc}{\lambda_i} + \frac{hc}{T} \cdot \frac{[-\partial \log S / \partial(1/T)]_i}{[\partial \log S_c / \partial(1/\lambda)]_i}, \quad (16)$$

where the subscript  $i$  refers to each "long-wavelength" data point ( $\lambda_i$ ), where spectral sensitivity data is measured. The derivatives  $[-\partial \log S / \partial(1/T)]_i$  and  $[\partial \log S_c / \partial(1/\lambda)]_i$  are also determined at the wavelength  $\lambda_i$ . For simplifications used in calculations, the reader is referred to the Methods sections of papers I and II.

Equation 16 is based on Stiles' model of the temperature dependence of the long-wavelength slope, but takes into account the curvature of the spectrum as proposed by Lewis (1955). Thus, Srebro's formula offers a simple way of estimating  $E_a$  based on Stiles' model refined by Lewis' ideas. This simple formula does not require explicit determination of the extra parameter  $m$ , but still takes into account its effect on the spectrum. Furthermore, each pair of data points (warm-cold) in the long-wavelength domain offers means of getting independent estimates of  $E_a$ . Because of these advantages, equation 16 has been used as the primary basis for activation energy estimates in this thesis (I–III).

### 3 Aims of the study

The purpose of this thesis was to elucidate the relation between three main functional properties of vertebrate visual pigments: the position of the absorbance spectrum, characterized by  $\lambda_{\max}$ , the minimum energy needed for photoactivation ( $E_a$ ) and the rate of thermal isomerizations ( $k$ ). The ultimate goal was to find a physical model, which could 1) explain the discrepancy between the estimates of the minimum energy needed for photoactivation ( $E_a$ ) and apparent Arrhenius activation energy estimates ( $E_{a,B}$ ) deduced from the temperature-dependence of thermal isomerizations and 2) explain the experimentally found correlation between  $\lambda_{\max}$  and thermal isomerization rates of visual pigments (Donner *et al.*, 1990; Firsov & Govardovskii, 1990; Fyhrquist, 1999; cf. Figs 2 and 3 in paper V). The specific goals of papers I–V are summarized below.

**Paper I.** The objective was to test experimentally the prediction of an inverse relation between  $E_a$  and  $\lambda_{\max}$  (SLB hypothesis) (Stiles, 1948; Lewis, 1955; Barlow, 1957). The minimum energy needed for photoactivation ( $E_a$ ) was estimated based on temperature effects in the long-wavelength domain of both spectrally similar and spectrally different visual pigments. The study included A1-based and A2-based visual pigments. Spectral sensitivity was measured solely by the electroretinogram (ERG) technique at two different temperatures in the wavelength range 397–752 nm.

**Paper II.** The objective was to test the accuracy of the physical models predicting temperature effects on visual pigment spectra and to test the SLB hypothesis with a refined method of  $E_a$  estimation. For these purposes, temperature effects on spectral properties of toad “red” and “green” rods were studied by single-cell microspectrophotometry (MSP) and, in the case of red rods, also by electroretinogram (ERG) recording. Temperature effects on  $\lambda_{\max}$  were characterized by microspectrophotometry (MSP). Absorbance spectra recorded by MSP at different temperatures were combined with spectral sensitivities recorded by ERG at the same temperatures to remove a number of potential artifacts connected with the use of ERG alone. The temperature dependence of the long-wavelength domain of the composite MSP & ERG spectra were used to estimate the minimum energy needed for the photoactivation ( $E_a$ ) of the red rod pigments of two closely related toad species.

**Paper III.** The objective was to study the relation between  $\lambda_{\max}$  and  $E_a$  in A2-based pigments. In addition, the effect of the chromophore switch on  $E_a$  and  $\lambda_{\max}$  was studied. For this purpose, temperature effects on three A2-based visual pigments and one A1/A2 pigment pair with the same opsin were studied with the

same methods as in paper II. The pigments studied allowed three pair-wise comparisons to elucidate the relation between  $\lambda_{\max}$  and  $E_a$ : 1) two pigments with the same opsin but different chromophores, 2) two A2 pigments with similar  $\lambda_{\max}$ , 3) two A2 pigments with different  $\lambda_{\max}$ .

**Paper IV.** The objective was to study a possible correlation between the minimum energy needed for photoactivation ( $E_a$ ) and  $1/\lambda_{\max}$  in the full experimental material collected. The study was based on 12 different visual pigments (the pigments from studies I–III plus two invertebrate A2 pigments). The effects of the chromophore switch and opsin shift on  $\lambda_{\max}$  and  $E_a$  were studied separately. An empirical relation between  $E_a$  and  $1/\lambda_{\max}$  was deduced and compared with the prediction of the SLB hypothesis.

**Paper V.** The objective was to formulate a new hypothesis explaining the discrepancy between the apparent Arrhenius activation energies ( $E_{a,B}$ ) and the photoactivation energies ( $E_a$ ) as well as the correlation between  $\lambda_{\max}$  and thermal isomerization rates. The model is based on the photoactivation energy estimates deduced in papers I–IV and the literature data on the rates of thermal isomerizations in vertebrate photoreceptors to which is applied the physical theory of the rate of thermal unimolecular reactions.

## 4 Materials and methods

### 4.1 A general note on experimental techniques

Two experimental techniques were used in this thesis. Absorbance spectra of visual pigments were recorded by single-cell microspectrophotometry (MSP) from the outer segments of isolated rods and cones (II–IV). The spectral sensitivities of rod and cone photoreceptors were measured by electroretinogram (ERG) recording of mass photoresponses across the isolated aspartate-superfused retina (I–IV). Both techniques were used for characterizing the temperature effects on spectral properties of visual pigments within the physiological temperature range (0 °C–38 °C).

MSP and ERG techniques were used, because together they offer accurate information of the spectral properties of visual pigments over a wide wavelength range. With MSP, the absorbance spectra can be studied with high resolution in the vicinity of the peak of the spectrum ( $\lambda_{\max}$ ). MSP allows the measurement of the absorbance spectrum on most amphibian rod photoreceptors with reasonable accuracy up to the long-wavelength point, where absorbance has dropped *ca.* 2 log units from its peak value. In this region, MSP is superior in accuracy compared to any electrophysiology, including the ERG. On the other hand, ERG as an electrophysiological method is superior in the long-wavelength domain. Because of the biological amplification of single photoisomerizations (see section 2.1.3) and the summation of responses originating from thousands of photoreceptors, the ERG technique allows very low variability and noise level in the responses. The spectral range that can be studied by electrophysiology is eventually limited only by the power of the light source. Thus, our ERG across the isolated retina allowed the measurement of spectral sensitivity up to a long-wavelength point, where spectral sensitivity had dropped even *ca.* 8 log units from its peak value.

MSP and ERG techniques have several other advantages, which make them suitable for this study: both of these techniques allow reliable and long-lasting recordings in the physiological temperature range. In addition, MSP is a fast and effective method for characterizing the absorbance spectra of single cells. MSP would allow the extension of the temperature range also beyond the limits used in this study. Contrary to the absorbance recordings on extracted visual pigments in solution, MSP offers a possibility to study the pigments in their natural environment inside the membranes of intact photoreceptor cells. The main disadvantage of this method is that the light intensity is limited: The more light that is used, the more visual pigments are bleached distorting the recorded

spectrum. Thus, high-resolution spectra can be obtained only by using low light intensity and by averaging recordings from a large number of cells.

In addition to the abovementioned benefits, the ERG technique has the advantage that photoreceptors in the intact retina are in their natural physiological environment. The main disadvantage of the ERG technique is that the signal contains several components even when the synaptic transmission to second-order cells has been blocked by aspartate. Thus, the signal component generated by the photoreceptor type under study has to be separated by special procedures (see below). When several photoreceptor types with quite similar light sensitivities and response kinetics are present in the same retina, this problem can severely limit the usability of the ERG method. Another disadvantage of the ERG method is that the shape of the spectral sensitivity curve is distorted in the short-wavelength region (near  $\lambda_{\max}$ ) due to so called “self-screening”. Essentially this phenomenon implies that when the light is travelling through a high total pigment density, as e.g. in the long outer segment of a rod, the absorption probability for photons in a broad band around  $\lambda_{\max}$  is close to 100% and does not reflect of the actual absorbance spectrum of a single pigment molecule.

Despite some disadvantages, the combination of MSP and ERG techniques proved to be effective for the accurate study of temperature effects on spectral properties of visual pigments. Alternative methods for studying spectral properties of visual pigments could hardly have been successfully applied in the present study with comparable effort. For example, the long-wavelength tail of the spectral sensitivity curve could be determined also by e.g. psychophysical spectral sensitivity measurements based on the threshold sensitivity of the whole animal at different wavelengths of monochromatic light. Although behavioural thresholds can be accurately measured in poikilothermic animals at different temperatures, the invested effort for each spectral point is considerable (cf. Aho *et al.*, 1993). Psychophysical experiments, on the other hand, are limited to a narrower temperature range than MSP and ERG recordings. Spectral sensitivity recordings by the suction pipette technique would at the moment be the best alternative to the ERG. Suction-pipette recordings allow the same temperature range and in a well-polished system might reach an accuracy comparable to that attained in this thesis.

In this chapter the main aspects of the methods used in this thesis are summarized. For a more detailed description of the methods, the reader is referred to the original papers (see Table 1 for references of specific methods).

**Table 1.** Specific methods of this thesis and their primary references.

Methods	References
<b>Experimental procedures:</b>	
<ul style="list-style-type: none"> <li>• ERG recordings</li> <li>• MSP recordings</li> </ul>	Papers I–III <sup>a</sup> Papers II, III <sup>b</sup>
<b>Analysis of absorbance &amp; spectral sensitivity spectra:</b>	
<ul style="list-style-type: none"> <li>• Extraction of porphyropsin spectra from mixed A1/A2 spectra</li> </ul>	Paper III
<ul style="list-style-type: none"> <li>• <math>\lambda_{\max}</math> estimation</li> </ul>	Paper II
<ul style="list-style-type: none"> <li>• Construction of composite MSP &amp; ERG spectra</li> </ul>	Paper II
<ul style="list-style-type: none"> <li>• <math>E_a</math> estimation based solely on ERG data</li> </ul>	Paper I
<ul style="list-style-type: none"> <li>• Refined method for <math>E_a</math> estimation based on composite ERG &amp; MSP spectra</li> </ul>	Paper II
<b>Statistical methods:</b>	
<ul style="list-style-type: none"> <li>• Error estimates for <math>E_a</math> and statistical testing of <math>E_a</math> estimates</li> </ul>	Papers I–III
<b>Methods used for constructing models based on <math>E_a</math> estimates:</b>	
<ul style="list-style-type: none"> <li>• The relation between <math>E_a</math> and <math>1/\lambda_{\max}</math></li> </ul>	Paper IV
<ul style="list-style-type: none"> <li>• The relation between <math>\log k</math> and <math>1/\lambda_{\max}</math></li> </ul>	Paper V

<sup>a</sup>Cf. Donner *et al.* (1988); Koskelainen *et al.* (1994); Pahlberg *et al.* (MS in preparation). <sup>b</sup>Cf. Govardovskii *et al.* (2000).

## 4.2 Visual pigments, animals and preparations

### *Visual pigments*

Table 2 lists all the visual pigments studied in this thesis. The experimental data stem from MSP and ERG measurements performed on 11 different vertebrate visual pigments *in situ* in photoreceptor cells. Recordings were in most cases performed at two to four different temperatures as shown in table 2. All of the vertebrate pigments studied belong to either amphibian or fish visual pigments. In addition, two invertebrate pigments belonging to two closely related crustaceans (*Mysis relicta*) were included in activation energy comparisons (paper IV). The original spectral sensitivity data of these invertebrate pigments is presented in the study by Pahlberg *et al.* (manuscript in preparation).

The following criteria were used when choosing the pigments for this study: 1) Both A1- and A2-based visual pigments were included. Two A1/A2 pigment pairs having the same opsin but different chromophores were selected particularly to elucidate the effect of the chromophore switch on  $E_a$ . 2) Both spectrally similar visual pigments with nearly identical  $\lambda_{\max}$  values as well as pigments with different  $\lambda_{\max}$  values were selected to study the variation of  $E_a$  within single  $\lambda_{\max}$  value as well as to find out the general relation between  $E_a$  and  $\lambda_{\max}$ . Together the  $\lambda_{\max}$  values of the visual pigments studied cover the range 433–629 nm. 3) Well-characterized model species allowing functional comparisons between  $\lambda_{\max}$ , pigment structure and the rate of thermal isomerizations ( $k$ ) were preferred. Thus, pigments for which  $k$  and the amino acid sequence of the opsin were available were regarded especially valuable for this study. The availability (A) or the absence (N) of the literature data for the opsin sequence and  $k$  is shown in table 2 for each pigment studied. In addition to the main criteria 1–3, some other points were taken into account as choosing the pigments: e.g. pigments were selected with emphasis on the possibility to study them effectively by MSP and ERG methods and pigments without polymorphism were often preferred to those with reported polymorphism.

**Table 2. (facing page)** Visual pigments studied in this thesis are classified according to the species, the photoreceptor type and the chromophore (Ch). Tabulated values of the peak sensitivity ( $\lambda_{\max}$ ) are given within the accuracy of 1 nm. Estimates are based on the best-fitting Govardovskii *et al.* (2000) nomogram fitted to the “room temperature” or “warm” (21–28 °C) absorbance spectra recorded by MSP in this thesis (with the exceptions of *Rana temporaria* L-cone pigments, see footnotes). Measurements performed by MSP and ERG techniques in this thesis, their temperatures and references (Ref.) related to the recordings are shown. The availability (A) or absence (N) of opsin sequence (Op) in the literature is marked as well as that of the rate of thermal isomerizations ( $k$ ). See footnotes for references.

Species & photoreceptor type	Ch	$\lambda_{\max}$ (nm)	Measurements		Ref.	Op	$k$
			MSP (°C)	ERG (°C)			
<i>Rana catesbeiana</i>							
rod (ventral retina)	A1	502 <sup>a</sup>	8.5; 28.5	8.5; 28.5	III, IV	A <sup>b</sup>	A <sup>c</sup>
rod (dorsal retina)	A2	525	8.5; 21; 28.5	8.5; 28.5	III, IV	A <sup>b</sup>	A <sup>c</sup>
<i>Rana temporaria</i>							
rod	A1	503 <sup>a</sup>	7.0; 28.0	5.4; 25.0	I, IV	A <sup>d</sup>	N
L-cone	A1	562 <sup>e</sup>	-	5.4; 25.0	I, IV	N	N
L-cone (tadpole)	A2	629 <sup>f</sup>	-	7.9; 24.6	I	N	N
<i>Bufo bufo</i>							
rod	A1	503 <sup>a</sup>	8.5; 28.5	8.5; 28.5	I, II	A <sup>d</sup>	A <sup>g</sup>
<i>Bufo marinus</i>							
“red” rod	A1	504 <sup>a</sup>	0; 8.5; 28.5; 40	8.5; 28.5	II	A <sup>d</sup>	A <sup>h</sup>
“green” rod	A1	433 <sup>a</sup>	0; 8.5; 28.5; 40	-	II	A <sup>i</sup>	A <sup>j</sup>
<i>Xenopus laevis</i>							
rod	A2	522 <sup>a</sup>	7.0; 27.0	7.0; 26.0	I, IV	A <sup>k</sup>	A <sup>l</sup>
<i>Carassius carassius</i>							
rod	A2	526	8.5; 28.5	8.5; 28.5	III	N	N
L-cone	A2	619	21	5.0; 15.0; 25.0	III	N	N
<i>Mysis relicta</i>							
Pojoviken Bay population	A2	530 <sup>m</sup>	21.0 <sup>m</sup>	7.0; 20.0 <sup>n</sup>	(IV) <sup>n</sup>	N	N
Lake Pääjärvi population	A2	553 <sup>m</sup>	21.0 <sup>m</sup>	5.0; 18.0 <sup>n</sup>	(IV) <sup>n</sup>	N	N

<sup>a</sup>For comparison, see Table 1 in Govardovskii *et al.* (2000), <sup>b</sup>Kayada *et al.* (1995), about the presence of single opsin in rhodopsin and porphyropsin rods, see Fong *et al.* (1985), <sup>c</sup>Donner *et al.* (1990), <sup>d</sup>Fyhrquist *et al.* (1998a), <sup>e</sup>Koskelainen *et al.* (1994), cf. Table 1 in paper 1. This value is based on the prediction of the nomogram by Govardovskii *et al.* (2000) for the A2-pigment pair of the corresponding A1 pigment (Koskelainen *et al.*, 1994), <sup>f</sup>Fyhrquist *et al.* (1998b), Firsov *et al.* (2002), <sup>g</sup>Baylor *et al.* (1980), <sup>h</sup>Hisatomi *et al.* (1999), <sup>i</sup>Matthews (1984), <sup>k</sup>Batni *et al.* (1996), <sup>l</sup>Fyhrquist *et al.* (1999), <sup>m</sup>Jokela-Määttä *et al.* (manuscript in preparation), <sup>n</sup>The ERG recordings in this case are based on Pahlberg *et al.* (manuscript in preparation); for  $E_a$  estimates see also paper IV.

### *Animals and preparations*

Animals were provided either by commercial suppliers or caught in the wild. Most of them were kept at room temperature and 12h light / 12h dark regime, and fed with appropriate food. The common frogs (*Rana temporaria*) and one portion of the common toads (*Bufo bufo*) were kept unfed in hibernating conditions (at ca. 5 °C). Bullfrogs (*Rana catesbeiana*) were kept in special light and temperature conditions favouring the formation of either A1 or A2 pigment (III; cf. Reuter *et al.*, 1971; Donner *et al.*, 1990). For studying the porphyropsin L-cones of the common frog (*Rana temporaria*), tadpoles at early developmental stages were selected for the study. At this stage they have the maximal A2-pigment content in the retina (I; cf. Reuter, 1969).

Animals were dark adapted for at least 12 hours at room temperature before the experiment. At the beginning of the experiment, the animal was decapitated, double-pithed and both eyes were removed under weak red light ( $\lambda > 680$  nm). The retina was isolated from the pigment epithelium in cooled (15 °C) Ringer solution (for Ringer composition, see paper II). For ERG recordings, the whole retina or a piece of it was used for recording. For MSP recordings, a small piece of the retina was gently pulled into pieces in a drop of Ringer on a coverslip to expose isolated cells or outer segments (see paper II for further details).

## **4.3 Single-cell microspectrophotometry (MSP) (II–III)**

### *Principle*

For about 40 years, single-cell microspectrophotometry has been a standard technique for measuring the absorbance of photoreceptor outer segments (Hanaoka & Fujimoto, 1957; Brown, 1961; Marks, 1963; Liebman & Entine, 1964; Brown & Wald, 1964; for review see Liebman, 1972; Bowmaker, 1984). The basic idea of microspectrophotometry is very simple: a monochromatic beam of light is passed through the photoreceptor outer segment and the intensity of the transmitted light is measured at each wavelength. Thus, the principle is the same as in standard spectrophotometry. Compared to standard spectrophotometry, the additional challenges of microspectrophotometry are related to the small dimensions of the cells as well as the limitations to the light intensity in the MSP recordings, where bleaching of visual pigment by bright light has to be avoided. Absorbance can be calculated based on the intensities of incident ( $I_i$ ) and transmitted ( $I_t$ ) light using the well-known Lambert-Beer law:

$$A(\lambda) = \log \frac{I_i}{I_t} = \varepsilon(\lambda)cl, \quad (17)$$

where  $A(\lambda)$  is absorbance at certain wavelength  $\lambda$ ,  $\varepsilon(\lambda)$  is molar extinction coefficient at the same wavelength,  $c$  is concentration and  $l$  is the solution thickness.

### Equipment

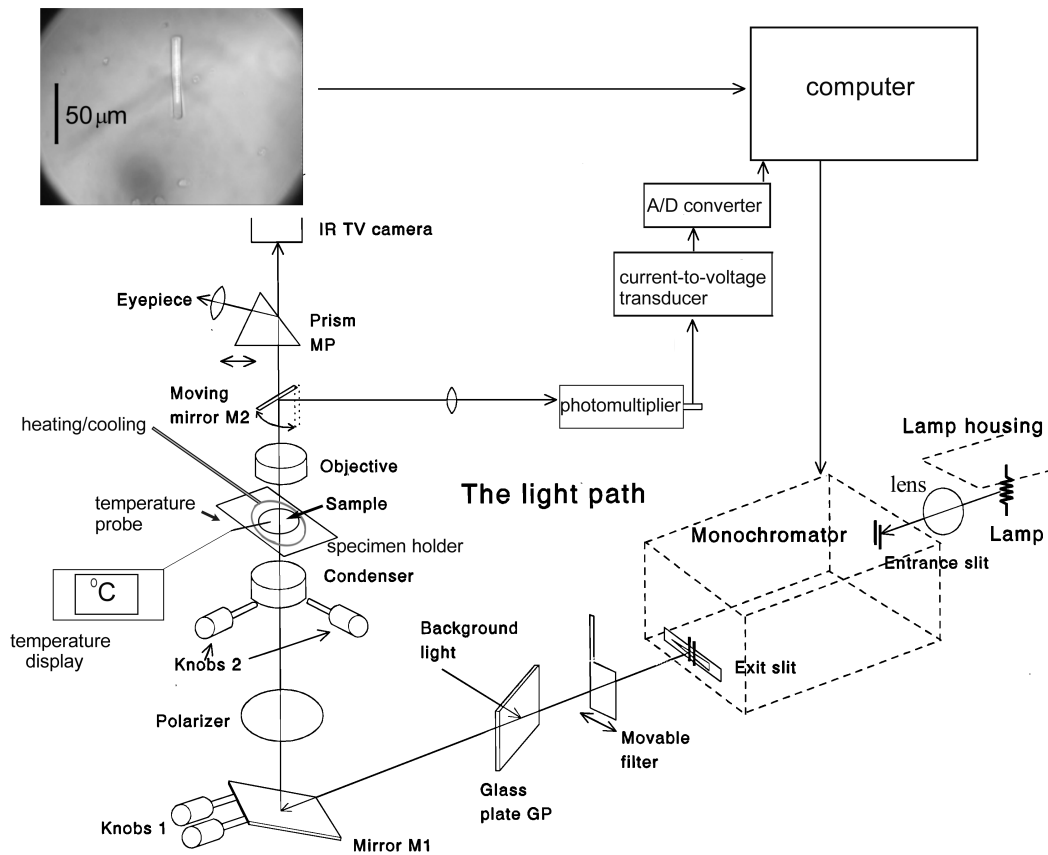


**Fig. 10.** A schematic drawing of the instrument used for MSP recordings (modified from Fig. 4 in Govardovskii, 1999).

The microspectrophotometer used in this study is illustrated in Fig. 10. It is a single-beam, computer-controlled MSP device described in Govardovskii & Zueva (2000). A halogen lamp serves as a light source. Spectral lights are obtained by a monochromator, where a computer-controlled diffraction grating was used for producing different wavelengths (see paper II). Light intensity was

controlled by the width of the entrance and exit slits of the monochromator as well as a movable, computer-controlled neutral density filter (O.D. *ca.* 1.0). A movable polarizer in the light beam allowed the polarization of light with the *e*-vector in the plane of the outer segment disks. The light beam was condensed on to the sample that was placed in the temperature-controlled specimen holder attached in the x-y plane of the microscope stage. The transmitted light could be directed by a movable mirror either to the eyepiece of the microscope or conducted to the photomultiplier during the spectral scan. Photomultiplier output was fed to the computer memory via a current-to-voltage transducer and an A/D converter.

#### *Recording protocol and purposes*

The MSP recordings were performed with the beam oriented at right angles to the long axis of the photoreceptor outer segment (OS), which was aligned parallel to the slit as shown in Fig. 10. The width of the beam was adjusted normally to *ca.* 1/5–1/3 of the OS diameter. The wavelength range scanned was normally 350–750 nm (scanning in ~ 1 nm steps with a speed of 250 nm/s). Optical densities were calculated against corresponding baseline recordings, which were measured separately for each cell in advance in the clear space near the cell. The wavelength calibration of the MSP instrument was performed using a mercury lamp and a standard neodymium glass, whose absorbance had been characterized by a standard spectrophotometer (see paper II). The wavelength calibration was checked regularly in each experiment by recording the absorbance spectrum of the same neodymium glass.

In each experiment, the absorbance spectra of several cells (*ca.* 20–100 depending on the species) were recorded at each temperature studied (for temperatures, see Table 2). For the final results, the spectra of several (*ca.* 3–6) experiments from different retinas were averaged. Measurements were performed at low light intensities resulting in less than *ca.* 1–2 % final bleaching of the visual pigment. In addition, recordings were performed in most cases at two different light intensities, which allowed the final spectra to be corrected for bleaching (cf. Govardovskii *et al.*, 2000).

In this study, MSP recordings were performed for three main purposes. Firstly, absorbance spectra were recorded by MSP at the same temperatures, where ERG recordings were performed in order to construct composite MSP & ERG spectra in a wide wavelength range (II–IV). Secondly, MSP spectra were recorded at an extended temperature range (0–38 °C) to study temperature effects on  $\lambda_{\max}$  (II). Thirdly, MSP spectra were recorded at room temperature to allow the determination of A1/A2 ratio based on Govardovskii *et al.* (2000) nomogram (III).

## 4.4 Electroretinogram recording (ERG) (I–IV)

### *Principle*

Electrophysiological measurement of spectral sensitivity has a simple principle: The light intensity (photons area<sup>-1</sup> time<sup>-1</sup>) needed to produce a signal corresponding to a certain low-amplitude threshold is measured at each wavelength of monochromatic light. The relative spectral sensitivity is defined as the normalized inverse criterion intensity:

$$S = \left( \frac{I(\lambda)}{I(\lambda_{\max})} \right)^{-1}, \quad (18)$$

where  $I(\lambda)$  is the light intensity at wavelength  $\lambda$  that is needed to generate the criterion signal corresponding to a certain threshold amplitude.

Because the quantum efficiency of rhodopsin is constant, the criterion signal corresponds to the absorption of the same average number of photons, and thus the conversion of the same average number of inactive rhodopsin molecules to the active state at each wavelength tested. Using this knowledge as a starting point, the relation between the relative spectral sensitivity and the relative absorbance can be deduced by a fairly straightforward analysis (for details, see Alpern *et al.*, 1987; Stavenga *et al.*, 2000):

$$S = \frac{1 - 10^{-A(\lambda)}}{1 - 10^{-A(\lambda_{\max})}}, \quad (19)$$

where  $A(\lambda)$  is the absorbance corresponding to the wavelength ( $\lambda$ ). In the ideal case, where the light intensity in the photoreceptor waveguide is homogenous (no “self-screening”), equation 19 can be simplified into the following form (cf. equation 17 for definitions):

$$S = \frac{A(\lambda)}{A(\lambda_{\max})} = \frac{\varepsilon(\lambda)}{\varepsilon(\lambda_{\max})}. \quad (20)$$

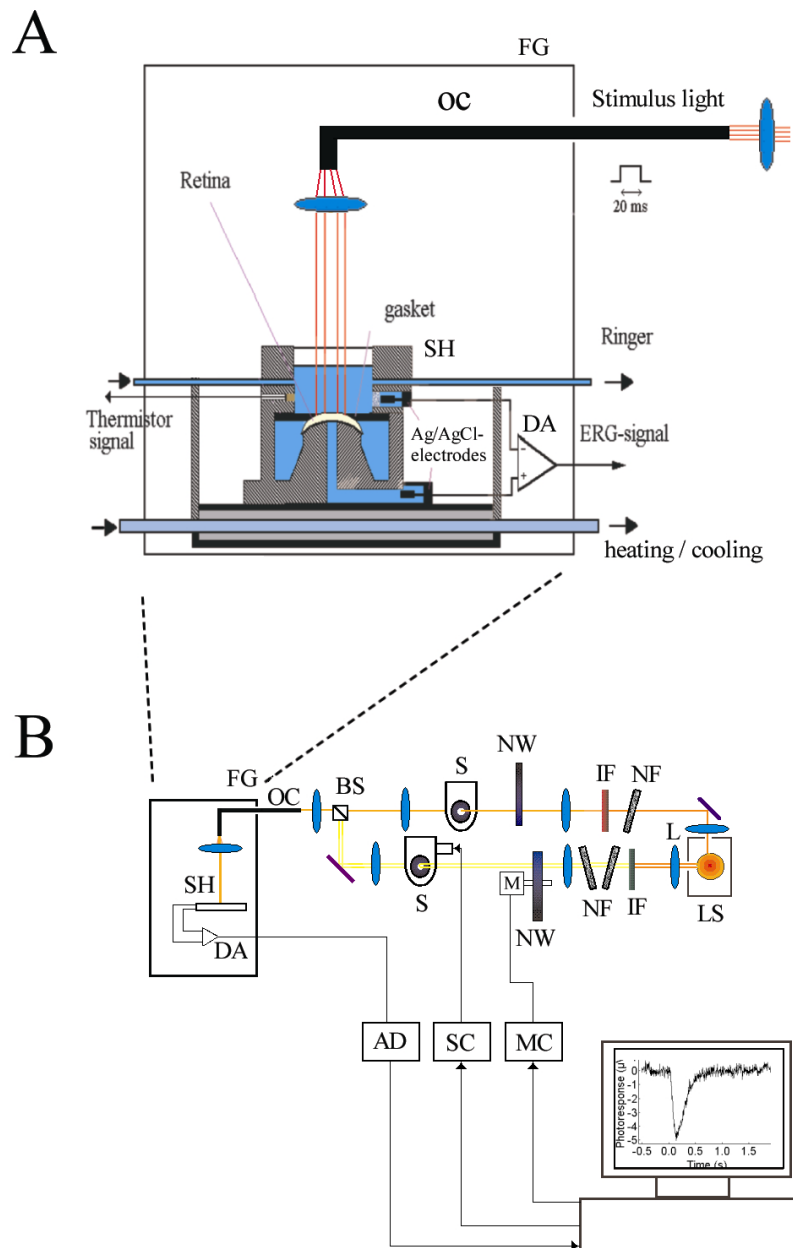


**Fig. 11.** The ERG setup: **(A)** the specimen holder in the light-tight Faraday cage and **(B)** a general view of optics and the whole setup; AD = analog-to-digital converter, BS = beam splitter, DA = differential amplifier, IF = interference filter, FG = light-tight Faraday cage, L = lens, LS = light source, M = stepmotor, MC = stepmotor controller, NW = neutral density wedge, NF = neutral density filter, OC = optic cable, S = shutter, SC = shutter controller, SH = specimen holder.

### *Equipment and stimulation*

The ERG setup is illustrated in Fig. 11. The retina was placed the distal (receptor) side upward in the specimen holder and perfused and illuminated from the upper (distal) side as shown in panel A. The mass receptor potential was recorded with two Ag/AgCl sintered electrodes placed at the distal and proximal sides of the retina. The DC signal was amplified (1000×) and led to the analog-to-digital (AD) converter, where the signal was further amplified (10–100×). In earlier recordings (I, II), an active 8-pole Bessel-type low-pass filter with cut-off frequency 20 Hz for rods and 100 Hz for cones was used. In later recordings (III), digital filtering was used. The temperature of the specimen holder was controlled by a small heat exchanger located in the specimen holder. Temperature was measured by a thermistor placed near the retina (for further details see paper II).

Panel B in Fig. 11 shows the stimulus system used for ERG recordings. The optic bench of the stimulus system had two light channels: one for the stimulus light and one for the background light. A halogen lamp (50 W) was used as a light source for both channels. Computer-controlled shutters were used for producing homogenous full-field flashes (normally 20 ms). The spectral composition of light was controlled by a set of interference filters with transmission half-bandwidths of *ca.* 10 nm. The transmission bands of the interference filters covered the wavelength range of *ca.* 400–800 nm. Light intensity was controlled by neutral density filters and neutral wedges in both the stimulus channel and the background channel. Light intensity was calibrated regularly for each interference filter by a calibrated photodiode. Stimulus and background light were combined by a beam-splitter (BS) (see panel B). An optic cable (OC) led the light to the specimen holder in the light-tight Faraday cage.

### *The ERG: isolation of responses from the photoreceptor type studied*

In the electroretinogram (ERG) technique, the light-induced changes in field potential across the retina are recorded. The voltage changes recorded by the ERG technique are generated by the light-evoked changes in all the radial currents in the resistive extracellular space of the retina. Even though synaptic transmission was always blocked by aspartate (2 mM) in our recordings, the ERG signal may still contain several components: photoreceptor responses of possibly more than one photoreceptor type as well as glial (Müller cell) responses. The aim in each spectral sensitivity recording was as far as possible to isolate the signal generated by the photoreceptor type studied. The following methods were applied to separate the desired signal component (shown in boldface):

**Photoreceptor component.** Glial (Müller) cells respond to the changes in the potassium concentration generated by the light-induced changes in the ion fluxes of photoreceptor cells. In part of the recordings, glial component was suppressed by blocking the potassium channels of Müller cells by  $Ba^{2+}$  added to Ringer solution (cf. Bolnick *et al.*, 1979; Donner & Hemilä, 1985). Even though the glial component could not be totally suppressed, it did not distort spectral sensitivity recordings mainly because of its slower kinetics compared to the photoreceptor responses.

**Rod responses.** Rod responses were separated from cone responses based on their slower kinetics (see paper I: panel C in Fig. 1). When two types of rods (red and green rods) were present in the same retina, the separation of the signal components of the different rod types was based on the large separation of their  $\lambda_{max}$  values. In this case, the long-wavelength part of the spectrum is totally dominated by red rods (see paper II). Thus, red-rod contribution was easy to separate from green rods in the most interesting wavelength domain. On the other hand, green-rod sensitivity could not be studied by the ERG technique in the long-wavelength domain.

**Cone responses.** Cone responses were separated from rod responses by two different techniques. 1) In the main pool of cone recordings, a double-flash technique was used (see Fig.1 in paper III; cf. Koskelainen *et al.*, 1994). In this method, a rod-saturating conditioning flash was followed by a test flash at a time, when cones had recovered but rods were still saturated. 2) In a few recordings (see paper I), the cone responses were separated from the rod responses by selective suppression of the rods with steady background light. Only the long-wavelength-sensitive (L) cones were studied in this thesis. Their spectral sensitivity dominates in the long-wavelength domain. The ERG-technique did not allow the isolation of the signals from other cone types with  $\lambda_{max}$  at shorter wavelengths.

#### *Recording protocol and analysis*

ERG recordings were performed on each retina at two or three different temperatures in the physiological temperature range (see Table 2 for temperatures). Recordings were performed on dark-adapted retinas. The recording protocol for determining spectral sensitivity is best shown in Fig. 1 in paper I and in Fig. 1 in paper II. As shown in these figures, spectral sensitivity at each test wavelength was determined relative to a reference wavelength chosen quite near the wavelength of maximum sensitivity. Response families at 4–7 different intensities were recorded repeatedly at the reference wavelength. Between consecutive response families at the reference wavelength, 3–20 dim-flash responses were recorded and averaged at 3–5 different test wavelengths. A

generalized Michaelis-function (intensity-response function) was fitted to the response families at the reference wavelength. Relative spectral sensitivity at each test wavelength was determined based on the lateral shift, which was needed to shift the corresponding intensity-response function recorded at the reference wavelength on intensity scale to match the averaged response at the test wavelength. (for a detailed description, see methods sections in papers I and II).

#### 4.5 General analysis (I–IV)

Absorbance spectra obtained by MSP and relative spectral sensitivities obtained by ERG at different temperature were used for further analysis to obtain estimates for  $\lambda_{\max}$ , to quantify the temperature effects on spectral sensitivity and to obtain estimates for  $E_a$ . Fig. 12 summarizes the main steps of the further analysis of absorbance and spectral sensitivity data. The methods are exemplified in the case of the common toad (*Bufo bufo*) red rod pigment. The methods summarized in Fig. 12 are discussed below under separate boldface subtitles.

**$\lambda_{\max}$  estimation.** The wavelength of the maximum absorbance ( $\lambda_{\max}$ ) was determined by fitting the visual pigment template of Govardovskii *et al.* (2000) to the absorbance spectra recorded by MSP. Only data recorded at room temperature or at “warm” temperatures (27–28.5 °C) were used for template fitting, since “cold” spectra are not perfectly well fitted by the nomogram (II). Therefore, temperature effects on  $\lambda_{\max}$  were studied by fitting, instead of the nomogram, a 2nd-order polynomial to a narrow area around the peak (normalized  $A \geq 0.9$ ). The goodness of fit was estimated by the least-square criterion.

**Analysis of the “purity” of the spectrum and separation of mixed visual pigment spectra.** The Govardovskii *et al.* (2000) templates for A1 and A2 pigments fitted to room-temperature or “warm” MSP spectra were used for studying, whether two chromophores were present. The purpose was to verify that the measured absorbance was due to a single chromophore (see paper II). Since the A1→A2 substitution broadens the absorbance spectrum, the presence of even a small fraction (*ca.* 1%) of the A2 chromophore could be detected by this method (see paper II). In addition, linear combinations of the A1 and the A2 templates of Govardovskii *et al.* (2000) were used to determine, which proportion of the “mixed” absorbances was due to A1 and A2 chromophores in porphyropsin rods of the bullfrog (*Rana catesbeiana*). The information was needed for extracting the pure A2 spectra from the mixed spectra at different temperatures (for a detailed description of extracting the pure A2 spectra, see paper III).

**Combination of spectral sensitivity and absorbance spectra.** ERG and MSP data recorded at the same temperature were used to construct composite spectra, which were accurate over a wide wavelength range. The spectra were glued together in the region, where both techniques offer accurate data and “self-screening” can be neglected for the present purpose. In this region of the spectrum, equation 20 is valid within reasonable accuracy allowing the combination of the two data sets. A detailed description of the anchoring of MSP and ERG data is included in paper II. As shown in Fig. 12, the anchoring was based on smoothing the MSP-data in the range of interest by a 2nd-order polynomial. ERG data was anchored by least-square criterion to the 2nd-order polynomial fitted to the MSP data.

**Combination of “cold” and “warm” spectra.** Spectra recorded at different temperatures have to be positioned optimally relative to each other in order to estimate the temperature effects on spectral sensitivity. When MSP data was present, each composite spectrum was normalized according to the peak sensitivity. Thus, the relative position of “cold” and “warm” spectra was determined solely by the normalization of MSP spectra. On the other hand, in some cases only ERG data was present (e.g. pigments studied in paper I). Then the relative anchoring of “cold” and “warm” spectra was based solely on ERG-data in the short-wavelength domain, where the physical models (Stiles, 1948; Lewis, 1955) predict a temperature-independent domain. For further details about the anchoring of “cold” and “warm” spectra in such cases, see paper I and paper III (for the methods used for the L-cones of the crucian carp).

**Final slope estimation.** The long-wavelength tail of spectral sensitivity data (log-normalized  $S$  vs. wavenumber) was characterized by the slope of the straight line fitted to the region, where absorbance had dropped typically more than *ca.* 2–3 log units from the peak value. In general, weighted linear regression was used, where each data point was weighted by  $1/SEM^2$ . For the most long-wavelength-sensitive pigments (the L-cones of crucian carp and the A2-based L-cones of common frog tadpoles) a bit looser criteria were applied (*ca.* 1.5 log units from the peak value). The long-wavelength slopes were compared to the predictions of Stiles’ (1948) model (see section 2.3.2 and papers II & III).

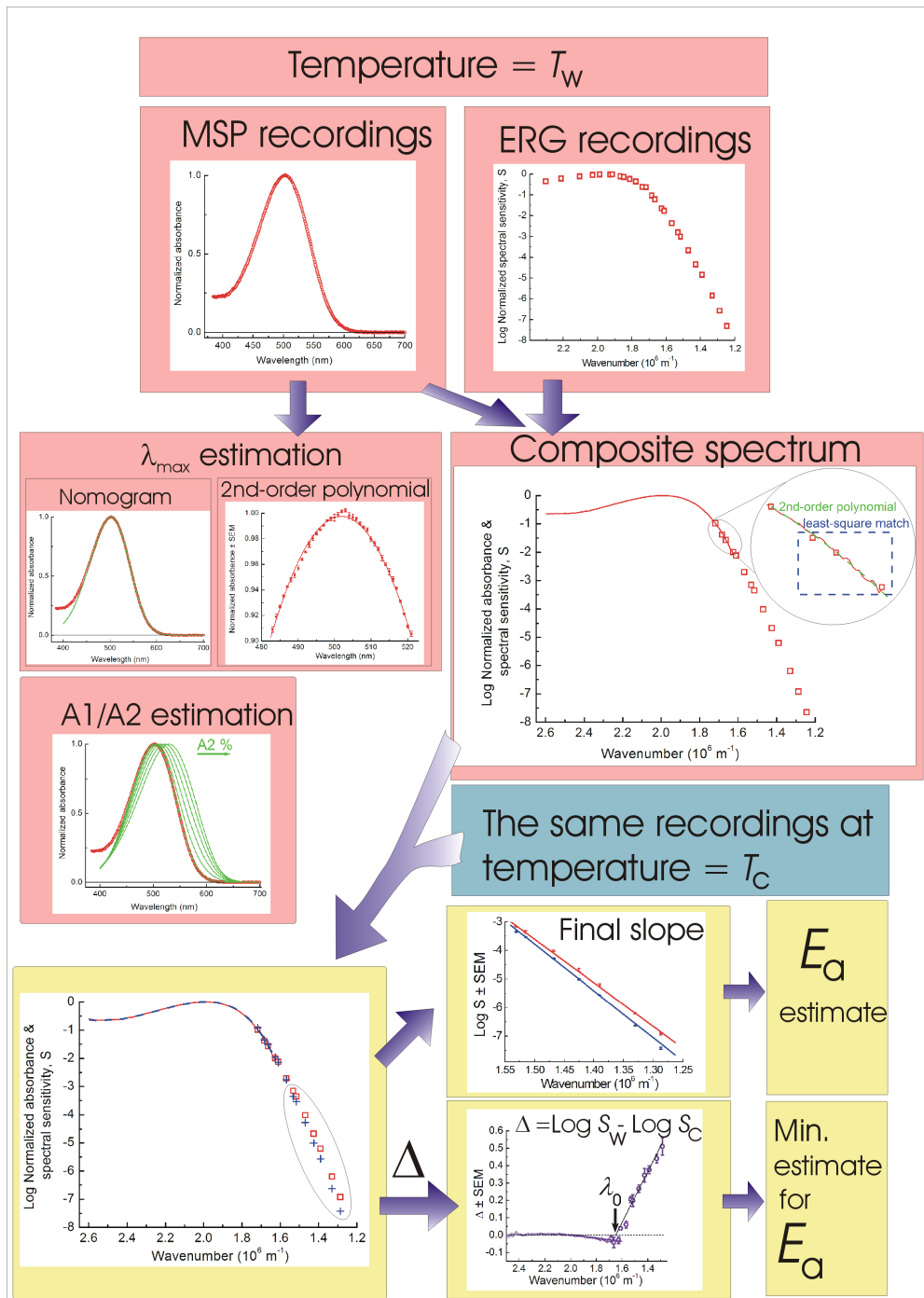


**Fig. 12.** Summary of the methods used for further analysis of the absorbance and spectral sensitivity data recorded at different temperatures. The methods are exemplified using the data obtained from common toad (*Bufo bufo*). See the text for the description of the methods illustrated in the figure.

**Construction of  $\Delta$ -spectra.** Temperature effects on spectra were visualized by plotting the difference between warm and cold spectra ( $\Delta = \log S_w - \log S_c$ ). These  $\Delta$ -spectra were constructed separately for the MSP and the ERG data and anchored together by means of a least-square match (for further details about anchoring, see paper II).

**Estimation of the minimum energy needed for photoactivation ( $E_a$ ).** The minimum energy needed for photoactivation ( $E_a$ ) was estimated based on the temperature effects in the long-wavelength domain. As discussed earlier in section 2.3.2, the estimation of  $E_a$  was based on equation 16 (Srebro, 1966; I & II). The method uses each pair of the data points (warm-cold) in the long-wavelength region to obtain independent estimates for  $E_a$ . In general, only data points for which a clear temperature effect was detected ( $\Delta > ca. 0.1$ ) were used for the analysis. For a detailed description of  $E_a$  estimation based on composite spectra, the reader is referred to the Methods section of paper II.

In addition,  $\Delta$ -spectra were used for getting the minimum estimate for  $E_a$ . For this purpose, a straight line with a slope predicted by Stiles' model was fitted to the long-wavelength ( $\Delta > ca. 0.1$ .) data points (see section 2.3.2 and e.g. Fig. 3C in paper II).

**Statistical methods.** Standard statistical methods were used to calculate the standard error of means (SEMs) for each data point of the averaged absorbance and spectral sensitivity spectra. The SEM estimates of the  $\Delta$ -spectra were calculated using the variances and the number of the original data points comprising cold and warm spectra. The SEMs of  $E_a$  estimates take into account two independent variance components. Firstly, the variance due to the vertical matching of the spectra when constructing the composite spectrum (II–IV). In paper I, where no MSP data was used this variance component is due to the vertical matching of the cold and warm ERG spectra in the short-wavelength domain. Secondly, the variance of individual point estimates of  $E_a$  in the long-wavelength domain was taken into account (for further details, see papers I & II). Confidence limits and statistical significant testing of  $E_a$  estimates were based on  $t$  distribution and student's  $t$ -test with the degrees of freedom according to the variance estimates of the individual  $E_a$  estimates (detailed description in papers I & II).

## 4.6 Methods for models (IV, V)

### *The relation between $E_a$ and $1/\lambda_{max}$ (IV)*

In paper IV,  $E_a$  estimates for all the visual pigments studied were plotted against  $1/\lambda_{max}$ . The slope of the best-fitting regression line was compared with the best-fitting line predicted by the SLB hypothesis. Three different cases were studied: 1)  $E_a$  estimates of all visual pigments pooled together, 2)  $E_a$  estimates comprising the chromophore switch in two A1/A2 pigment pairs and 3)  $E_a$  estimates in seven pigments having the same (A2) chromophore. In all cases, the weighting factor  $1/SEM^2$  of the  $E_a$  estimates was used in the regression analysis. The error in  $\lambda_{max}$  values was negligible

### *Constructing the model for thermal activation of visual pigments (V)*

In paper V, the discrepancy between the estimates of photoactivation energy ( $E_a$ ) and the apparent Arrhenius activation energies ( $E_{a,B}$ ) deduced from the temperature dependence of the rate of thermal isomerizations was studied with the aid of the Hinshelwood model (see section 2.2.3). The data of thermal isomerization rates was obtained from the literature (see Tables 1 and 2 in paper V) and corrected for the same temperature (21 °C). The aim was to test, whether both the temperature-dependence of the rate of thermal isomerizations ( $k$ ) as well as the experimentally observed correlation between  $k$  and  $\lambda_{max}$  (Donner *et al.*, 1990; Firsov & Govardovskii, 1990; Fyhrquist, 1999; cf. Figs 2 and 3 in paper V) could be explained with approximately the same energy barrier for thermal activation and photoactivation. The construction of the model presented in paper V involves the following steps (1–5):

#### **Hypothesis:**

- 1) The energy barriers for thermal and photic activations are approximately the same ( $E_{a,H} \approx E_a$ ), but different numbers of vibrational modes ( $n/2$ ) are involved in photic and thermal activation processes.

#### **Assumptions:**

- 2) The number of “square terms” ( $n$ ) and thereby the number of vibrational modes ( $n/2$ ) involved in thermal activation needed to totally account for the difference between the apparent Arrhenius activation energy ( $E_{a,B}$ ) and the apparent Hinshelwood activation energy ( $E_{a,H}$ ) was estimated by equation 6. Because it was assumed that  $E_{a,H} \approx E_a$ , only  $E_a$  and  $E_{a,B}$  were

needed for the estimation of  $n$ . For this purpose, the difference between  $E_a$  and  $E_{a,B}$  was calculated for the red rods of the cane toad (*Bufo marinus*), where both  $E_{a,B}$  (Baylor *et al.*, 1980) and  $E_a$  (III) were available.

- 3) It was assumed that  $n$  does not vary considerably between different visual pigments.

**Model testing:**

- 4) The empirical relation between  $E_a$  and  $1/\lambda_{\max}$  deduced in paper IV was used to see, whether the new model could explain the experimentally observed relation between the rate of thermal isomerizations ( $k$ ) and  $1/\lambda_{\max}$  in both rod and cone visual pigments. The model was tested under the simple assumption that the pre-exponential factor ( $A_H$ ) is constant within the groups of rod and cone pigments, respectively (see equation 5).
- 5) The model was also tested by pair-wise comparison of the thermal activation rates of the A1/A2 rod pigment pair of the bullfrog. The prediction of the model for the relation between the activation rates was calculated by equation 5 using the corresponding photoactivation energy estimates (III). It was again assumed that the pre-exponential factor is approximately the same for both pigments.

## 5 Results

### 5.1 Temperature effects on spectral sensitivity (I–IV)

#### *Temperature effects in the long-wavelength domain (I–IV)*

The effect of temperature on spectral sensitivity was qualitatively similar in the long-wavelength domain of all visual pigments studied in papers I–IV: the relative sensitivity was higher at higher temperatures as predicted by Stiles (1948). For visualization of the temperature effects on expanded scale (Log normalized  $S$  vs. wavenumber), see Fig. 3 in paper II and Fig. 4 in paper III. As exemplified by these figures, an approximately linear decline of log-normalized sensitivity vs. wavenumber was found for all pigments and temperatures in the long-wavelength domain. Table 3 summarizes the final slopes of “cold” and “warm” spectra plotted on logarithmic ordinates against wavenumber for all vertebrate visual pigments studied in papers I–IV.

As shown by the final column of Table 3, the ratio of “cold” and “warm” slopes ( $K_C/K_W$ ) is in excellent agreement with the prediction of Stiles’ (1948) model. On the other hand, the absolute slopes are somewhat (*ca.* 10–30%) shallower than predicted. The long-wavelength limbs of the spectra show also small but systematic curvature towards longer wavelengths so that the data points at the longest wavelengths fall systematically below the regression line (see Fig. 3 in paper II and Fig. 4 in paper III). The shallower than predicted slope as well as the small systematic curvature of the final limb of the spectra can be explained by Lewis’ (1955) refinement to Stiles’ theory (for theoretical background, see section 2.3.2 and for further discussion section 6.1).

### *Temperature effects in the short-wavelength domain (II, III)*

MSP recordings on rod pigments showed that temperature affects also the short-wavelength domain of the spectra by shifting the wavelength of maximum absorbance ( $\lambda_{\max}$ ). It was shown in paper II on *Bufo marinus* rod pigments that temperature effects on  $\lambda_{\max}$  differ in red and green rods. In all seven red rod pigments studied, a small but systematic shift in  $\lambda_{\max}$  towards longer wavelengths was detected, as temperature was lowered (II & III). The temperature effect on  $\lambda_{\max}$  of the red rods was quite satisfactorily described by a linear relation between  $\lambda_{\max}$  and temperature, although a slight curvature in this relation was found (see Fig. 6 in paper II). The average effect ( $\Delta\lambda_{\max} \pm \text{SEM}$ ) in the seven red-rod pigments studied was  $-0.53 \text{ nm} \pm 0.07 \text{ nm}$  per  $10 \text{ }^\circ\text{C}$  rise in temperature. This result is in good agreement with the absorbance measurements on extracted A1 and A2 pigments in solution interpolated to the same temperature range (St. George, 1952; Yoshizawa & Horiuchi, 1969; Yoshizawa, 1972; see also Fig. 4 in paper II).

The effect of temperature on the spectral absorbance of green rods was quite different. No statistically significant dependence between  $\lambda_{\max}$  and temperature was found (see Fig. 6 in paper II). The  $\lambda_{\max}$  of *Bufo marinus* green rods remained the same (432.6 nm) within the accuracy of 0.1 nm even in the extended temperature range studied in paper II (0–38  $^\circ\text{C}$ ). For a discussion on the possible reasons underlying the differences in the short-wavelength temperature effects between the green and the red rods, see Discussion section in paper II.

**Table 3. (facing page)** The final slopes ( $K = \partial \text{Log } S / \partial (1/\lambda)$ ) of vertebrate visual pigment spectra measured in the present thesis at “cold”, ‘C’ and “warm”, ‘W’ temperatures (temperatures given in parentheses). The slopes were obtained as described in the Materials and methods section. Values for the coefficient of determination ( $r^2$ ) of the regression analysis are listed in separate columns for “cold” and “warm” temperatures. The ratios  $K_C/K_W$  measure the size of the temperature effect in the long-wavelength sensitivity. The final column gives the predictions by Stiles’ (1948) model for  $K_C$ ,  $K_W$  and the ratio  $K_C/K_W$ . The deviations of the empirical values (in percents) from the prediction of Stiles’ model are given in parenthesis.

Species & photoreceptor type, chromophore	$K_C$ $10^{-5}$ m	$r^2$	$K_W$ $10^{-5}$ m	$r^2$	$K_C / K_W$	Stiles' predictions $K_C / K_W$ $K_C$ ( $10^{-5}$ m) $K_W$ ( $10^{-5}$ m)
<i>Rana catesbeiana</i>						
rod (A1)	1.64 (8.5 °C)	0.999	1.55 (28.5 °C)	0.999	1.062	$K_C / K_W = 1.071$ (-0.9 %) $K_C = 2.219$ (-26 %) $K_W = 2.071$ (-25 %)
rod (A2)	1.66 (8.5 °C)	0.998	1.57 (28.5 °C)	0.9995	1.054	$K_C / K_W = 1.071$ (-1.5 %) $K_C = 2.219$ (-25 %) $K_W = 2.071$ (-24 %)
<i>Rana temporaria</i>						
rod (A1)	1.71 (5.4 °C)	0.998	1.58 (25.0 °C)	0.9996	1.086	$K_C / K_W = 1.070$ (+1.4 %) $K_C = 2.243$ (-24 %) $K_W = 2.096$ (-25 %)
L-cone (A1)	1.68 (5.4 °C)	0.999	1.55 (25.0 °C)	0.9998	1.082	$K_C / K_W = 1.070$ (+1.1 %) $K_C = 2.243$ (-25 %) $K_W = 2.096$ (-26 %)
L-cone (tadpole) (A2)	1.67 (7.9 °C)	-*	1.59 (24.6 °C)	-*	1.053	$K_C / K_W = 1.059$ (-0.6 %) $K_C = 2.223$ (-25 %) $K_W = 2.099$ (-24 %)
<i>Bufo bufo</i>						
rod (A1)	1.64 (8.5 °C)	0.998	1.52 (28.5 °C)	0.999	1.075	$K_C / K_W = 1.071$ (+0.3 %) $K_C = 2.219$ (-26 %) $K_W = 2.071$ (-27 %)
<i>Bufo marinus</i>						
“red” rod (A1)	1.68 (8.5 °C)	0.999	1.57 (28.5 °C)	0.9995	1.073	$K_C / K_W = 1.071$ (+0.2 %) $K_C = 2.219$ (-24 %) $K_W = 2.071$ (-24 %)
<i>Xenopus laevis</i>						
rod (A2)	1.62 (7.0 °C)	0.998	1.52 (26.0 °C)	0.9997	1.069	$K_C / K_W = 1.068$ (+0.1 %) $K_C = 2.230$ (-27 %) $K_W = 2.089$ (-27 %)
<i>Carassius carassius</i>						
rod (A2)	1.57 (8.5 °C)	0.998	1.45 (28.5 °C)	0.999	1.079	$K_C / K_W = 1.071$ (+0.8 %) $K_C = 2.219$ (-29 %) $K_W = 2.071$ (-30 %)
L-cone (A2)	1.99 (5.0 °C)	0.997	1.77 (25.0 °C)	0.996	1.123	$K_C / K_W = 1.072$ (+4.7 %) $K_C = 2.246$ (-11 %) $K_W = 2.096$ (-15 %)

\*The slope is based only on two data points giving the trivial result:  $r^2 = 1$ .

## 5.2 Photoactivation energy estimates and their relation to $1/\lambda_{\max}$ (I–IV)

Paper IV summarizes the results of  $E_a$  estimates for the visual pigments studied. The primary  $E_a$  estimates, the corresponding SEMs and the minimum estimates for  $E_a$  obtained from  $\Delta$ -spectra interpreted by Stiles' model are listed in Table 4 with the corresponding  $\lambda_{\max}$  values of the pigments (for references of  $\lambda_{\max}$  values, see Table 2). The primary  $E_a$  estimates with their SEMs are plotted against  $1/\lambda_{\max}$  in Fig. 2 in paper IV and compared to the prediction of the Stiles-Lewis-Barlow (SLB) relation.

**Table 4.** The primary estimates of the minimum energy needed for photoactivation ( $E_a$ ) based on papers I–IV. The final column shows the minimum estimates for  $E_a$  obtained by fitting a straight line to the final limb of  $\Delta$ -spectra with the slope predicted by Stiles' simple formula (see the Materials and methods section).

Species & photoreceptor type, chromophore	$\lambda_{\max}$ (nm)	$E_a \pm$ SEM (kcal/mol)	Minimum estimate for $E_a$ (kcal/mol)
<i>Rana catesbeiana</i>			
rod (A1)	502	46.5 $\pm$ 0.8 (III)	45.2
rod (A2)	525	44.2 $\pm$ 0.9 (III)	43.0
<i>Rana temporaria</i>			
rod (A1)	503	45.7 $\pm$ 0.4 (I)	44.3
L-cone (A1)	562	45.5 $\pm$ 0.4 (I)	44.4
L-cone (tadpole) (A2)	629	40.4 $\pm$ 1.6 (I)	38.9
<i>Bufo bufo</i>			
rod (A1)	503	48.8 $\pm$ 0.5 (II)	47.1
<i>Bufo marinus</i>			
“red” rod (A1)	504	44.3 $\pm$ 0.6 (II)	43.4
<i>Xenopus laevis</i>			
rod (A2)	522	43.3 $\pm$ 1.3 (IV)	42.9
<i>Carassius carassius</i>			
rod (A2)	526	42.3 $\pm$ 0.6 (III)	41.9
L-cone (A2)	619	38.3 $\pm$ 0.4 (III)	38.3
<i>Mysis relicta</i>			
Pojoviken Bay population (A2)	530	47.8 $\pm$ 1.8*	44.8
Lake Pääjärvi population (A2)	553	41.5 $\pm$ 0.7*	40.4

\*Activation energy estimates for *Mysis relicta* are based on Pahlberg *et al.* (MS in preparation).

The following main results were obtained considering the relation between  $E_a$  and  $\lambda_{\max}$  based on studied in papers I–IV:

- 1) The simple physical idea of the one-to-one inverse proportion between  $E_a$  and  $\lambda_{\max}$  ( $E_a = \text{const.} \times (1/\lambda_{\max})$ , here termed SLB-relation) is not strictly valid among either the A1 or the A2 pigments studied. For example, two pigments with approximately the same  $\lambda_{\max}$  can have statistically significantly different  $E_a$  estimates (cf. e.g. the  $E_a$  estimates of *Bufo bufo* and *Bufo marinus* rod pigments). On the other hand, pigments with clearly different  $\lambda_{\max}$  can have approximately the same  $E_a$  (cf. e.g.  $E_a$  estimates of *Rana temporaria* rod and L-cone pigments).
- 2) There is, however, a strong correlation between  $E_a$  and  $1/\lambda_{\max}$  ( $r^2 = 0.73$ ), which is not very different from the best-fitting SLB-relation: The regression coefficient of the empirically found correlation was 84% of the one predicted by the best-fitting SLB-relation for the 12 visual pigments studied. The following empirical relation was found between  $E_a$  and  $1/\lambda_{\max}$ :

$$E_a = 7.10 \text{ kcal mol}^{-1} + 19800 \text{ nm kcal mol}^{-1} \cdot \frac{1}{\lambda_{\max}}. \quad (21)$$

- 3) The correlation between  $E_a$  and  $1/\lambda_{\max}$  can be decomposed into chromophore change and the effect of the opsin. For the chromophore change (studied in two A1/A2 pigment pairs) the SLB relation was valid within the experimental error. For the opsin shift in  $\lambda_{\max}$  (studied within the group of A2 pigments) the correlation was shallower than predicted by the SLB relation: the regression coefficient was only 72% of the best SLB fit.

### 5.3 Model for thermal activation of visual pigments (V)

It was shown in paper V that the same temperature-dependence of the dark event rates observed by Baylor *et al.* (1980) for *Bufo marinus* rods can be explained by a considerably higher activation energy ( $E_{a,H}$ ) than the one predicted by the simple Arrhenius theory ( $E_{a,B}$ ), if the internal (vibrational) energy of rhodopsin is involved. With *ca.* 39 vibrational modes ( $n/2$ ) involved in thermal activation or more accurately 79 “square terms” ( $n$ ), the temperature-dependence of the dark event rate observed by Baylor *et al.* (1980) can be explained even with the same

energy barrier as estimated for photoactivation of *Bufo marinus* red rods in paper II (see Fig. 1 in paper V).

In addition, the model predicted the relation between logarithmic thermal activation rates ( $\log k$ ) and  $1/\lambda_{\max}$  for both rod and cone pigments in good agreement with the experimental data available (see Figs 2 and 3 in paper V for rod and cone results, respectively). The predictions for thermal activation rates were obtained by the simplifying assumptions presented in the Materials and methods section: 1) the same number of “square terms” ( $n = 79$ ) was assumed for all pigments, 2) approximately the same energy barrier was assumed for thermal activation and photoactivation ( $E_{a,H} \approx E_a$ ), which was obtained from the empirical relation found in paper IV (see equation 21) and 3) the pre-exponential factor ( $A_H$ ) was assumed to be constant within the groups of rod and cone pigments respectively. The accuracy of these simplifying assumptions is discussed in the original paper V and in section 6.3.

The model was also tested by the pair-wise comparison of the experimentally determined thermal activation rates of the A1/A2 pigment pair of the bullfrog (*Rana catesbeiana*) with the prediction of the model. The experimentally determined ratio  $k_{A2}/k_{A1} \approx 10$  (Donner *et al.*, 1990) is in good agreement with the prediction of the theory ( $k_{A2}/k_{A1} = 7.6$ ) proposed in paper V.

The following conclusions can be drawn from the results presented above (V): the model fulfills both of the requirements listed in section 2.2.3 by explaining 1) the temperature-dependence of thermal activation rates and 2) the correlation between  $1/\lambda_{\max}$  and  $\log k$ . The second prerequisite is fulfilled much better than in the simple model predicted by Horace Barlow (HB), which also predicts the  $\lambda_{\max}$ -dependence for  $k$  based on Arrhenius equation and thereby the Boltzmann distribution. The  $\lambda_{\max}$  relation predicted by the HB hypothesis for  $k$  is, however, far too steep (see Figs 2 & 3 in paper V). Furthermore, the model presented in paper V questions the need for two different molecular routes for visual pigment activation: a low-barrier route for thermal activation and a high-barrier route for photoactivation.

It should also be noted that the model presented in paper V does not require that the thermal barrier and the photoactivation energy are exactly the same. As shown in paper V, a small energy “offset” ( $E_a - E_{a,H}$ ) between the photoactivation energy and the energy barrier for thermal activation is allowable as long as the two are coupled. It was also shown that a model based on the Boltzmann statistics such as the HB model gives a correlation that is always too steep between  $1/\lambda_{\max}$  and  $\log k$  even if the energy “offset” is allowed.

## 6 General discussion

### 6.1 The validity of the physical models for spectral sensitivity and photoactivation energy

We have used the spectral sensitivities of photoreceptors obtained by electroretinogram recording across the isolated retina and microspectrophotometric measurements of absorbance in single photoreceptor outer segments to assess the validity of the physical models used for estimation of the photoactivation energy ( $E_a$ ) (Stiles, 1948; Lewis, 1955). As discussed earlier in section 2.3.2, the underlying assumptions of these models are clear, plausible, and in good agreement with our experimental data. According to these models: 1) a minimum energy is needed for photoactivation and 2) thermal energy can contribute to photon energy in the activation process. In the section below, the models and their applicability for  $E_a$  estimation are further discussed on the basis of the specific results on spectral sensitivity and its temperature-dependence reported in papers I–IV. The purpose is to analyze the limitations of the models and the effect of these on  $E_a$  estimates.

Firstly, one may criticize the models, because they give reasonable estimates of the shape of the spectrum only in the long-wavelength domain. A physical theory explaining the shape of the entire spectrum would, of course, be much better for studying the relation between  $\lambda_{\max}$  and  $\lambda_0$  (or  $E_a$ ). In the absence of such a theory, however, Stiles' and Lewis' models are useful. They do not require any reference to  $\lambda_{\max}$ . They deal only with the long-wavelength slope that appears as a consequence of the fact that a minimum energy is needed for photoactivation and this energy can be partly supplemented by heat. This long-wavelength part of the spectrum starts at  $\lambda_0$  ( $> \lambda_{\max}$ ) and is all that is needed for  $E_a$  estimation.

As shown in the Results section, the absolute slopes of the experimentally determined spectra are shallower than predicted by Stiles' model (see Table 3) and show a small but systematic curvature towards longer wavelengths. This was explained by the refinements of Lewis (1955), which are taken into account in the formula (equation 16) used for  $E_a$  estimation. Using the  $\lambda_0$  values deduced from the  $E_a$  estimates both the slight curvature of the absolute slope (see equation 12) as well as the experimentally observed temperature effects on spectral sensitivity in the long-wavelength domain (see equation 15) are predicted if approximately 2–4 vibrational modes ( $1 \leq m \leq 3$ ) are involved in photoactivation. This analysis also suggests that the final slopes predicted by the models have not yet been reached at the longest wavelengths studied here.

In principle, differences in the temperature effects in the long-wavelength domain could arise from differences in the numbers of vibrational modes ( $m+1$ ) involved in photoactivation of different pigments instead of differences in  $E_a$ . As shown by the above analysis, small differences in  $m$  cannot be excluded without more accurate data of the curvature of the final slope of the measured spectra. However, the variation of  $m$  within this range (1–3) could at most account for a variation in  $E_a$  estimates of  $\Delta mRT = 2 RT \leq ca. 1.2$  kcal/mol in the temperature range studied. Thus, the measured differences in  $E_a$  values cannot by any means be totally explained by differences in the number of vibrational modes involved in photoactivation of different visual pigments. Above all, as long as  $m$  does not vary between different pigments, the interspecies comparisons of photoactivation energies remain essentially unaffected (II).

The accuracy of the  $E_a$  estimates also depends on the assumption that the temperature effects measured in the long-wavelength domain result wholly from changes in the distribution of rhodopsin molecules on thermal energy levels. This assumption is an approximation, which is not strictly valid. Firstly, the differences in relative sensitivity in the long-wavelength domain between “warm” and “cold” spectra depend on the relative positioning of the spectra in the short-wavelength range, which the models assume to be temperature-independent. However, temperature effects are also apparent in the short-wavelength region causing a systematic error in  $E_a$  of at most *ca.* 0.5 kcal/mol (II). This may indicate a temperature effect on  $E_a$  itself (see paper II). Secondly, some slight differences in self-screening may affect the data even in the region, where MSP and ERG spectra are glued together. The worst-case estimate for the ensuing error in  $E_a$  in our case is negligible however ( $< 0.1$  kcal/mol) (II).

The range of  $E_a$  estimates obtained in this thesis (38–49 kcal/mol, I–IV) is comparable with the data available in the literature. As discussed earlier, previous studies about the energetics of photoactivation are based only on a few model pigments. Mathies (1999) estimated that the energy gap between the ground state and the excited state is *ca.* 46 kcal/mol, as the retinal chromophore leaves the excited state. Birge & Vought (2000) estimated the ground-state barrier of the isomerization of the protein bound chromophore to be *ca.* 45 kcal/mol based on photocalorimetric studies on bovine rhodopsin (Cooper, 1979; Schick *et al.*, 1987). Bleaching studies on frog and bovine rhodopsin extracts (Lythgoe & Quilliam, 1938; St. George, 1952) give photoactivation energy estimates in the range 44–49 kcal/mol.

## 6.2 The relation between the wavelength of maximum absorbance ( $\lambda_{\max}$ ) and photoactivation energy ( $E_a$ )

In papers I–IV, it was shown that there is no tight physical coupling between  $E_a$  and  $1/\lambda_{\max}$ , but still a general correlation between these two. In the case of the chromophore switch, the correlation is in agreement with the one predicted by the SLB relation ( $E_a = \text{const.} \times 1/\lambda_{\max}$ ). In the case of opsin shift, a shallower-than-predicted correlation is found between  $E_a$  and  $1/\lambda_{\max}$ . In the following section, the physical interpretation of these results is discussed.

The result that  $E_a$  and  $\lambda_{\max}$  can be tuned at least partly independently can be interpreted with the aid of a schematic diagram representing the potential energy surfaces for photoactivation (see Fig. 3). As a first approximation one may consider a situation, where only the distance between the ground state and the 1st electronically excited state is changed but the shapes of both of the potential energy surfaces remain the same. Then one would predict that the minimum energy needed for photoactivation ( $E_a$ ) would change by the same factor as the energy corresponding to the most probable transition, and thereby  $\lambda_{\max}$ . On the other hand, if the change in the distance between the potential energy surfaces is accompanied by changes in their shapes, it follows that  $E_a$  and  $\lambda_{\max}$  would change at least partly independently. Thus, the results of paper IV could be interpreted in the following way: 1) When the chromophore is switched, the shapes of the energy surfaces remain mainly unchanged but the gap between the surfaces is changed. 2) Opsin-induced changes in  $\lambda_{\max}$  and  $E_a$  change the shapes of the potential energy surfaces to a larger extent, allowing some degree of independent tuning of  $E_a$  and  $\lambda_{\max}$ .

Because the chromophore switch from A1 to A2 seemed to follow the SLB relation (I, III, IV), it can be seen as a simple physical operation, where the red-shift of the  $\lambda_{\max}$  of the pigment is tightly coupled to the lowering of  $E_a$ . To the extent that the photoactivation energy and the energy barrier for thermal activation are coupled, the chromophore switch would always entail a predictable increase in the thermal noise. It should be noted, however, that the experimental data is based only on two A1/A2 pairs studied (IV). It is a trivial truth that the examination of a large number of A1/A2 pairs combined to different opsins could reveal deviations from the SLB relation. It seems unlikely, however, that different opsins should affect the  $E_a$ - $\lambda_{\max}$  relation of the chromophore switch very differently (IV).

The model presented in paper V helps to interpret the shallower than predicted relation between  $E_a$  and  $1/\lambda_{\max}$  observed when different opsins are compared (IV).

Given that  $E_a$  and  $\lambda_{\max}$  can be tuned at least partly independently and assuming that the energy barrier for thermal activation correlates with  $E_a$  (V), one could expect the  $E_a$  values of the long-wavelength-sensitive pigments to be tuned as high as possible by evolution (IV). This would flatten the relation between  $E_a$  and  $\lambda_{\max}$  compared with the simple SLB relation.

### **6.3 The relation between the wavelength of maximum absorbance ( $\lambda_{\max}$ ) and thermal activation rates of visual pigments**

The model presented in paper V offers an explanation for the large discrepancy between the apparent Arrhenius activation energies and the photoactivation energies of visual pigments. At the same time, it explains the experimentally determined relation between thermal event rates ( $k$ ) and the position of the peak absorbance ( $\lambda_{\max}$ ) of visual pigments. The model demonstrates that it is not necessary to look for a low-barrier route for thermal activation process. However, the model is based on a number of assumptions the accuracy of which has to be discussed (see below) and also extended to further experimental tests.

#### *The correlation between photoactivation energy and thermal activation energy*

Although the model was tested under the simplest assumption that the minimum energy needed for photoactivation is exactly the same as the energy barrier for thermal activation, it works well also if a small “offset” is assumed between these two energies. As emphasized in paper V, the only requirement is that these two energies correlate. This assumption is in agreement with a recent estimate by Mathies (1999) according to which the ground-to-excited state energy gap is only *ca.* 5–6 kcal/mol as the retinal chromophore leaves the excited state. It can be expected, that the extremely high speed of photoactivation requires the energy gap between the ground-state and the excited-state energy surfaces to be small in the direction of the activation coordinate (Mathies, 1999; cf. paper V).

Why should the thermal reaction and the photon-triggered reaction (after relaxation to the ground-state surface) proceed along the same route on the ground-state potential energy surface? This question cannot be fully answered without precise modeling of both activation processes. At least theoretically, the molecular route to metarhodopsin II could be very different for photic and thermal activations. By entirely intuitive reasoning, one could, however, expect the two to proceed along the same route. Maximizing the thermal stability of the molecule would require high energy barriers for activation in all directions on the ground-

state surface. In the direction of photoactivation, however, the high quantum efficiency of photoactivation requires the ground-state potential energy surface to be no higher than the excited-state surface. Since similar constraints to the height of the ground-state potential energy barrier are not *a priori* to be expected in the other directions of the ground-state potential energy surface, the lowest energy barrier could be expected to be found in the direction of photoactivation reaction. This teleological argument supports the idea that photic and thermal activation should proceed along the same route (V).

*The number of vibrational modes ( $n/2$ ) involved in activation*

The model presented in paper V is based on the theory of Hinshelwood (1933), which predicts that the thermal energy involved in vibrational modes is involved in the chemical reactions of complex molecules. The curvature of the final slopes of spectral sensitivity data plotted as logarithmic sensitivity vs. wavenumber suggests that vibrational energy is also involved in photic activation (Lewis, 1955). With respect to the number of vibrational modes involved, however, the proposed model raises two important questions: First, is the total number of vibrational modes (*ca.* 39) needed for thermal activation plausible? Second, why is the number of vibrational modes different for photic and thermal activation processes?

The first question can be addressed by relating the number of vibrational modes needed for thermal activation to the total number available within the molecule. As shown in paper V, there are *ca.* 141 vibrational modes in the 11-*cis* retinaldehyde. Thus, there are more than enough vibrational modes already in the chromophore part of the molecule, which means that the model does not require the vibrational modes of the opsin part to be involved. If *ca.* 39 vibrations are involved in thermal activation, this comprises less than one third of those available in the chromophore. This is in good agreement with results obtained for the thermal decomposition of some other organic molecules. For instance, for the activation of cyclopropane, the theory of Hinshelwood suggest that one third of the 21 vibrations are involved in activation (see Moore (1962, p. 282)). Furthermore, Hinshelwood (1942, pp. 81–82) found that  $n = 45-50$  for the decomposition of azoisopropane and  $n = ca. 25$  for azomethane, respectively (see also St. George, 1952). It should also be noted that even less than 39 vibrations are needed for rhodopsin if there is some “offset” between the minimum energy needed for photoactivation and the energy barrier for thermal activation, as discussed above. Moreover, it is known that there is energy transfer from the opsin to the chromophore.

The second question emerges from a comparison of the long-wavelength domain of visual pigment spectra with the prediction of Lewis' model. As discussed in section 6.1, the spectral sensitivity data is in agreement with the idea that approximately 2–4 vibrational modes are involved in the photoactivation process. This number is much smaller than that obtained in paper V for thermal activation. One possibility for the difference was suggested by St. George (1952): “*As to the portion of the molecule which is involved in activation, the increase in  $n$  towards long wave lengths fits the idea that an increasingly larger part of the protein comes into play as the thermal component of the activation becomes larger*”. Intuitively one could also assume that the process involving the absorption of the photon in a very short time window can involve a different number of vibrational modes than a purely thermal process. However, this whole question requires further study.

#### *The pre-exponential factor*

As discussed in paper V, the rates of thermal isomerizations plotted on logarithmic ordinates against  $1/\lambda_{\max}$  have approximately the same slopes for rods and cones, but the difference in absolute values is *ca.* 4 log-units. This supports the idea that the systematic variation arises from the  $\lambda_{\max}$ -dependence of the energy barrier for thermal activation. The difference in absolute values between rods and cones is accounted for by the pre-exponential factor in this model. What, then, is the physical interpretation of the pre-exponential factor and why is it so different in rods and cones? These questions are discussed in some detail in paper V. The difference may arise from the more “closed” structure of the chromophore pocket of rods compared to cones. Resolving this question must await more accurate models of rod and cone opsins.

## 7 Conclusions

1. There is no strict physical coupling between the photoactivation energy ( $E_a$ ) and the wavelength of maximum absorbance ( $\lambda_{\max}$ ), e.g. of the type  $E_a = \text{const.} \times 1/\lambda_{\max}$  (here termed the SLB relation). This is true for both A1 and A2 pigments.
2. However,  $E_a$  and  $1/\lambda_{\max}$  showed a significant correlation in the whole set of pigments studied ( $r^2 = 0.73$ ) and the regression line did not differ very much from the best-fitting SLB relation.
3. For  $\lambda_{\max}$  shifts due to chromophore change (studied in two A1/A2 pigment pairs) the SLB relation was valid within experimental error. For opsin-dependent  $\lambda_{\max}$  shifts (studied within the group of A2 pigments) the experimental relation was shallower than the SLB prediction.
4. All earlier estimates of thermal activation energies have been calculated from data on the temperature-dependence of thermal activation rates without observing that the energy is derived from a large number of vibrational modes of the visual pigment molecule. Yet the statistics (thus temperature-dependence) of thermal activation depends critically on the number of modes involved.
5. A new model taking this into account is proposed. It is shown that the low estimates for thermal activation energies hitherto accepted (20–25 kcal/mol) may only indicate the failure to do so in the Arrhenius model.
6. Given that energies for activation by light and by heat may in fact be quite similar, the two processes may follow the same molecular route from a very early stage. However, the numbers of vibrational modes contributing to activation appear to be smaller in reactions involving photon absorption than in purely thermal reactions.
7. The model, together with the general relation between  $E_a$  and  $\lambda_{\max}$  experimentally determined in the present work, correctly predicts the empirical correlation between the rate of thermal activations and  $\lambda_{\max}$  for rod as well as cone pigments.

## References

- Aho, A.-C., Donner, K., Hydén, C., Larsen, L. O., & Reuter, T. (1988). Low retinal noise in animals with low body temperature allows high visual sensitivity. *Nature* **334**, 348–350.
- Aho, A.-C., Donner, K., Hydén, C., Reuter, T., & Orlov, O. Y. (1987). Retinal noise, the performance of retinal ganglion cells, and visual sensitivity in the dark-adapted frog. *Journal of the Optical Society of America A-Optics & Image Science* **4**, 2321–2329.
- Aho, A.-C., Donner, K., & Reuter, T. (1993). Retinal origins of the temperature effect on absolute visual sensitivity in frogs. *Journal of Physiology* **463**, 501–521.
- Alpern, M., Fulton, A. B., & Baker, B. N. (1987). “Self-screening” of rhodopsin in rod outer segments. *Vision Research* **27**, 1459–1470.
- Arnis, S. & Hofmann, K. P. (1993). Two different forms of metarhodopsin II: Schiff base deprotonation precedes proton uptake and signaling state. *Proceedings of the National Academy of Sciences of the United States of America* **90**, 7849–7853.
- Arshavsky, V. Y., Lamb, T. D., & Pugh, E. N., Jr. (2002). G proteins and phototransduction. *Annual Review of Physiology* **64**, 153–187.
- Autrum, H. (1943). Über kleinste Reize bei Sinnesorganen. *Biologisches Zentralblatt* **63**, 209–236.
- Barlow, H. B. (1956). Retinal noise and absolute threshold. *Journal of the Optical Society of America* **46**, 634–639.
- Barlow, H. B. (1957). Purkinje shift and retinal noise. *Nature* **179**, 255–256.
- Barlow, H. B. (1958). Intrinsic noise of cones. In *Visual problems of colour*, Vol II, pp. 617–630. London: Her Majesty’s Stationery Office.
- Barlow, H. B. (1977). Retinal and central factors in human vision limited by noise. In *Vertebrate Photoreception*, eds. Barlow, H. B. & Fatt, P., pp. 337–358. London-New York-San Francisco: Academic Press.
- Barlow, H. B. (1982). What causes trichromacy? A theoretical analysis using comb-filtered spectra. *Vision Research* **22**, 635–643.
- Barlow, H. B. (1988). The thermal limit to seeing. *Nature* **334**, 296–297.
- Barlow, R. B., Birge, R. R., Kaplan, E., & Tallent, J. R. (1993). On the molecular origin of photoreceptor noise. *Nature* **366**, 64–66.
- Batni, S., Scalzetti, L., Moody, S. A., & Knox, B. E. (1996). Characterization of the *Xenopus* rhodopsin gene. *Journal of Biological Chemistry* **271**, 3179–3186.
- Baylor, D. A., Lamb, T. D., & Yau, K. W. (1979). Responses of retinal rods to single photons. *Journal of Physiology* **288**, 613–634.

- Baylor, D. A., Matthews, G., & Yau, K. W. (1980). Two components of electrical dark noise in toad retinal rod outer segments. *Journal of Physiology* **309**, 591–621.
- Baylor, D. A., Nunn, B. J., & Schnapf, J. L. (1984). The photocurrent, noise and spectral sensitivity of rods of the monkey *Macaca fascicularis*. *Journal of Physiology* **357**, 575–607.
- Baylor, D. A., Nunn, B. J., & Schnapf, J. L. (1987). Spectral sensitivity of cones of the monkey *Macaca fascicularis*. *Journal of Physiology* **390**, 145–160.
- Birge, R. R. (1990). Nature of the primary photochemical events in rhodopsin and bacteriorhodopsin. *Biochimica et Biophysica Acta* **1016**, 293–327.
- Birge, R. R. & Barlow, R. B. (1995). On the molecular origins of thermal noise in vertebrate and invertebrate photoreceptors. *Biophysical Chemistry* **55**, 115–126.
- Birge, R. R. & Vought, B. W. (2000). Energetics of rhodopsin photobleaching: photocalorimetric studies of energy storage in early and later intermediates. *Methods in Enzymology* **315**, 143–163.
- Boll, F. (1876). Zur Anatomie und Physiologie der Retina. *Monatsberichte der Königlich-Preussischen Akademie der Wissenschaften zu Berlin* **23**, 783–787.
- Boll, F. (1877). Zur Anatomie und Physiologie der Retina. *Archiv für Anatomie und Physiologie. (Physiologische Abteilung)*, 4–36.
- Bolnick, D. A., Walther, A. E., & Sillman, A. J. (1979). Barium suppresses slow PIII in perfused bullfrog retina. *Vision Research* **19**, 117–119.
- Bowmaker, J. K. (1984). Microspectrophotometry of vertebrate photoreceptors. A brief review. *Vision Research* **24**, 1641–1650.
- Bownds, D. (1967). Site of attachment of retinal in rhodopsin. *Nature* **216**, 1178–1181.
- Bridges, C. D. B. (1956). The visual pigments of the rainbow trout (*Salmo irideus*). *Journal of Physiology* **134**, 620–629.
- Bridges, C. D. B. (1965). Variability and relationships of fish visual pigments. *Vision Research* **5**, 239–251.
- Bridges, C. D. B. (1967). Spectroscopic properties of porphyropsins. *Vision Research* **7**, 349–369.
- Bridges, C. D. B. (1972). The rhodopsin-porphyrpsin visual system. In *Handbook of Sensory Physiology, VII/1. Photochemistry of Vision*, ed. Dartnall, H. J. A., pp. 417–480. Berlin-Heidelberg-New York: Springer.
- Brown, P. K. (1961). A system for microspectrophotometry employing a commercial recording spectrophotometer. *Journal of the Optical Society of America* **51**, 1000–1008.
- Brown, P. K. & Wald, G. (1964). Visual pigments in single rods and cones of the human retina. *Science* **144**, 45–52.

- Burns, M. E. & Baylor, D. A. (2001). Activation, deactivation, and adaptation in vertebrate photoreceptor cells. *Annual Review of Neuroscience* **24**, 779–805.
- Burns, M. E. & Lamb, T. D. (2003). Visual transduction by rod and cone photoreceptors. In *The Visual Neurosciences*, eds. Chalupa, L. M. & Werner, L. S., pp. 215–233. MIT Press.
- Cooper, A. (1979). Energy uptake in the first step of visual excitation. *Nature* **282**, 531–533.
- Cooper, A. (1981). Rhodopsin photoenergetics: lumirhodopsin and the complete energy profile. *FEBS Letters* **123**, 324–326.
- Cooper, A. & Converse, C. A. (1976). Energetics of primary processes in visual excitation: photocalorimetry of rhodopsin in rod outer segment membranes. *Biochemistry* **15**, 2970–2978.
- Cornwall, M. C., MacNichol, E. F., Jr., & Fein, A. (1984). Absorbance and spectral sensitivity measurements of rod photoreceptors of the tiger salamander, *Ambystoma tigrinum*. *Vision Research* **24**, 1651–1659.
- Corson, D. W. & Fein, A. (1980). The pH dependence of discrete wave frequency in *Limulus* ventral photoreceptors. *Brain Research* **193**, 558–561.
- Crescitelli, F. (1977). Ionochromic behavior of Grecko visual pigments. *Science* **195**, 187–188.
- Dartnall, H. J. A. (1953). The interpretation of spectral sensitivity curves. *British Medical Bulletin* **9**, 24–30.
- Dartnall, H. J. A. (1955). Visual pigments of the bleak (*Alburnus lucidus*). *Journal of Physiology* **128**, 131–156.
- Dartnall, H. J. A. (1968). The photosensitivities of visual pigments in the presence of hydroxylamine. *Vision Research* **8**, 339–358.
- Dartnall, H. J. A. & Lythgoe, J. N. (1965). The spectral clustering of visual pigments. *Vision Research* **5**, 81–100.
- Dawis, S. M. (1981). Polynomial expressions of pigment nomograms. *Vision Research* **21**, 1427–1430.
- Denton, E. J. & Pirenne, M. H. (1954). The visual sensitivity of the toad *Xenopus laevis*. *Journal of Physiology* **125**, 181–207.
- de Vries, H. (1948). Der Einfluss der Temperatur des Auges auf die spektrale Empfindlichkeitskurve. *Experientia* **4**, 357–358.
- Donner, K. (1992). Noise and the absolute thresholds of cone and rod vision. *Vision Research* **32**, 853–866.

- Donner, K., Firsov, M. L., & Govardovskii, V. I. (1990). The frequency of isomerization-like 'dark' events in rhodopsin and porphyropsin rods of the bull-frog retina. *Journal of Physiology* **428**, 673–692.
- Donner, K. & Hemilä, S. (1985). Rhodopsin phosphorylation inhibited by adenosine in frog rods: lack of effects on excitation. *Comparative Biochemistry and Physiology* **81A**, 431–439.
- Donner, K., Hemilä, S., & Koskelainen, A. (1988). Temperature-dependence of rod photoresponses from the aspartate- treated retina of the frog (*Rana temporaria*). *Acta Physiologica Scandinavica* **134**, 535–541.
- Ebrey, T. & Koutalos, Y. (2001). Vertebrate photoreceptors. *Progress in Retinal & Eye Research* **20**, 49–94.
- Ebrey, T. G. & Honig, B. (1977). New wavelength dependent visual pigment nomograms. *Vision Research* **17**, 147–151.
- Fager, L. Y. & Fager, R. S. (1979). Halide control of color of the chicken cone pigment iodopsin. *Experimental Eye Research* **29**, 401–408.
- Filipek, S., Stenkamp, R. E., Teller, D. C., & Palczewski, K. (2003). G protein-coupled receptor rhodopsin: A prospectus. *Annual Review of Physiology* **65**, 851–879.
- Firsov, M. L., Donner, K., & Govardovskii, V. I. (2002). pH and rate of "dark" events in toad retinal rods: test of a hypothesis on the molecular origin of photoreceptor noise. *Journal of Physiology* **539**, 3–46.
- Firsov, M. L. & Govardovskii, V. I. (1990). Dark noise of visual pigments with different absorption maxima. *Sensornye Sistemy* **4**, 25–34 (in Russian).
- Fong, S. L., Landers, R. A., & Bridges, C. D. B. (1985). Varieties of rhodopsin in frog rod outer segment membranes: analysis by isoelectric focusing. *Vision Research* **25**, 1387–1397.
- Freedman, K., Becker, R. S., Hannak, D., & Bayer, E. (1986). Investigation into the spectroscopy and photoisomerization of a series of poly(ethylene glycol) peptide Schiff bases of 11-*cis* retinal. *Photochemistry & Photobiology* **43**, 291–295.
- Fyhrquist, N. (1999). Spectral and thermal properties of amphibian visual pigments related to molecular structure. *Dissertationes Biocentri Viikki Universitatis Helsingiensis* **18/99**.
- Fyhrquist, N., Donner, K., Hargrave, P. A., McDowell, J. H., Popp, M. P., & Smith, W. C. (1998a). Rhodopsins from three frog and toad species: sequences and functional comparisons. *Experimental Eye Research* **66**, 295–305.
- Fyhrquist, N., Govardovskii, V., Leibrock, C., & Reuter, T. (1998b). Rod pigment and rod noise in the European toad *Bufo bufo*. *Vision Research* **38**, 483–486.
- Goldsmith, T. H. (1990). Optimization, constraint, and history in the evolution of eyes. *The Quarterly Review of Biology* **65**, 281–322.

- Govardovskii, V. I. (1999). *Computer-controlled recording microspectrophotometer* (Manual), Helsinki, 33 p.
- Govardovskii, V. I., Fyhrquist, N., Reuter, T., Kuzmin, D. G., & Donner, K. (2000). In search of the visual pigment template. *Visual Neuroscience* **17**, 509–528.
- Govardovskii, V. I. & Zueva, L. V. (2000). Fast microspectrophotometer for studying the photolysis of visual pigments *in situ*. *Sensornye Sistemy* **14**, 288–296. (In Russian).
- Han, M., Lin, S. W., Minkova, M., Smith, S. O., & Sakmar, T. P. (1996a). Functional interaction of transmembrane helices 3 and 6 in rhodopsin. Replacement of phenylalanine 261 by alanine causes reversion of phenotype of a glycine 121 replacement mutant. *Journal of Biological Chemistry* **271**, 32337–32342.
- Han, M., Lin, S. W., Smith, S. O., & Sakmar, T. P. (1996b). The effects of amino acid replacements of glycine 121 on transmembrane helix 3 of rhodopsin. *Journal of Biological Chemistry* **271**, 32330–32336.
- Hanaoka, T. & Fujimoto, K. (1957). Absorption spectrum of a single cone in carp retina. *Japanese Journal of Physiology* **7**, 276–285.
- Hargrave, P. A., McDowell, J. H., Curtis, D. R., Wang, J. K., Juszczak, E., Fong, S. L., Rao, J. K., & Argos, P. (1983). The structure of bovine rhodopsin. *Biophysics of Structure & Mechanism* **9**, 235–244.
- Hárosi, F. I. & MacNichol, E. F., Jr. (1974). Dichroic microspectrophotometer: a computer-assisted, rapid, wavelength-scanning photometer for measuring linear dichroism in single cells. *Journal of the Optical Society of America* **64**, 903–918.
- Hecht, S., Schlaer, S., & Pirenne, M. H. (1942). Energy, quanta, and vision. *Journal of General Physiology* **25**, 819–840.
- Hecht, S. & Williams, R. E. (1922). The visibility of monochromatic radiation and the absorption spectrum of visual purple. *The Journal of General Physiology* **5**, 1–33.
- Hinshelwood, C. N. (1933). *The Kinetics of Chemical Change in Gaseous Systems*. Oxford, United Kingdom: Clarendon Press.
- Hinshelwood, C. N. (1942). *The Kinetics of Chemical Change*. Oxford, United Kingdom: Clarendon Press.
- Hisatomi, O., Takahashi, Y., Taniguchi, Y., Tsukahara, Y., & Tokunaga, F. (1999). Primary structure of a visual pigment in bullfrog green rods. *FEBS Letters* **447**, 44–48.
- Hong, K., Knudsen, P. J., & Hubbell, W. L. (1982). Purification of rhodopsin on hydroxyapatite columns, detergent exchange, and recombination with phospholipids. *Methods in Enzymology* **81**, 144–150.
- Hough, E. A. & Ruddock, K. H. (1969). The Purkinje shift. *Vision Research* **9**, 313–315.
- Hubbard, R. (1958a). The thermal stability of rhodopsin and opsin. *Journal of General Physiology* **42**, 259–280.

- Hubbard, R. (1958b). Bleaching of rhodopsin by light and by heat. *Nature* **181**, 1126.
- Hubbard, R. (1966). The stereoisomerization of 11-*cis*-retinal. *Journal of Biological Chemistry* **241**, 1814–1818.
- Hubbard, R., Bownds, D., & Yoshizawa, T. (1965). The chemistry of visual photoreception. *Cold Spring Harbor Symposia on Quantitative Biology*, Abstract book, 301–315.
- Hubbard, R., Brown, P. K., & Kropf, A. (1959). Vertebrate lumi- and metarhodopsins. *Nature* **183**, 442–446.
- Hug, S. J., Lewis, J. W., Einterz, C. M., Thorgeirsson, T. E., & Kliger, D. S. (1990). Nanosecond photolysis of rhodopsin: evidence for a new, blue-shifted intermediate. *Biochemistry* **29**, 1475–1485.
- Imai, H., Mizukami, T., Imamoto, Y., & Shichida, Y. (1994). Direct observation of the thermal equilibria among lumirhodopsin, metarhodopsin I, and metarhodopsin II in chicken rhodopsin. *Biochemistry* **33**, 14351–14358.
- Jokela-Määttä, M., Pahlberg, J., Lindström, M., Porter, M., Zak, P., Ostrovskii, M., Cronin, T., & Donner, K. Visual pigments and spectral sensitivity in three subspecies of *Mysis relicta* (Crustacea). (MS in preparation)
- Jurkowitz, L. (1959). Photochemical and stereochemical properties of carotenoids at low temperatures. (I) Photochemical behaviour of retinene. *Nature* **184**, 614–617.
- Kakitani, T. (1999). General discussion II. *Novartis Foundation Symposium* **224**, 90–101.
- Kakitani, T., Akiyama, R., Hatano, Y., Imamoto, Y., Shichida, Y., Verdegem, P., & Lugtenburg, J. (1998). Deuterium substitution effect on the excited-state dynamics of rhodopsin. *Journal of Physical Chemistry B* **102**, 1334–1339.
- Kayada, S., Hisatomi, O., & Tokunaga, F. (1995). Cloning and expression of frog rhodopsin cDNA. *Comparative Biochemistry & Physiology. Part B, Biochemistry & Molecular Biology* **110**, 599–604.
- Kito, Y., Suzuki, T., Azuma, M., & Sekoguti, Y. (1968). Absorption spectrum of rhodopsin denatured with acid. *Nature* **218**, 955–957.
- Kleinschmidt, J. & Harosi, F. I. (1992). Anion sensitivity and spectral tuning of cone visual pigments in situ. *Proceedings of the National Academy of Sciences of the United States of America* **89**, 9181–9185.
- Knowles, A. (1976). The effect of chloride ions upon chicken visual pigments. *Biochemical & Biophysical Research Communications* **73**, 56–62.
- Knowles, A. (1980). The chloride effect in chicken red cone receptors. *Vision Research* **20**, 475–483.
- Kochendoerfer, G. G., Lin, S. W., Sakmar, T. P., & Mathies, R. A. (1999). How color visual pigments are tuned. *Trends in Biochemical Sciences* **24**, 300–305.

- Koskelainen, A., Hemilä, S., & Donner, K. (1994). Spectral sensitivities of short- and long-wavelength sensitive cone mechanisms in the frog retina. *Acta Physiologica Scandinavica* **152**, 115–124.
- Kühne, W. (1877) Zur Photochemie der Netzhaut. *Verhandlungen des naturhistorisch-medizinischen Vereins zu Heidelberg* **1**, 484–492.
- Kühne, W. (1879). Chemische Vorgänge in der Netzhaut. In *Handbuch der Physiologie*, ed. Herrmann, L., pp. 235–239, Leipzig: Vogel. [An English translation by Ruth Hubbard and George Wald appears in *Vision Research* **17**, 1269–1316 (1977)].
- Lamb, T. D. (1984). Effects of temperature changes on toad rod photocurrents. *Journal of Physiology* **346**, 557–578.
- Lamb, T. D. (1995). Photoreceptor spectral sensitivities: common shape in the long-wavelength region. *Vision Research* **35**, 3083–3091.
- Lewis, P. R. (1955). A theoretical interpretation of spectral sensitivity curves at long wavelengths. *Journal of Physiology* **130**, 45–52.
- Liebman, P. A. (1972). Microspectrophotometry of photoreceptors. In *Handbook of Sensory Physiology, VII/1. Photochemistry of Vision*, ed. Dartnall, H. J. A., pp. 481–528. Berlin-Heidelberg-New York: Springer.
- Liebman, P. A. & Entine, G. (1964). Sensitive low-light-level microspectrophotometer detection of photosensitive pigments of retinal cones. *Journal of the Optical Society of America* **54**, 1451–1459.
- Lin, S. W. & Sakmar, T. P. (1996). Specific tryptophan UV-absorbance changes are probes of the transition of rhodopsin to its active state. *Biochemistry* **35**, 11149–11159.
- Lin, S. W. & Sakmar, T. P. (1999). Colour tuning mechanisms of visual pigments. *Novartis Foundation Symposium* **224**, 124–135.
- Loeb, J. N., Brown, P. K., & Wald, G. (1959). Photochemical and stereochemical properties of carotenoids at low temperatures. (2) *Cis-trans* isomerism and steric hindrance. *Nature* **184**, 617–620.
- Loppnow, G. R. & Mathies, R. A. (1988). Excited-state structure and isomerization dynamics of the retinal chromophore in rhodopsin from resonance Raman intensities [published erratum appears in *Biophysical Journal* (1989) **55**(3), following 583]. *Biophysical Journal* **54**, 35–43.
- Lythgoe, J. N. & Quilliam, J. P. (1938). The thermal decomposition of visual purple. *Journal of Physiology* **93**, 24–38.
- Ma, J., Znoiko, S., Othersen, K. L., Ryan, J. C., Das, J., Isayama, T., Kono, M., Oprian, D. D., Corson, D. W., Cornwall, M. C., Cameron, D. A., Harosi, F. I., Makino, C. L., & Crouch, R. K. (2001). A visual pigment expressed in both rod and cone photoreceptors. *Neuron* **32**, 451–461.

- MacNichol, E. F. (1978). A photon-counting microspectrophotometer for the study of single vertebrate photoreceptor cells. In *Frontiers of Visual Science*, eds. Cool, S. J. & Smith, E. L., pp. 194–208. New York: Springer.
- MacNichol, E. F., Jr. (1986). A unifying presentation of photopigment spectra. *Vision Research* **26**, 1543–1556.
- Mansfield, R. J. W. (1985). Primate photopigments and cone mechanisms. In *The Visual System*, eds. Fein, A. & Levine, J. S., pp. 89–106. New York: Liss.
- Marks, W. B. (1963). Difference spectra of the visual pigments in single goldfish cones. Ph.D. Thesis. Johns Hopkins University.
- Marks, W. B., Dobbelle, W. H., & MacNichol, E. F. (1964). Visual pigments of single primate cones. *Science* **143**, 1181–1182.
- Mathies, R. A. (1999). Photons, femtoseconds and dipolar interactions: a molecular picture of the primary events in vision. *Novartis Foundation Symposium* **224**, 70–84.
- Matthews, G. (1984). Dark noise in the outer segment membrane current of green rod photoreceptors from toad retina. *Journal of Physiology* **349**, 607–618.
- Matthews, R. G., Hubbard, R., Brown, P. K., & Wald, G. (1963). Tautomeric forms of metarhodopsin. *Journal of General Physiology* **47**, 215–240.
- Maximov, V. V. (1988). Approximation of visual pigment absorbance spectra. *Sensornyye Sistemy* **2**, 3–9.
- McFarland, W. N. & Allen, D. M. (1977). The effect of extrinsic factors on two distinctive rhodopsin-porphyrin systems. *Canadian Journal of Zoology* **55**, 1000–1009.
- Metzler, D. E. & Harris, C. M. (1978). Shapes of spectral bands of visual pigments. *Vision Research* **18**, 1417–1420.
- Moore, W. J. (1962). *Physical Chemistry*. 3rd ed. Eaglewood Cliffs N.J.: Prentice Hall.
- Mortimer, R. G. (1993). *Physical Chemistry*, pp. 821–823, Redwood City, California: The Benjamin/Cummings Publishing Company.
- Motto, M. G., Sheves, M., Tsujimoto, K., Balogh-Nair, V., & Nakanishi, K. (1980). Opsin shifts in bovine rhodopsin and bacteriorhodopsin. Comparison of two external charge models. *Journal of American Chemical Society* **102**, 7947–7949.
- Munz, F. W. & Schwanzara, S. A. (1967). A nomogram for retinene<sub>2</sub>-based visual pigments. *Vision Research* **7**, 111–120.
- Naka, K. I. & Rushton, W. A. (1966). S-potentials from colour units in the retina of fish (Cyprinidae). *Journal of Physiology* **185**, 536–555.

- Nakagawa, M., Iwasa, T., Kikkawa, S., Tsuda, M., & Ebrey, T. G. (1999). How vertebrate and invertebrate visual pigments differ in their mechanism of photoactivation. *Proceedings of the National Academy of Sciences of the United States of America* **96**, 6189–6192.
- Nathans, J. (1990a). Determinants of visual pigment absorbance: identification of the retinylidene Schiff's base counterion in bovine rhodopsin. *Biochemistry* **29**, 9746–9752.
- Nathans, J. (1990b). Determinants of visual pigment absorbance: role of charged amino acids in the putative transmembrane segments. *Biochemistry* **29**, 937–942.
- Nathans, J. & Hogness, D. S. (1983). Isolation, sequence analysis, and intron-exon arrangement of the gene encoding bovine rhodopsin. *Cell* **34**, 807–814.
- Nathans, J. & Hogness, D. S. (1984). Isolation and nucleotide sequence of the gene encoding human rhodopsin. *Proceedings of the National Academy of Sciences of the United States of America* **81**, 4851–4855.
- Nathans, J., Thomas, D., & Hogness, D. S. (1986). Molecular genetics of human color vision: the genes encoding blue, green, and red pigments. *Science* **232**, 193–202.
- Novitskii, I. I., Zak, P. P., & Ostrovskii, M. A. (1989). The effect of anions on spectral properties of iodopsin and native cones in the frog retina (microspectrophotometric study). *Bioorganicheskaiia Khimiia* **15**, 1037–1043 (in Russian).
- Okada, T., Ernst, O. P., Palczewski, K., & Hofmann, K. P. (2001). Activation of rhodopsin: new insights from structural and biochemical studies. *Trends in Biochemical Sciences* **26**, 318–324.
- Ovchinnikov, Y. A. (1982). Rhodopsin and bacteriorhodopsin: structure-function relationships. *FEBS Letters* **148**, 179–191.
- Ovchinnikov, Y. A., Abdulaev, N. G., Feigina, M. Y., Artamonov, I. D., Zolotarev, A. S., Kostina, M. B., Bogachuk, A. S., Miroshnikov, A. I., Martynov, V. I., & Kudelin, A. B. (1982). The complete amino acid sequence of visual rhodopsin. *Bioorganicheskaiia Khimiia* **8**, 1011–1014.
- Pahlberg, J., Lindström, M., Ala-Laurila, P., Fyhrquist-Vanni, N., Koskelainen, A., & Donner, K. The photoactivation energy of the visual pigment in two populations of *Mysis relicta* (*Mysidacea*, *Crustacea*) determined from temperature effects on spectral sensitivity. (MS in preparation)
- Palacios, A. G., Goldsmith, T. H., & Bernard, G. D. (1996). Sensitivity of cones from a cyprinid fish (*Danio aequipinnatus*) to ultraviolet and visible light. *Visual Neuroscience* **13**, 411–421.
- Palczewski, K., Kumasaka, T., Hori, T., Behnke, C. A., Motoshima, H., Fox, B. A., Le, T. I., Teller, D. C., Okada, T., Stenkamp, R. E., Yamamoto, M., & Miyano, M. (2000). Crystal structure of rhodopsin: A G protein-coupled receptor. *Science* **289**, 739–745.

- Partridge, J. C. & DeGrip, W. J. (1991). A new template for rhodopsin (vitamin A1 based) visual pigments. *Vision Research* **31**, 619–630.
- Reuter, T. (1969). Visual pigments and ganglion cell activity in the retinae of tadpoles and adult frogs (*Rana temporaria* L.). *Acta Zoologica Fennica* **122**, 1–64.
- Reuter, T. E., White, R. H., & Wald, G. (1971). Rhodopsin and porphyropsin fields in the adult bullfrog retina. *Journal of General Physiology* **58**, 351–371.
- Rieke, F. (2000). Mechanisms of single-photon detection in rod photoreceptors. *Methods in Enzymology* **316**, 186–202.
- Rieke, F. & Baylor, D. A. (1996). Molecular origin of continuous dark noise in rod photoreceptors. *Biophysical Journal* **71**, 2553–2572.
- Rieke, F. & Baylor, D. A. (1998). Single-photon detection by rod cells of the retina. *Reviews of Modern Physics* **70**, 1027–1036.
- Rieke, F. & Baylor, D. A. (2000). Origin and functional impact of dark noise in retinal cones. *Neuron* **26**, 181–186.
- Sakitt, B. (1972). Counting every quantum. *Journal of Physiology* **223**, 131–150.
- Sakmar, T. P., Franke, R. R., & Khorana, H. G. (1989). Glutamic acid-113 serves as the retinylidene Schiff base counterion in bovine rhodopsin. *Proceedings of the National Academy of Sciences of the United States of America* **86**, 8309–8313.
- Sakmar, T. P., Menon, S. T., Marin, E. P., & Awad, E. S. (2002). Rhodopsin: insights from recent structural studies. *Annual Review of Biophysics & Biomolecular Structure* **31**, 443–484.
- Sampath, A. P. & Baylor, D. A. (2002). Molecular mechanism of spontaneous pigment activation in retinal cones. *Biophysical Journal* **83**, 184–193.
- Schertler, G. F., Villa, C., & Henderson, R. (1993). Projection structure of rhodopsin. *Nature* **362**, 770–772.
- Schick, G. A., Cooper, T. M., Holloway, R. A., Murray, L. P., & Birge, R. R. (1987). Energy storage in the primary photochemical events of rhodopsin and isorhodopsin. *Biochemistry* **26**, 2556–2562.
- Schnapf, J. L., Nunn, B. J., Meister, M., & Baylor, D. A. (1990). Visual transduction in cones of the monkey *Macaca fascicularis*. *Journal of Physiology* **427**, 681–713.
- Schoenlein, R. W., Peteanu, L. A., Mathies, R. A., & Shank, C. V. (1991). The first step in vision: femtosecond isomerization of rhodopsin. *Science* **254**, 412–415.
- Schultze, M. (1866). Zur Anatomie und Physiologie der Retina. *Archiv für Mikroskopische Anatomie* **2**, 175–286.
- Shichida, Y. & Imai, H. (1998). Visual pigment: G-protein-coupled receptor for light signals. *Cellular & Molecular Life Sciences* **54**, 1299–1315.

- Shichida, Y., Matuoka, S., & Yoshizawa, T. (1984). Formation of photorhodopsin, a precursor of bathorhodopsin, detected by picosecond laser photolysis at room temperature. *Photobiochemistry and Photobiophysics* **7**, 221–228.
- Srebro, R. (1966). A thermal component of excitation in the lateral eye of *Limulus*. *Journal of Physiology* **187**, 417–425.
- Stavenga, D. G., Oberwinkler, J., & Postma, M. (2000). Modelling primary visual processes in insect photoreceptors. In *Handbook of Biological Physics 3. Molecular Mechanisms in Visual Transduction*, 1st ed., eds. Stavenga, D. G., Degrip, W. J., Pugh, E. N., Jr., pp. 527–574. Amsterdam-London-New York-Oxford-Paris-Shannon-Tokyo: Elsevier Science.
- Stavenga, D. G., Smits, R. P., & Hoenders, B. J. (1993). Simple exponential functions describing the absorbance bands of visual pigment spectra. *Vision Research* **33**, 1011–1017.
- Steinfeld, J. I., Francisco, J. S., & Hase, W. L. (1999). *Chemical Kinetics and Dynamics*. 2nd ed., pp. 325–389. New Jersey: Prentice Hall.
- St. George, R. C. C. (1952). The interplay of light and heat in bleaching rhodopsin. *Journal of General Physiology* **35**, 495–517.
- Stiles, W. S. (1948). The physical interpretation of the spectral sensitivity curve of the eye. In *Transactions of the Optical Convention of the Worshipful Company of Spectacle Makers*, pp. 97–107. London: Spectacle Makers' Co.
- Szundi, I., Mah, T. L., Lewis, J. W., Jager, S., Ernst, O. P., Hofmann, K. P., & Kliger, D. S. (1998). Proton transfer reactions linked to rhodopsin activation. *Biochemistry* **37**, 14237–14244.
- Tachibanaki, S., Imai, H., Terakita, A., & Shichida, Y. (1998). Identification of a new intermediate state that binds but not activates transducin in the bleaching process of bovine rhodopsin. *FEBS Letters* **425**, 126–130.
- Thorgeirsson, T. E., Lewis, J. W., Wallace-Williams, S. E., & Kliger, D. S. (1993). Effects of temperature on rhodopsin photointermediates from lumirhodopsin to metarhodopsin II. *Biochemistry* **32**, 13861–13872.
- Unger, V. M., Hargrave, P. A., Baldwin, J. M., & Schertler, G. F. (1997). Arrangement of rhodopsin transmembrane alpha-helices. *Nature* **389**, 203–206.
- van der Velden, H. A. (1946). The number of quanta necessary for the perception of light in the human eye. *Ophthalmologica* **111**, 321–331.
- Wald, G. (1933). Vitamin A in the retina. *Nature (London)* **132**, 316–317.
- Wald, G. (1935). Carotenoids and the visual cycle. *Journal of General Physiology* **19**, 351–371.
- Wald, G. (1945). Human vision and the spectrum. *Science* **101**, 653–658.

- Wald, G. (1959). Photochemical and stereochemical properties of carotenoids at low temperatures. (3) Discussion. *Nature* **184**, 620–624.
- Wald, G. (1968). Molecular basis of visual excitation. *Science* **162**, 230–239.
- Wald, G., Brown, P. K. & Smith, P. H. (1953). Cyanopsin a new pigment of cone vision. *Science* **118**, 505–508.
- Wang, Q., Schoenlein, R. W., Peteanu, L. A., Mathies, R. A., & Shank, C. V. (1994). Vibrationally coherent photochemistry in the femtosecond primary event of vision. *Science* **266**, 422–424.
- Wang, Z., Asenjo, A. B., & Oprian, D. D. (1993). Identification of the Cl(-)-binding site in the human red and green color vision pigments. *Biochemistry* **32**, 2125–2130.
- Williams, T. P. & Milby, S. E. (1968). The thermal decomposition of some visual pigments. *Vision Research* **8**, 359–367.
- Yokoyama, S. (1996). Molecular evolution of retinal and nonretinal opsins. *Genes to Cells*, **1**, 787–794.
- Yokoyama, S. & Yokoyama, R. (1996). Adaptive evolution of photoreceptors and visual pigments in vertebrates. *Annual Review of Ecology & Systematics* **27**, 543–567.
- Yokoyama, S. & Yokoyama, R. (2000). Comparative molecular biology of visual pigments. In *Molecular Mechanisms in Visual Transduction*, eds. Stavenga, D. G., DeGrip, W. J., & Pugh, E. N., pp. 259–296. Elsevier, Amsterdam-London-New York-Oxford-Paris-Shannon-Tokyo.
- Yoshizawa, T. (1972). The behaviour of visual pigments at low temperatures. In *Handbook of Sensory Physiology, VII/1. Photochemistry of Vision*, ed. Dartnall, H. J. A., pp. 147–179. Berlin-Heidelberg-New York: Springer.
- Yoshizawa, T. & Horiuchi, S. (1969). Intermediates in the photolytic process of porphyropsin. *Experimental Eye Research* **8**, 243–244.
- Yoshizawa, T. & Kito, Y. (1958). Chemistry of the rhodopsin cycle. *Nature* **182**, 1605.
- Yoshizawa, T., Shichida, Y., & Matuoka, S. (1984). Primary intermediates of rhodopsin studied by low temperature spectrophotometry and laser photolysis. Bathorhodopsin, hpsorhodopsin and photorhodopsin. *Vision Research* **24**, 1455–1463.
- Zak, P. P., Ostrovsky, M. A., & Bowmaker, J. K. (2001). Ionochromic properties of long-wave-sensitive cones in the goldfish retina: an electrophysiological and microspectrophotometric study. *Vision Research* **41**, 1755–1763.
- Zhukovsky, E. A. & Oprian, D. D. (1989). Effect of carboxylic acid side chains on the absorption maximum of visual pigments. *Science* **246**, 928–930.